Final Report on SERDP SEED Project

3D Geophysical Data Collection and Analysis for UXO Discrimination

SERDP SEED Project 1357

Revision 0

Prepared by

Environmental Sciences Division
Oak Ridge National Laboratory

June 2004

Report Documentation Page

Form Approved
OMB No. 0704-0188

1. REPORT DATE	2. REPORT TYPE	3. DATES COVERED
JUN 2004	**Final**	**-**

4. TITLE AND SUBTITLE	5a. CONTRACT NUMBER
3D Geophysical Data Collection and Analysis for UXO Discrimination	5b. GRANT NUMBER
	5c. PROGRAM ELEMENT NUMBER
6. AUTHOR(S)	5d. PROJECT NUMBER
T. Jeffrey Gamey	**UX-1357**
	5e. TASK NUMBER
	5f. WORK UNIT NUMBER
7. PERFORMING ORGANIZATION NAME(S) AND ADDRESS(ES)	8. PERFORMING ORGANIZATION REPORT NUMBER
Battelle 105 Mitchell Road, Suite 103 Oak Ridge, TN 37830	
9. SPONSORING/MONITORING AGENCY NAME(S) AND ADDRESS(ES)	10. SPONSOR/MONITOR'S ACRONYM(S)
Strategic Environmental Research & Development Program 901 N Stuart Street, Suite 303 Arlington, VA 22203	**SERDP**
	11. SPONSOR/MONITOR'S REPORT NUMBER(S)

12. DISTRIBUTION/AVAILABILITY STATEMENT
Approved for public release, distribution unlimited

13. SUPPLEMENTARY NOTES
The original document contains color images.

14. ABSTRACT

15. SUBJECT TERMS

16. SECURITY CLASSIFICATION OF:			17. LIMITATION OF ABSTRACT	18. NUMBER OF PAGES	19a. NAME OF RESPONSIBLE PERSON
a. REPORT	b. ABSTRACT	c. THIS PAGE			
unclassified	**unclassified**	**unclassified**	**UU**	**108**	

Standard Form 298 (Rev. 8-98)
Prescribed by ANSI Std Z39-18

Table of Contents

List of Acronyms

AGL	Above ground level
AS	Analytic signal
ASCII	American Standard Code for Information Interchange
DAS	Data analysis system
DoD	Department of Defense
EM	Electromagnetic
FUDS	Formerly Used Defense Sites
GPS, DGPS	(Differential) Global Positioning System
MTADS	Multi-Sensor Towed Array Detection System
ORNL	Oak Ridge National Laboratory
SERDP	Strategic Environmental Research & Development Program
UXO	Unexploded Ordnance
VG	Vertical (magnetic) gradient

List of Figures

List of Tables

Acknowledgements

This work was funded by the Strategic Environmental Research and Development Program under the direction of Dr. Brad Smith and Dr. Anne Andrews. The report was written by employees of Oak Ridge National Laboratory. Oak Ridge National Laboratory is managed by UT-Battelle, LLC for the U.S. Department of Energy under contract DE-AC05-00OR22725. A contractor of the U. S. Government has authored the submitted manuscript. Accordingly, the U.S. Government retains a nonexclusive, royalty-free license to publish or reproduce the published form of this contribution, or allow others to do so, for U. S. Government purposes.

3D Geophysical Data Collection and Analysis for UXO Discrimination

SERDP-SEED: UXSEED-1357

Oak Ridge National Laboratory, PO Box 2008, Oak Ridge, Tennessee 37831-6038;
T. Jeffrey Gamey, phone 865-574-6316, fax 865-576-8646, email gameytj@ornl.gov

Background

Ordnance detection and discrimination techniques are typically based on two-dimensional representations of geophysical data such as contoured grids. These grids are created by interpolating data collected along transect lines. Without the use of wheeled carts (which pose their own set of unique restrictions) the assumption that all data are collected at a common height above the ground is routinely violated. Differences in sensor height between adjacent lines cause systematic and pseudo-random distortions in the gridded data which are not based on geophysical changes. The resulting anomalies are easily misinterpreted, or require filters which reduce the reliability of inversion routines. Field efforts to collect data of the quality required for adequate inversion are painstakingly conducted to achieve a measure of uniformity. The time, effort, and training required by these efforts have seldom been translated into cost-effective project implementation.

Objective

The objective of this research is to determine some of the benefits accrued by collecting and processing three-dimensionally positioned data (3D) for unexploded ordnance (UXO) detection and discrimination versus traditional two-dimensional (2D) approaches.

Technical approach

The technical approach taken here was strictly model-based in that no geophysical data were collected at this stage of the project. Although the techniques are equally applicable to electromagnetic as well as magnetic data sets, only magnetic data were modeled at this stage. 2D and 3D collection scenarios were devised and tested over a variety of single and double target models. Simulated targets included 60mm and 20mm shells at relatively deep burial depths and close proximity. Moderate levels of noise were added to the positions and to the synthetic magnetic readings.

In this project, 3D processing, visualization, detection and discrimination techniques were developed as analogs to the 2D techniques most commonly in current use. Comparisons were made between the 2D and 3D techniques to evaluate the relative merits of the 3D approach.

A new collection procedure was devised to maximize the utility of the 3D approach. This is principally a “reacquisition” or “cued investigation” approach in which an operator is directed to an anomalous location on a dig list and proceeds to collect data over the target area by waving the sensor randomly over the center point. This is similar to the approach

currently used by OE Technicians with analog magnetometers, only in this case the instruments would be digital and capable of recording 3D positioned data. Eventually, the processing and inversion techniques developed here can be implemented on a real-time basis in order to minimize field time.

Processing techniques were extended to 3D using commercial software. A variety of "gridding" routines were tested for their ability to reliably interpolate potential field data and an optimal technique was chosen. Hanning filter coefficients were also calculated and programmed to smooth the data in three-dimensions.

Visualization techniques are irrelevant to numerical inversion routines, but are required for operator input. For example, without a simple visualization technique the operator cannot tell whether to invert for one or more objects. A variety of standard visualization techniques were examined, but the most effective was the Gradient String. This is a unique concept devised specifically for this project. A Gradient Strings traces a line of maximum magnetic gradient through the three-dimensional data space above a target. This reduces the solid cube of data into a single strand which points directly to the target or targets.

Discrimination techniques included a variety of 3D analogs to 2D techniques. For the purposes of this report, discrimination is differentiated from detection in that detection is limited to identifying the number of targets, whereas discrimination attempts to determine specific parameters such as depth, size and orientation. In particular, higher order gradients were used to estimate depths (Salem et al, 2002), as was a simple Euler deconvolution. The MTADS-DAS dipole model code was used to estimate depth and size. The commercial ModelVisionPro software was used to estimate depth, size and orientation. Discrimination in this study does not include differentiating UXO from non-UXO.

Summary

The 3D acquisition and processing methodology was shown to be better than the standard 2D method for detection and location of closely spaced targets in all cases. The Gradient String approach detected all of the targets and located them in (x, y) more accurately than the comparable technique of 2D analytic signal peaks. Depth estimates using the analytic signal ratio and Euler deconvolution were five times more accurate using the 3D data. The most accurate technique was the 3D ModelVision spherical inversion, which averaged location errors of 9cm and depth errors of 2cm.

Tests showed that detection and inversion of 2D *noise-free* data was comparable to the 3D *noise-free* data in most cases. This is not unexpected for potential field data. The introduction of noise, however (1cm of positional noise and 0.1nT of magnetometer noise), created significant problems for the 2D data. In general, the data were insufficient to invert or (in some cases) detect multiple objects even with tight line spacing. The 3D data also suffered from the noise, particularly at low heights where gradients were

strongest, but detection and location capabilities were almost always 2-5 times better than the comparable 2D data.

The Gradient String technique proved to be an excellent method of detecting and visualizing multiple targets within the data space. The various inversion techniques generally improved the 2D results, but in almost all cases the 3D processing outperformed the comparable 2D processing. The 3D data provided enough additional information to improve detection and depth estimates by up to 5 times, but not enough to determine more complex parameters such as dimensions and orientation.

Table 1: Average location errors by method. Failures in the dipole inversion are generally the result of insufficient signal strength.

		2D data set	3D data set
Peak detection	horiz-error	0.18 m	0.09 m
AS ratio depth	vert-error*	0.21 m	0.10 m
Euler depth	vert-error*	0.24 m	0.06 m
Dipole inv	radial-error	0.12 m (9 failures)	0.28 m (1 failure)
Sphere inv	radial-error	0.14 m	0.09 m
Ellipse inv	radial-error	0.17 m	0.18 m

* vertical error listed here is at location with horizontal error given for peak detection (i.e. Euler 2D radial error = $\sqrt{(0.18^2 + 0.24^2)} = 0.30$m)

Several lines of development are suggested by the results of this project. Implementation of feedback mechanisms and an extension of the 3D techniques to electromagnetic methods are recommended to extract the additional features such as orientation from the data. More advanced data segmentation techniques are also recommended in order to more effectively resolve model parameters. Discrepancies between the various software packages for ellipsoid model signatures were found and need to be resolved. Test-stand measurements to verify signature shapes and field trials to verify performance standards are required. Similarly, tests to improve inversion results for target shape and orientation and for discrimination between UXO and non-UXO are still required to fully implement this 3D technique.

Accomplishments

Introduction

This project is broken down into several parts, each with its own method and conclusions, and most flowing sequentially from one to the other. For reporting continuity, these topics are covered individually rather than providing method for all parts and then results for all parts. These topics include:

- Project Conception
- Data Collection and Modeling
- Gridding, Filtering and Processing
- Visualization and Gradient Strings
- Detection
- Depth Estimation
- Euler Deconvolution
- Dipole Inversion
- Solid-body Inversion (Sphere)
- Solid-body Inversion (Ellipsoid)

Project Conception

Many geophysical data sets, collection procedures and presentation techniques are described as 3-dimensional. For the purposes of clarity, a distinction must be made between the number of dimensions of the positioning data recorded during the survey and the number of dimensions of the presentation format. The traditional survey records two dimensions of position data (x, y) and presents the geophysical results as:

- 1D profiles (a projection against a single axis of time or horizontal position, with the data as the second axis),
- 2D grids/contours (a projection against two horizontal position axes using contours or colors to represent the data axis),
- or 3D surfaces/curves/nets (a projection against two horizontal position axes, using the illusion of a third vertical axis in data units to represent the geophysics, often including color and/or contours for emphasis of the data).

Even with the recording of 3D positional data (x, y, height), none of the aforementioned presentation techniques display or accommodate the addition of height information. Generally, the height is assumed to be constant and the data are forced onto a 2D grid. We must also recognize the limitations of all two-dimensional media (paper and screens). Even 3D surfaces are technically 2D presentations using illusions of perspective and shading to appear 3D. It is extremely difficult to represent 3D points on a 2D screen or map, and this does not yet include a dimension for the geophysical data. Occasionally, the perspective of a 3D presentation is rotated, thus adding time to enhance the illusion of dimension. Exchanging our 2D media for 3D holographic presentations would still require some form of transparency plus rotation of the image or movement of the observer in order to fully interpret it, just as any solid object would. A 3-dimensional representation therefore presents several fundamental obstacles to the observer.

Multi-dimensional data sets require that we either reduce the information to its most relevant form for presentation, or think and present data in terms of matrices and functions with n-dependent variables. This applies equally to 3D positioned data from a single sensor, multiple responses from a single sensor (ie EM time gates), or integrated multi-sensor data sets. Although this makes them ideal candidates for computer analysis, which is based almost entirely on linear matrices, the human factor is still required for control and judgment, hence the requirement for visualization.

A single geophysical measurement at one point in space rarely has any significance. A measurement requires spatial correlation with neighboring points (1D profile) to give data meaning. Similarly, consecutive profiles allow the data to be spatially correlated in two dimensions – down line and across line. The traditional approach to geophysical mapping therefore is to collect data along parallel transects (1D) at a nominal height and present the results as a grid (2D). Each added dimension brings a new level of relevance to the interpretation, but there are drawbacks.

Single profiles present the data with great resolution and fidelity since they are not subject to gridding interpolation, but can be difficult to interpret. The most obvious shortfall is the lack of information to the sides of a profile anomaly. By presenting the data with reference to neighboring points on both sides, the 2D perspective makes it much simpler to discriminate discrete targets from broader anomalies. This simplification is an important part of the interpretation process.

Data processing techniques based on 2D data sets also have significant advantages over their 1D counterparts. There are many advantages to analyzing data that have been spatially correlated in two dimensions. Spatial filters, for example, can remove uncorrelated noise thereby enhancing the signal-noise ratio. FFT processes, such as analytic signal, can also enhance features more reliably and with fewer assumptions when applied to grids than to profiles.

The disadvantage of 2D presentations is that they assume that all of the data were collected on a common plane, although this is rarely true. Whenever a data point is collected at different height than the adjacent data points, the gridding process creates an artifact in the grid. Depending on the severity and distribution of these artifacts, any interpretation based on the gridded data will be more or less flawed. As a result, many additional 2D data processing steps must be incorporated into the work flow in order to correct for the "common plane" assumption and produce a viable interpretation. In addition to the gridding process, which generally desamples data down-line and interpolates data between lines, filtering or deletion of data points must be applied to produce a satisfactory grid. In some cases, these additional steps may reduce data quality more than they enhance it.

The impact of variable sensor height on gridded data has been addressed by many others and the effects on both magnetic and electromagnetic data are well documented. Numerous studies have been done to limit, quantify or correct these effects. Techniques include wheeled carts to control height, altimeters and other positioning systems to measure height, and various upward or downward continuation algorithms to correct readings to a nominal height. Advances in positioning systems and computing capabilities now allow collection and storage of geophysical, position and height data in a single database. Software packages for data inversion are taking advantage of increased power and are inverting data with height information. Although the technology has incorporated several aspects of 3D data, all of these are attempts to solve the problem of continually forcing 3D data into a 2D format.

To date, the best inversion solutions ignore the 2D format altogether and work entirely with profile data. Although this work flow avoids many of the problems, it does not take advantage of any of the positive elements of 2D processing such as noise reduction or FFT algorithms. Processing benefits are limited to one dimension of spatial correlation (down-line). Only filters and processes that can be applied to profiles are used.

The only way to take advantage of spatial correlation of data collected with 3D positioning is to process it in three dimensions. Not only does this effectively deal with the problems associated with changes in height, but it offers the potential of spatially correlating the data vertically as well as horizontally. This also provides an opportunity to enhance the state-of-the-art inversion techniques by incorporating the benefits of spatial correlation prior to inversion.

This project was therefore designed to examine the steps necessary to maximize the utility of 3D positioned data, to develop the groundwork for some of the tools that may be required, and to quantify the benefits accrued through such a process.

Data Collection and Modeling

For logistical and testing purposes, this project assumed that the data were collected as part of a cued investigation (to follow-up a previously detected anomaly) using magnetometer sensors. The techniques are, however, equally applicable to traditional survey collection and to electromagnetic data after additional experimentation with 3D gridding and inversion techniques. After an initial geophysical survey, specific anomalies are identified for additional follow-up. Prior to excavation, the operator collects a "cloud" of data points at irregularly spaced intervals around the pre-determined location. The "cloud" of data is then interpolated into a 3D lattice for processing and analysis (Figure 1).

Forward models were created to develop and test new 3D algorithms and to test the comparison between 2D and 3D capabilities. Initial testing of new routines and software was done with simple dipole models. For the final evaluation of the 3D techniques, new models were created using the MAGMOD code as the basic kernel. It had the advantage of modeling ordnance-like sources, and was independent of the various inversion codes being tested. The user interface and output formats of the original Matlab code were revised to accommodate the specific project requirements. This included acceptance of a list of 3D measurement points, output of results in 3D, grid orientations other than magnetic North, and modeling multiple targets.

The final list of models included single and closely spaced ordnance at various depths and orientations. The various target parameters are listed below. Non-varying parameters are listed in Table 2, variable parameters in Table 3. Scale representations of the models against the 2D color contours are shown in Appendix B-1.

Target locations were chosen to represent a scenario in which a single anomaly may be reasonably detected on a standard survey. Line spacing and noise levels were set to simulate a search for small UXO (20mm) on a mixed-use range. The results of the 2D simulation show an anomaly that would be selected for further follow-up. The reacquisition phase should be sufficient to determine if there is more than one target contributing to the original anomaly and its/their basic parameters (position, depth, size). Targets were placed close enough together to overlap signatures at typical sensor heights, but still have distinct positive peaks that would be considered separate hits with a 0.5m search radius. Burial depths were guided by maximum penetration limits estimated by USAESCH. The deepest 60mm targets were placed at 90% of the maximum penetration depth, while the 20mm targets were placed at approximately 25% of maximum depth.

Table 2: Non-varying target parameters for final set of models. Target dimensions were obtained from ordnance tables. Relative permeability is the default used by the Magmod code. Remanence has been set to zero, and the effects of demagnetization and octupole components have been included.

60mm equivalent sphere	
Diameter	0.102m
Relative permeability	500
20mm equivalent sphere	
Diameter	0.034m
Relative permeability	500
60mm ellipsoid	
Major axis length	0.200m
Semi-major axis length	0.060m
Minor axis length	0.060m
Relative permeability	500
20mm ellipsoid	
Major axis length	0.069m
Semi-major axis length	0.020m
Minor axis length	0.020m
Relative permeability	500
Earth's field	
Strength	50,000nT
Inclination	70°N
Declination	0°E

Table 3: Variable target parameters for final set of models. Negative depth is below ground. Azimuth is the horizontal angle between the major axis and grid North (positive CW). Dip is the vertical angle between the major axis and horizontal (positive down).

Model	Type	X	Y	Depth	Azim	Dip
1	60mm sph	-0.1	-0.2	-0.2	0	0
2	60mm sph	-0.1	-0.2	-0.6	0	0
3	60mm sph 20mm sph	-0.1 +0.1	-0.2 +0.3	-0.6 -0.05	0 0	0 0
4	60mm ellip	-0.1	-0.2	-0.2	0	0
5	60mm ellip	-0.1	-0.2	-0.6	0	0
6	60mm ellip	-0.1	-0.2	-0.6	0	90
7	60mm ellip 20mm ellip	-0.1 +0.1	-0.2 +0.3	-0.6 -0.05	0 0	0 0
8	60mm ellip 20mm ellip	-0.1 +0.1	-0.2 +0.3	-0.6 -0.05	0 0	90 90
9	60mm ellip 20mm ellip	-0.1 +0.1	-0.2 +0.3	-0.6 -0.05	110 45	65 40

Data sampling for the 2D and 3D data sets were based on traverse lines and cued investigations respectively. For the 2D set, lines were spaced 0.5m apart at a nominal 0.35m height. Five lines were sampled, covering +/- 1m from the target. Lines 1,3,5 were set exactly at 0.35m (including the line closest to the targets), while Line 2 was set at 0.40m and Line 4 was set at 0.30m. This reflected the inherent irregularity of adjacent line heights without unduly biasing the overall average or the line closest to the targets. Down line data spacing was set at 0.05m, which corresponded to a slow walking speed of 0.5m/s at a 10Hz sample rate. Although roughly half normal walking speed (and twice the data density), this was consistent with the level of care required to maintain a 0.5m line spacing.

The 3D set was based on a 0.05m sample increment over a range of +/- 1m horizontally from the center point (0, 0) and from 0.1m-0.6m height. A random selection of 300 data points were taken from this set with a bias toward those closest to (0, 0, 0). This simulated a 30 second collection period at 10Hz sample rate over the target of interest.

Model results for the 2D and 3D point sets were generated using the modified MAGMOD code. Normally distributed noise of 0.01m was added to the positions in (x, y, z) and 0.1nT noise was added to the magnetic field. No additional noise was added to simulate heading, diurnal or operator error. These effects would only impact the 2D data, since the 3D data would have a constant heading, the diurnal would vary only slightly over the 30sec collection period, and the operator would remain stationary.

In total, there were 205 data points in the 2D data sets and 300 points in the 3D data set. Although this gave a slight advantage to the 3D data set in terms of the number of raw data points, it was the premise of this research that the collection methodology provides the greatest advantage. These are the data sets used for the inversion comparison. Figure 2 illustrates the basic data distribution for the 2D and 3D collection scenarios over two selected models.

Throughout this study a control model was input to determine the limitations of any given technique. “Model 3t” was created as a fully-populated noise-free version of “Model 3” at 5cm intervals. For this model, all grid and lattice nodes were filled with synthetic data without noise. This included 1681 data points (41x41 grid points) for the 2D data set and 18,491 data points (41x41x11 lattice points) for the 3D data set. This was intended to provide perfect input data to the algorithms with sufficient resolution to obviate the need for gridding, filtering or other processing. These results are shown in red in all tables and are not included in the average error calculations. A similar “Model 9t” was created specifically for the 3D ellipsoid inversion and is covered in detail in the appropriate section.

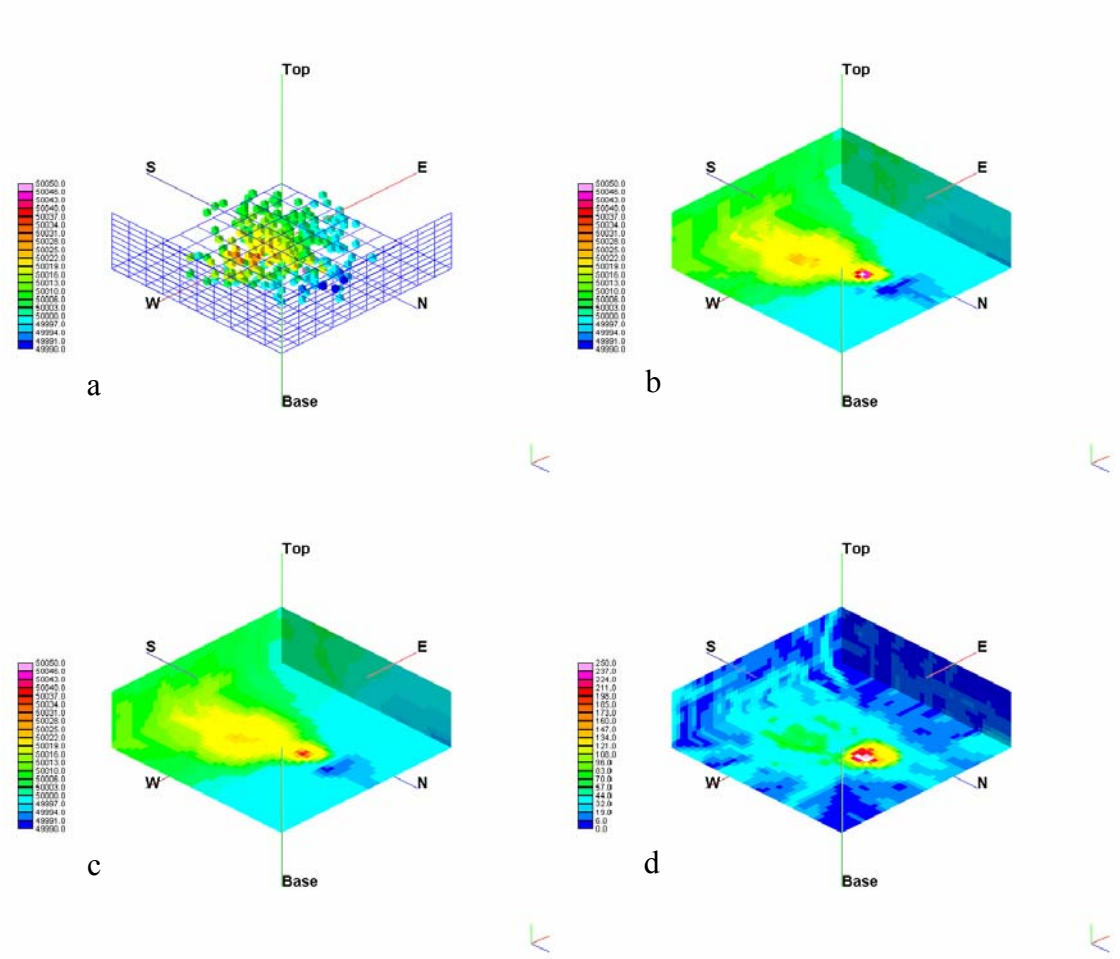

Figure 1: Sample of 3D processing stream from (a) "cloud" of collected data points to (b) interpolated grid to (c) filtered grid to (d) analytic signal. View is from beneath in the SE in order to illustrate the greater dynamic range data at the lowest altitudes. Data shown represent Model 3. Scale of data box is 2m x 2m x 0.5m.

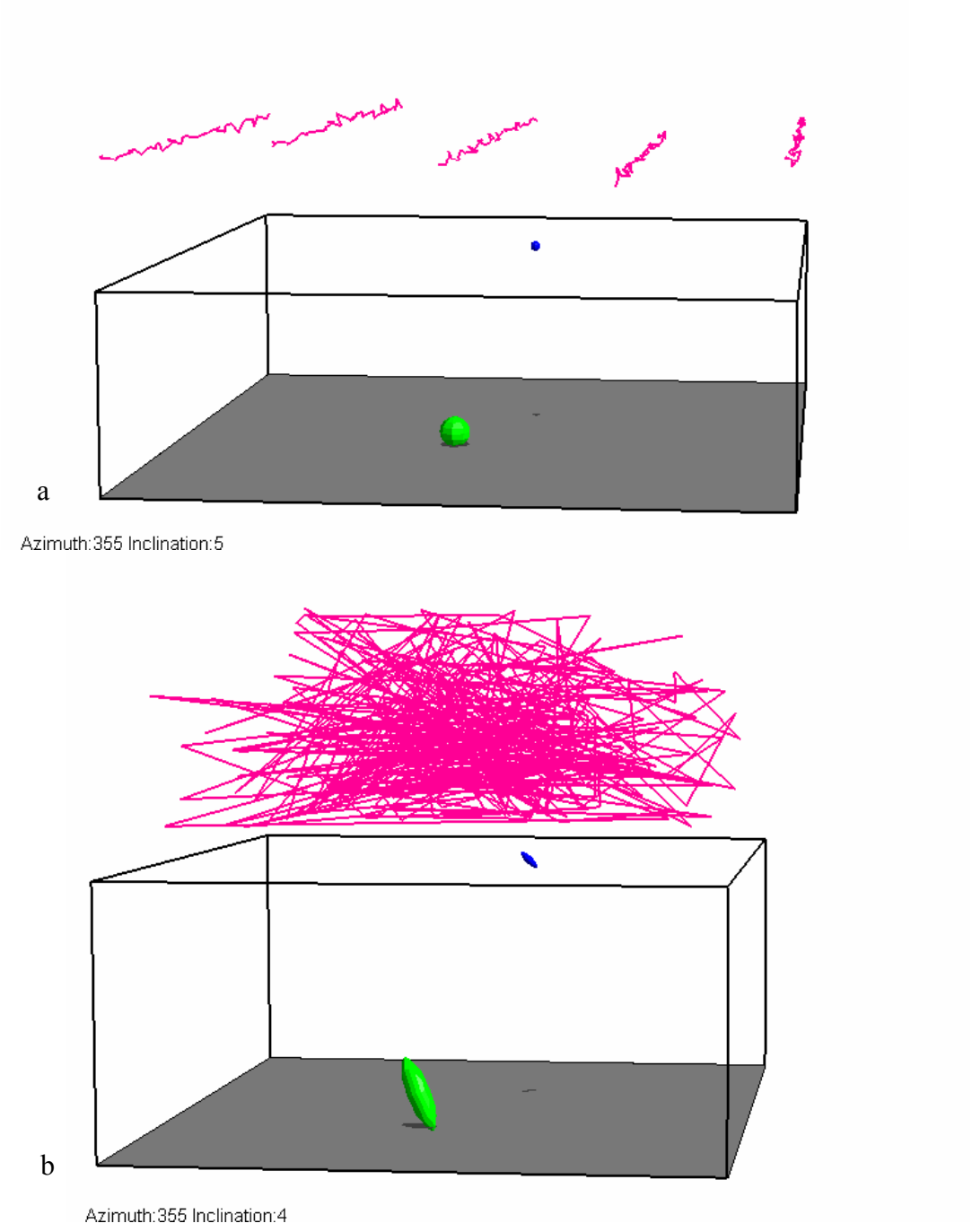

Figure 2: Visualization of data collection scenarios and selected models. The data points (red) are common to analysis of all models. (a) 2D data collection based on 0.5m line spacing with random noise at slightly varying line heights, presented over spherical targets (60mm blue, 20mm green) from Model 3. Scale of box is approximately 2m x 2m x 0.6m. (b) 3D data collection based on random points centered over the target with noise added, presented over ellipsoid targets from Model 9. Scale of box approximately 1.5m x 1.5m x 0.7m.

Gridding, Filtering and Processing

The 2D gridding was achieved using the Geosoft minimum curvature routine. Experience has shown this to be an acceptable default for potential field data. Representations of the 2D gridded data are shown in Appendix B-1.

No such standard existed for 3D gridding. Prior to choosing a 3D gridding algorithm and attendant parameters, an investigation was conducted into the relative outputs of the techniques available. Matlab and Rockware both offered 3D gridding routines, but Matlab offered a far more limited range of techniques. It was therefore decided to concentrate on the Rockware software.

Two closely spaced objects were modeled at 0.1m increments in (x, y, z) and subjected to six 3D gridding algorithms in Rockworks2002. The six gridding routines examined were labeled: closest point, isotropic distance, anisotropic distance, weighted distance, directional weighted and vertical biased. Each of these techniques is described in Appendix B-5, which is taken from the software help manual. The directionally weighted and vertically biased routines were designed to emphasize horizontal stratigraphic units only. In order to accommodate this orientation, the input data were rotated before gridding so that up was North.

Solid models (lattices) were created with each algorithm to test how well each represented the true data. The quality of the gridding was determined as the standard deviation of the difference between the solid model output and the original modeled data. The quality of the fit between the lattice results and the true model deteriorated with the amount of interpolation required by successive decimation of the input data, especially in the high gradient area near the center of the target. Results are provided in Table 4.

All gridding routines used a "declustering" technique to reduce memory requirements from oversampling. This process averaged all data points within a single lattice cell before interpolating. This served to reduce noise in closely spaced readings and to reduce the volume of input to the gridding routine. None of these tests required declustering at this stage since all input were undersampled rather than oversampled. It was later learned that this option altered the position of the data by *rounding* the position to the nearest node and averaging. This simplified the interpolation process, but reduced the intended accuracy of the positioning to that of the lattice interval. This option was turned off for subsequent operations.

The first test of gridding routines used a fully populated input data set. For each of the nodes in the final lattice, an input of modeled data was provided. Under these conditions, no interpolation was required and all routines faithfully returned identical values to the true modeled data.

The second test required interpolation between regularly spaced inputs. Input data were provided at 0.2m intervals in (x, y, z) and were interpolated to 0.1m intervals. This represented a data set desampled to $1/8^{th}$ the original density. The best gridding

algorithm for this case was the anisotropic, followed by the weighted distance and vertical bias techniques, which are variants of the anisotropic.

The third test also used 1/8th input data density, but positions were distributed randomly throughout the 3D space. The best algorithm was again the anisotropic technique, although the fit was somewhat poorer than with the regular distribution. Only the closest point techniques showed a better fit than the previous regular distribution.

The fourth test used 1/8th input data density, but input points were drawn preferentially from the center of the 3D space. Half of the points were located randomly within 1m of the center point of the space. This represents desampling to 1 point out of every 2 within this hemisphere. The remaining points were randomly distributed throughout the remaining space, representing desampling to 1 out of every 14 nodes. All techniques showed improvement over the random distribution due to the relative increase in sampling in the highest gradient area. The anisotropic technique again produced the best fit.

Table 4: Standard deviation of error between lattice output and true data

Gridding method	closest point	iso-tropic	aniso-tropic	dist wt'd	dir wt'd	vert wt'd
Fully populated	0.0	0.0	0.0	0.0	0.0	0.0
Desampled points	0.51	0.68	0.20	0.25	0.38	0.39
Random distribution	0.45	0.69	0.32	0.45	0.50	0.45
Concentrated distribution	0.41	0.62	0.28	0.30	0.31	0.40

Having established the optimal 3D gridding routine for use on this project, filters and processing techniques were developed. The 2D filtering and processing applications were conducted with Geosoft routines. New filtering routines had to be developed for the Rockware 3D models. The only filter available was an average filter. This filter is a moving filter which takes a simple average of all points touching the center point of the moving window (square roll-off). Coefficients for a 3D Hanning filter (cosine roll-off) were derived and programmed. The coefficients for the 3 point (3x3x3 pts) 3D Hanning filter are provided in Table 5.

Table 5: Coefficients of 3-point 3D Hanning filter

Lower layer			middle layer			upper layer		
0.006	0.030	0.006	0.030	0.074	0.030	0.006	0.030	0.006
0.030	0.074	0.030	0.074	0.148	0.074	0.030	0.074	0.030
0.006	0.030	0.006	0.030	0.074	0.030	0.006	0.030	0.006

In addition, programs were written to calculate the analytic signal (AS) from the 3D total field data. This was relatively simple in that the vertical gradient could be calculated directly from adjacent nodes in the interpolated lattice just as the horizontal gradients are in 2D methods. This removed the necessity of using FFT routines. The Hanning filter and native Rockware utilities were all compatible with the new AS file output.

Visualization and Gradient Strings

A variety of visualization techniques were available through the Rockware software for the total field and analytic signal data. These included slices in various directions (horizontally to create grids, vertically to create cross sections, multiple cross sections to create fences), iso-surfaces (3D analog of a single contour line) and transparencies. Figure 3 illustrates some of these concepts. Color was used in all cases to represent the amplitude of the geophysical data. Although all of these techniques are easily understood and applied to a wide variety of three-dimensional data sets, they require considerable user control of placement, color and thresholds in order to adequately visualize the data. For the purposes of smooth potential fields (or electromagnetic fields), a simpler technique has been devised which we call Gradient Strings. These are essentially lines through the lattice tracing maximum rate of change in the field. For magnetic data, one can imagine layers of stacked analytic signal grids with a line connecting the peaks from one layer to the next (Figure 4).

The aim of this technique is to reduce the data set to its most important qualities and allow simple visualization with as few control parameters as possible. The underlying assumption is that maximum gradient lines for legitimate sources will be continuous and will increase in magnitude with proximity to the ground. Noise, which might otherwise be picked as a possible target, will lack this continuity through 3D space. Similarly, multiple targets that may appear as a single target on the original survey data can be resolved as distinct gradient strings. Processing options based on Gradient String information can include spatial windows, cut-off thresholds, and filter strengths. Strings can be down-selected based on amplitude, length and continuity. If the line branches with depth, the operator is faced with the possibility of multiple targets or a single large target in the very near surface.

For a string to be valid, therefore, it must (a) exceed an intensity threshold (b) be continuous over several layers and (c) increase in intensity with depth. The result is a line through the 3D data space that points directly to the target. To further aid in interpretation, the line is color-coded to gradient intensity.

These gradient strings and the numerical inversion provide mutual feedback into the decision making process. The visualization and manipulation of gradient strings will allow the operator to refine processing parameters and to deselect targets from noise or to pin-point multiple targets within close proximity to one another. In return, the inversion will provide quantitative results in the form of fit coefficients.

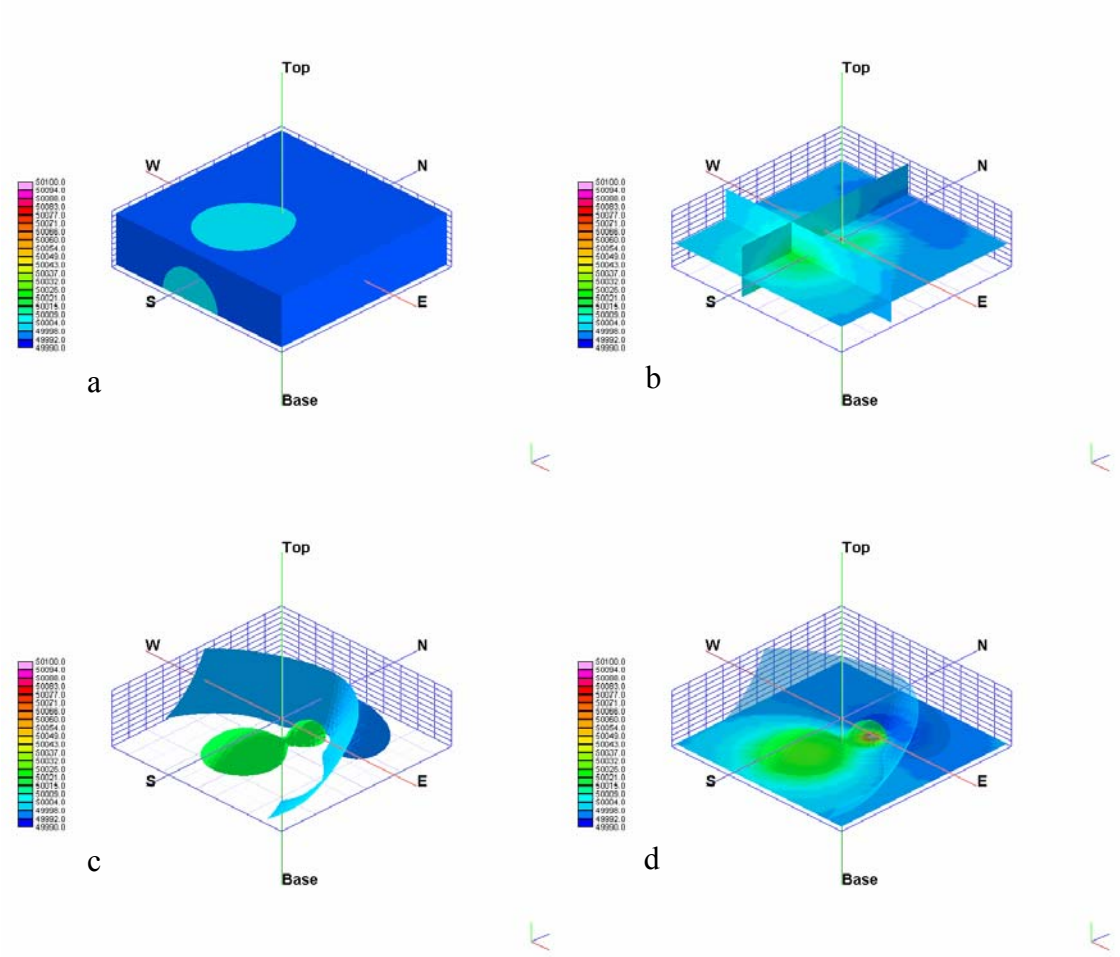

Figure 3: These graphics illustrate some of the problems and complexities associated with visualization of 3D data. (a) A solid model showing the outer surfaces. (b) Slices through the solid in three orthogonal directions. (c) Three iso-surfaces at 49997nT, 50000nT and 50017nT. (d) Transparencies of the iso-surfaces combined with a horizontal slice. Total field units in nT. An example of a visualization limitation would be a poor choice of iso-surface in (c) which either missed or grouped the anomalies.

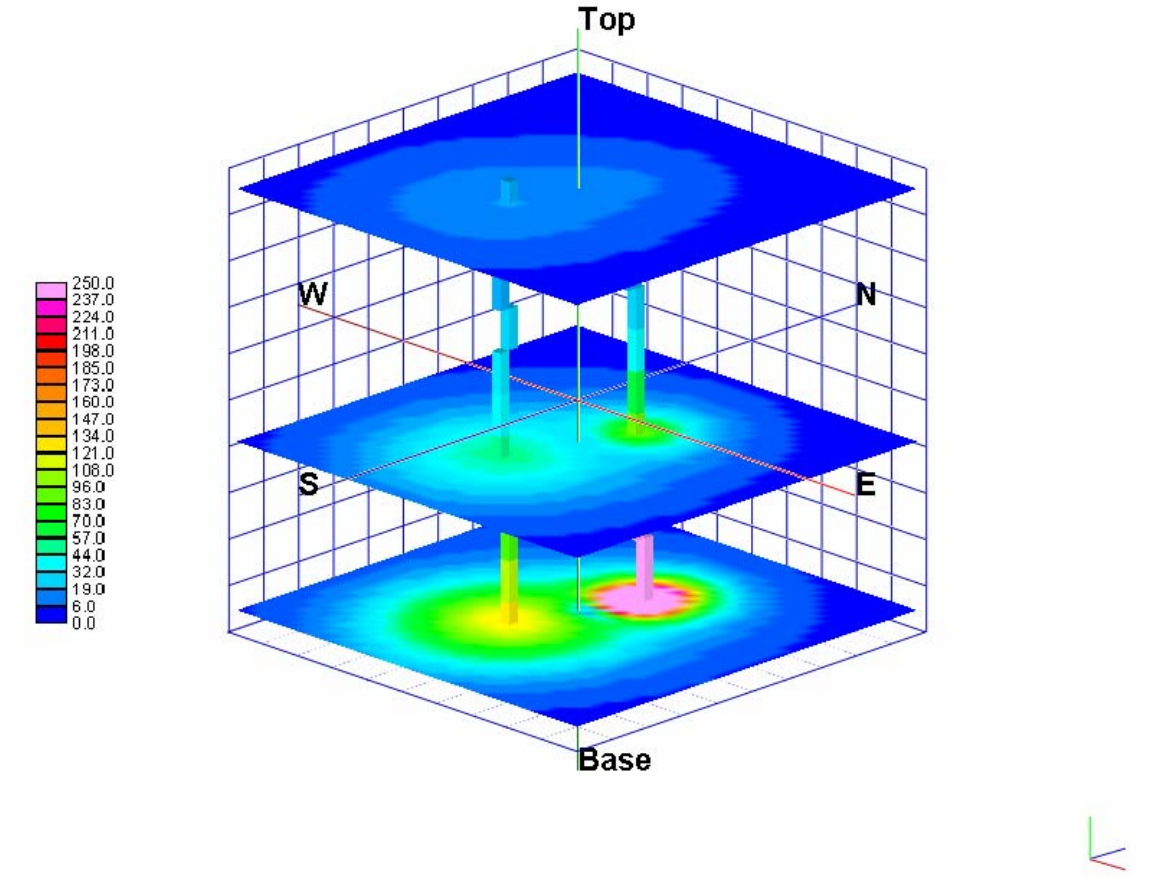

Figure 4: Illustration of Gradient String creation from 3D analytic signal of Model 3t (noise-free version of Model 3). Horizontal scale covers 2m x 2m, vertical scale has been stretched and features layers at 0.1m, 0.30m, and 0.55m. Analytic signal units in nT/m.

Detection

For the purposes of this study, detection was defined as the ability to reduce the data to a single point in (x, y) for each synthetic target. This basic level of detection was conducted using the Analytic Signal peaks for the 2D data, and the Gradient Strings for the 3D data. Both of these processes used the Analytic Signal data derived from the total field and output a point location in two dimensions that approximated the center of the target. A 10cm grid and lattice interval was used throughout. Although the accuracy of the Analytic Signal is limited to the grid cell size, it is by far the simplest and most reliable method of anomaly detection. Subsequent depth and size calculations (Euler, dipole inversion, etc) may use total field data but the basic detection is best achieved through Analytic Signal.

Detection calculations based on unfiltered data produced a number of false positive responses with amplitudes comparable to the primary peaks. A 3-point Hanning filter was therefore applied to the total field data prior to calculation of the Analytic Signal in order to smooth the interpolation errors. This eliminated all false positive responses from the detection list. Smoothing also produced one false negative response, missing the 60mm target in Model 9 (Table 6). In this case, the total field was flat enough that there was no Analytic Signal peak above 0.1nT/m. No other model had a peak less than 22nT/m.

Errors were measured as the horizontal offset from the detection point to the true target location. The 2D data showed errors that were slightly higher than the 3D data, and are largely the result of the 0.5m line spacing. All models, except for the fully-populated noise-free version of Model 3 (designated Model 3t), picked targets directly under the nominal survey line. This would indicate that the introduction of noise to the positioning and magnetic data surpassed the capability of the data to interpolate target locations between lines, even at this relatively tight spacing. The higher lateral spatial resolution in the 3D data was sufficient to overcome this problem.

Table 6: 2D Analytic Signal target locations. Average horizontal error 0.18m with one false negative.

	60mm	xy-error	20mm	xy-error
True	-0.1 -0.2		0.1 0.3	
Model 1	-0.0 -0.3	0.14	Not modeled	--
Model 2	-0.0 -0.3	0.14	Not modeled	--
Model 3	-0.0 -0.3	0.14	0.0 0.2	0.14
Model 3t	-0.1 -0.3	0.10	0.1 0.2	0.10
Model 4	-0.0 -0.3	0.14	Not modeled	--
Model 5	-0.0 -0.5	0.32	Not modeled	--
Model 6	-0.0 -0.3	0.14	Not modeled	--
Model 7	-0.0 -0.5	0.32	0.0 0.5	0.22
Model 8	-0.0 -0.3	0.14	0.0 0.2	0.14
Model 9	No detection	--	0.0 0.2	0.14

As described by Salem et al. (2002), there is a consistent shift of the AS peak to the magnetic South by an amount dependent upon the target depth and the field inclination. Without knowing the true depth, this cannot be calculated to adjust the AS peak locations. The average shift observed, however, is consistent with the typical range of UXO burial depths. As will be discussed later, the use of the depth estimates from other techniques can be used to refine the horizontal position estimate of the Analytic Signal.

From the filtered 3D data, Gradient Strings were calculated through the solid lattice of the Analytic Signal data. The most consistent results were obtained using a 10cm lattice size. Smaller intervals displayed sufficient noise and non-dipole effects to disconnect the Gradient Strings. The larger grid smoothed the noise and allowed the gradient to be calculated over a longer baseline. The 10cm baseline was generally longer than the wavelength of the non-dipole effects, thus effectively masking them. Strings less than 3 points in length, and having a maximum value <35nT/m were deleted as noise. In all cases, the remaining strings were continuously increasing in amplitude with proximity to the ground. Graphical results are shown in Appendix B-2.

Most of the models with the deeply buried 60mm target (2,3,6,7,8) had difficulty maintaining a continuous string throughout the entire data volume. Usually, strong gradient noise at an intermediate height split the strand into two discontinuous parts and had to be reconnected manually. Models 4, 5 and 9 had the same target depth but were able to maintain a continuous string. It may therefore be concluded that the Gradient String method has some limits regarding its ability to maintain a continuous string. These limits appear to be reached only at the maximum expected burial depth with the moderately high noise levels provided and can be solved with manual inspection. Further experimentation can be expected to remedy this minor flaw in automation.

Target location with this method was within one lattice point in every case but one. A smaller lattice size improved resolution but decreased string continuity. Final results for each model are presented in Table 7. Numbers in brackets are averages over the length of the string.

Table 7: Gradient String target locations. Average horizontal error 0.09m.

	60mm	xy-error	20mm	xy-error
True	-0.1 -0.2		0.1 0.3	
Model 1	-0.2 -0.2 (-0.12 -0.28)	0.1 (0.08)	Not modeled	--
Model 2	-0.1 -0.1 (-0.13 -0.28)	0.1 (0.09)	Not modeled	--
Model 3	-0.2 -0.2 (-0.20 -0.33)	0.1 (0.17)	0.0 0.3 (0.08 0.27)	0.1 (0.04)
Model 3t	-0.1 -0.3 (-0.10 -0.32)	0.1 (0.12)	0.1 0.3 (0.10 0.26)	0.0 (0.04)
Model 4	-0.2 -0.2 (-0.15 -0.32)	0.1 (0.13)	Not modeled	--
Model 5	-0.2 -0.2 (-0.18 -0.27)	0.1 (0.11)	Not modeled	--
Model 6	-0.1 -0.3 (-0.12 -0.22)	0.1 (0.02)	Not modeled	--
Model 7	-0.2 -0.2 (-0.18 -0.28)	0.1 (0.12)	0.0 0.3 (0.08 0.25)	0.1 (0.06)
Model 8	-0.1 -0.3 (-0.14 -0.30)	0.1 (0.11)	0.1 0.4 (0.10 0.32)	0.1 (0.02)
Model 9	-0.0 -0.4 (-0.12 -0.30)	0.4 (0.10)	0.1 0.3 (0.08 0.23)	0.0 (0.08)

In conclusion, the gradient string method successfully identified the number of targets in each model with an automated approach, and located them within one grid cell of the true location. A 10cm lattice was used to reduce the effects of strong gradients in the analytic signal at the lowest heights, which affected the final target location accuracy. Some models required visual inspection to connect a pair of disjointed gradient strings. It is worth noting that the inaccuracy in the target location is partially the result of the theoretical limitations of the analytic signal, as demonstrated by the noise-free data. This can be reduced by feedback using depth estimates from other analysis techniques.

Depth Estimation

Calculations for target depth were conducted using the ratio of analytic signals (after Salem et al., 2002). This technique uses the equation

$Z=4*AS_1/AS_2$

where AS_1 is the analytic signal of the total field and AS_2 is the analytic signal of the vertical gradient (a second order gradient, units of nT/m^2).

For the 2D data, these parameters were calculated using the Geosoft FFT algorithms from the gridded data. For the 3D data, they were calculated from the total field lattice data. The point of calculation is the peak of the AS_1. For the 3D data, this was taken at the average (x, y) location of the AS_1 peak, but at a height of 0.3m. This accounted for the boundary errors inherent in the calculation. For example, if the data at 0.1m were used, the vertical gradient calculations would be based on data outside the bounds of the collected data space. It also made the 2D and 3D results more comparable, since they were calculated at 0.3m and 0.35m respectively.

It was also found that the unfiltered total field data produced significantly better depth estimates than the filtered data. The application of a filter reduced and broadened the peak amplitudes thereby increasing the apparent depth of the target by approximately two times. Final depths and errors are presented in Tables 8 & 9. In most cases, the vertical accuracy is the same or better than the horizontal accuracy. The generally poorer performance of the 20mm depth estimates is attributed to the lower signal-noise ratio at the 0.3m calculation height. The use of a smaller lattice interval may have improved these results by reducing the effective calculation height thereby increasing the signal-noise ratio at the point of calculation. Instead, it was decided to maintain the 10cm interval from the Gradient String calculation for the sake of continuity and comparison to the 2D data.

The 2D depth estimates showed nearly five times greater error than the 3D data, averaging 0.29m depth error for the 60mm compared to 0.06m for the 3D data. In general, the depth of the 60mm is underestimated by one-half while the 20mm is overestimated. It is interesting to note that the noise-free data accurately returned the depth of the 60mm, but not the 20mm target.

The 3D data showed exceptionally good depth estimates for the 60mm, but did less well on the smaller 20mm target. Having calculated the depth, it would now be possible to refine the horizontal positions from the Gradient Strings and further improve the accuracy to approximately 5cm radially from the target center. This is an iterative feedback approach that should be explored in more detail in subsequent studies.

Table 8: 2D analytic signal depth estimates. Average depth error 0.21m.

	60mm	z-error	20mm	z-error
True	0.60*		0.05	
Model 1	0.10	0.10	Not modeled	--
Model 2	0.22	0.38	Not modeled	--
Model 3	0.29	0.31	0.04	0.01
Model 3t	0.63	0.03	0.13	0.08
Model 4	0.03	0.17	Not modeled	--
Model 5	0.22	0.38	Not modeled	--
Model 6	0.30	0.30	Not modeled	--
Model 7	0.23	0.37	0.02	0.03
Model 8	0.37	0.23	0.10	0.05
Model 9	0.21†	0.39	0.08	0.03

*depth of models 1 and 4 is 0.20m

†whereas no peak was detected for this target in the filtered data, the depths were calculated from unfiltered data which did show a peak at location (-0.0, -0.5)

Table 9: 3D analytic signal depth estimates. Average depth error 0.10m.

	60mm	z-error	20mm	z-error
True	0.60*		0.05	
Model 1	0.07	0.13	Not modeled	--
Model 2	0.56	0.04	Not modeled	--
Model 3	0.59	0.01	0.25	0.20
Model 3t	0.57	0.03	0.00	0.05
Model 4	0.23	0.03	Not modeled	--
Model 5	0.56	0.04	Not modeled	--
Model 6	0.58	0.02	Not modeled	--
Model 7	0.58	0.02	0.01	0.04
Model 8	0.48	0.12	0.27	0.23
Model 9	0.47	0.13	0.29	0.24

*depth of models 1 and 4 is 0.20m

Euler Deconvolution

The Euler equation

$$(x-x_0)\frac{\partial T}{\partial x}+(y-y_0)\frac{\partial T}{\partial y}+(z-z_0)\frac{\partial T}{\partial z}=N(F-T)$$

can be written as

$$\frac{\partial T}{\partial x}x_0+\frac{\partial T}{\partial y}y_0+\frac{\partial T}{\partial z}z_0=\frac{\partial T}{\partial x}x+\frac{\partial T}{\partial y}y+\frac{\partial T}{\partial z}z-N(F-T)$$

or

$$\left[\frac{\partial T}{\partial x}\frac{\partial T}{\partial y}\frac{\partial T}{\partial z}\right]*\begin{bmatrix}x_0\\y_0\\z_0\end{bmatrix}=[B]$$

where (x, y, z) is the sample location, (x_0, y_0, z_0) is the target location, T is the measured total field around the anomaly, F is the background magnetic field, and N is an index number associated with the dimensionality of the target.

A window of points around the sample location produces a set of equations of this form which can be solved as a series of linear equations in the form *AX=B*. The size of the window is generally determined by the spatial extent of the anomaly in order to improve the signal content of the least squares equations. This window should be large enough to encompass a reasonable portion of the anomaly, but small enough that it does not include signals from overlapping anomalies. For these tests, a simple 3x3 or 3x3x3 window was used to produce 9 or 27 equations for the 2D and 3D respectively. The index parameter N was set to 2.8 to achieve the best results in both 2D and 3D processing. As with the analytic signal depth calculations, better results were obtained using the unfiltered rather that the filtered total field data.

As with the analytic signal depth calculation, the Euler calculation was run at the average (x, y) location specified by the gradient calculation and at a height of 0.3m. This allowed a buffer zone for the vertical gradient calculation and conveniently corresponded to the height of the 2D calculation for closer comparison.

Euler deconvolution of the 2D data was conducted using the Geosoft grid routines, since the intention was to compare the 3D method against current industry standards. These are more sophisticated in their data conditioning than was possible for the 3D data in this project. This condition notwithstanding, the 3D technique again produced average depth errors approximately five times smaller than the 2D data (0.03m and 0.14m respectively for the 60mm target). This is roughly half that of the AS ratio technique described above.

Table 10: 2D Euler depth estimates. Average depth error 0.24m.

	60mm	z-error	20mm	z-error
True	0.60*		0.05	
Model 1	0.23‡	0.03	Not modeled	--
Model 2	0.46	0.14	Not modeled	--
Model 3	0.45	0.15	0.56	0.51
Model 3t	0.57	0.03	0.24	0.19
Model 4	0.23‡	0.03	Not modeled	--
Model 5	0.58	0.02	Not modeled	--
Model 6	0.26	0.34	Not modeled	--
Model 7	0.15	0.45	0.43	0.38
Model 8	0.48	0.12	0.53	0.48
Model 9	0.49†	0.11	0.47	0.42

*depth of models 1 and 4 is 0.20m
‡required manual adjustment of window size
†whereas no peak was detected for this target in the filtered data, the depths were calculated from unfiltered data which did show a peak at location (-0.0, -0.5)

Table 11: 3D Euler depth estimates. Average depth error 0.06m.

	60mm	z-error	20mm	z-error
True	0.60*		0.05	
Model 1	0.19	0.01	Not modeled	--
Model 2	0.61	0.01	Not modeled	--
Model 3	0.64	0.04	0.19	0.14
Model 3t	0.61	0.01	0.03	0.02
Model 4	0.24	0.04	Not modeled	--
Model 5	0.56	0.04	Not modeled	--
Model 6	0.57	0.03	Not modeled	--
Model 7	0.58	0.02	0.07	0.04
Model 8	0.63	0.03	0.28	0.23
Model 9	0.62	0.02	0.20	0.15

*depth of models 1 and 4 is 0.20m

Dipole Inversion

The first inversion for parameters other than depth was conducted using the MTADS-DAS dipole inversion code. This code operates on a set of (x, y, z, mag) data that may or may not be broken into lines. As such it is well suited to this project. It uses its own gridding algorithm to create a presentation data set that is used to manually isolate anomalies for inversion, but it operates on the original point data set. It is therefore independent of the 2D or 3D gridding process and makes full use of 3D positioning data, but does not benefit from the advantages of down-line, cross-line, or vertical smoothing through interpolation or filtering.

This code operates on one anomaly at a time. Where signatures overlap, data must be manually divided between anomalies based on position. For this project, where the detection algorithms identified multiple targets (Models 3, 7, 8, 9) the dividing line was drawn from (x, y) coordinates (-1, 1)-(0, 0)-(1, 0). Figure 5 illustrates the demarcation line used for segmentation. This effectively bisected the total field peaks, but the troughs were too closely overlapped to separate and were therefore attributed to the more northerly 20mm target. This segmentation process made it difficult for the program to invert the data in several instances. For this reason, where multiple anomalies were detected, they were also inverted as a single "combined" anomaly for comparison. This is comparable to the UXAnalyze inversion results discussed below.

The most obvious difference between the 2D and 3D data was the failure of the code to invert the 2D data for any of the 20mm targets and half of the 60mm targets. The DAS code inverted the 3D data for all targets except for Model 6. There were also some irregularities in the fit coefficients that have not been explained. For example, the noise-free data in the 2D Model 3t were inverted for the combined anomalies with a better fit than the 60mm alone. The 2D Model 7 was able to invert the single 60mm, but did not have sufficient signal to invert the combined anomalies. The 3D Model 1 was inverted for the 60mm for position with reasonable accuracy, but output a fit coefficient of 0.

The poor performance is attributed primarily to data segmentation problems, but there were also difficulties with the IDL-based version of the MTADS-DAS dipole inversion code. It is more restrictive than the UXAnalyze code currently under development by AETC and Geosoft which uses the same inversion engine. It was specifically designed to process and analyze MTADS survey data, and as a result many parameters are hardwired or defaulted to MTADS specifications. This made it extremely difficult to implement for this 3D SEED Project. AETC generously contributed the time and effort to invert these Models using their UXAnalyze code while still under development. The results are shown in Appendix B-3. This resolved more of the 2D data sets than the IDL-based code used here, but where both codes reached a solution the accuracy of the target positioning was comparable. Also, if the anomalies are treated as "combined" targets, the number of inversion failures is the same for both methods.

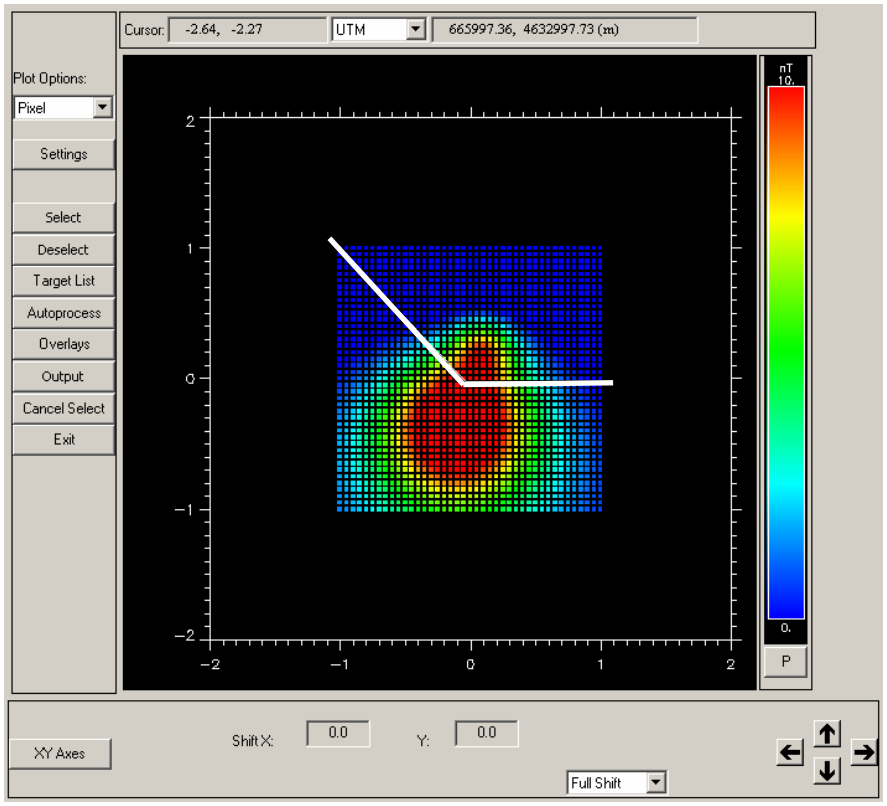

Figure 5: Screen capture showing demarcation line used to segment data into separate anomalies where multiple anomalies were detected.

Table 12: 2D data fit coefficients.

	Fit (60mm)	Fit (20mm)	Fit (comb)
Model 1	0.976	Not modeled	--
Model 2	0.973	Not modeled	--
Model 3	Not strong enough	Not strong enough	0.940
Model 3t	0.890	Not strong enough	0.908
Model 4	0.957	Not modeled	--
Model 5	Not strong enough	Not modeled	--
Model 6	0.982	Not modeled	--
Model 7	0.949	Not strong enough	Not strong enough
Model 8	Not strong enough	Not strong enough	0.951
Model 9	Not strong enough	Not strong enough	0.846

Table 13: 2D dipole inversion results. Average location error 0.12m with nine failures.

	60mm				Error	20mm				Error
	X	Y	Z	size		X	Y	Z	size	
True	-0.10	-0.20	0.60*	0.10		0.10	0.30	0.05	0.03	
Model 1	-0.18	-0.18	0.16	0.05	0.09	Not modeled				
Model 2	-0.08	-0.13	0.49	0.04	0.13	Not modeled				
Model 3	--				--	--				--
Model 3t	-0.20	-0.13	0.31	0.03	0.32	--				--
Model 4	-0.11	-0.18	0.20	0.05	0.02	Not modeled				
Model 5	--				--	Not modeled				
Model 6	-0.10	-0.11	0.49	0.06	0.14	Not modeled				
Model 7	-0.22	-0.20	0.45	0.04	0.19	--				--
Model 8	--				--	--				--
Model 9	--				--	--				--

*depth of models 1 and 4 is 0.20m

Table 14: 3D data fit coefficient.

	Fit (60mm)	Fit (20mm)	Fit (comb)
Model 1	0.000	Not modeled	--
Model 2	0.791	Not modeled	--
Model 3	0.948	0.693	0.299
Model 3t	0.913	0.004	0.001
Model 4	0.823	Not modeled	--
Model 5	0.494	Not modeled	--
Model 6	Too much change	Not modeled	--
Model 7	0.421	0.658	λ optimize prob
Model 8	0.922	0.635	0.603
Model 9	0.773	0.166	0.513

Table 15: 3D dipole inversion results. Average location error 0.28m with one failure.

	60mm				Error	20mm				Error
	X	Y	Z	size		X	Y	Z	size	
True	-0.10	-0.20	0.60*	0.10		0.10	0.30	0.05	0.03	
Model 1	-0.05	-0.28	-0.12	0.00	0.33	Not modeled				
Model 2	-0.26	-0.28	0.35	0.03	0.31	Not modeled				
Model 3	-0.28	-0.20	0.43	0.04	0.25	0.03	0.16	0.04	0.01	0.16
Model 3t	-0.17	-0.15	0.46	0.04	0.16	0.10	0.37	-0.10	0.00	0.17
Model 4	-0.17	-0.24	0.14	0.03	0.10	Not modeled				
Model 5	-0.35	-0.22	0.18	0.02	0.49	Not modeled				
Model 6	--				--	Not modeled				
Model 7	-0.25	-0.33	0.16	0.01	0.48	0.02	0.34	-0.01	0.01	0.11
Model 8	+0.05	-0.32	0.28	0.04	0.37	0.03	0.16	0.04	0.01	0.16
Model 9	-0.15	-0.19	0.19	0.03	0.41	0.07	0.23	-0.16	0.01	0.22

*depth of models 1 and 4 is 0.20m

The positions reported by the DAS inversion results were comparable in (x, y) accuracy to the analytic signal and Gradient String results. The largest contribution to radial position error came from the depth estimates, which were underestimated in all cases. Several depths were calculated as above the ground surface. The 60mm depth estimates from the 3D data set showed greater average error than the 2D data (0.25m and 0.12m respectively). In general, the dipole inversion of the 2D models generated better depth estimates than the 2D Euler and analytic signal ratio methods, but the dipole inversion of 3D models was 4-10 times worse. There were so few successful 2D models however that this is a doubtful statistic.

Although inclination, azimuth and moment information were also generated by this program, these parameters are linked to remanence rather than target orientation. Since this was not a variable in the target models, the expectation is that these parameters should align with the background field within +/- 30°. The observed results were generally consistent with this expectation, although results may be significantly distorted by the segmentation process, which separated much of the negative lobe of the 60mm target from the rest of the signature.

There are at least three reasons for the generally poor performance of this technique. The first is the requirement for segmentation of the data. As has been stated above, this had the effect of separating the negative and positive peaks in some of the strongest anomalies. The second was the possible mis-match in attempting to fit a point dipole to an ellipsoidal model. This was reflected in the poorer results of Models 4-9. Inversion for multiple targets, and for shapes other than a dipole is presented in the next section. A third problem was that the inclination, declination and background field strength were hardwired to the IGRF lookup table at the latitude and longitude provided. Although the inclination and declination could be adequately represented, the field strength of 50,000nT could not be. This information is not provided by the program, but it is estimated that the field strength used by the software was approximately 55,000nT. The program would therefore expect much stronger anomalies than the input data presented, and would consequently underestimate the depths of the calculated dipoles.

Solid-body Inversion

Inversion of the data for shaped bodies (spheres and ellipsoids) was conducted using the ModelVision software from Encom. This program was used to invert for spheres and ellipsoids from a pre-set starting model. The vendor recommends a more finely tuned starting model through manual manipulation of target parameters for each data set, but this was ignored in order to assure uniformity for testing purposes. This software had the advantage of inverting for multiple targets without the need for segmentation. The disadvantage is that the fit coefficient is an aggregate over the entire data set rather than being target specific.

The 2D and 3D data sets were inverted once for spheres, and then again for ellipsoids. For spheres, starting models included one or two targets (as determined by the previous detection procedure) with locations of (-0.1, -0.3, 0.5) and (0.1, 0.3, 0.5) with a radius of 0.1m for both. Ellipsoid starting models were centered on the same locations, but had axes lengths of (major 0.05, semi-major 0.02, minor 0.02) and orientations of (azimuth 90°, plunge 0°, rotation 0°). Maximum ranges for each variable were set to allow sufficient change in the model, and a maximum of 20 iterations were allowed.

Each spherical inversion included four free inversion parameters: X, Y, Z, radius. Each ellipsoidal inversion included nine free inversion parameters: X, Y, Z, axis-A, axis-B, axis-C, azimuth, plunge, rotation. Susceptibility was fixed at 3 SI for all models. Models with two targets (Models 3, 7, 8, 9) doubled the number of free parameters. RMS error for multiple target models is an aggregate fit over the entire data set. It should be noted here that Models 1-3 were synthesized from spheres, whereas Models 4-9 were synthesized from ellipsoids.

Tables 16-19 show the 2D inversion results, while Tables 20-23 show the comparable 3D inversion results. Tables 16 and 20 show the general fit coefficients. Tables 17 and 21 show the inversion results (positions) when testing for spherical models. Tables 18/19 and 22/23 show the inversion results (positions and dimensions) when testing for ellipsoidal models.

Table 16: 2D RMS error when fitting a sphere or ellipsoid to the data.

	RMS error (sph)	RMS error (ellip)
Model 1	1.25	1.23
Model 2	1.29	1.28
Model 3	1.25	1.47
Model 3t	0.01	0.03
Model 4	5.52	5.46
Model 5	8.30	8.23
Model 6	2.49	2.50
Model 7	7.50	7.45
Model 8	2.40	2.06
Model 9	3.83	3.80

Table 17: 2D Spherical inversion results (fitting a spherical model). Average location error 0.14m.

	60mm				Error	20mm				Error
	X	Y	Z	rad		X	Y	Z	rad	
True	-0.10	-0.20	0.60*	0.05		0.10	0.30	0.05	0.02	
Model 1	-0.10	-0.20	0.20	0.05	0.00	Not modeled				--
Model 2	-0.10	-0.20	0.60	0.05	0.00	Not modeled				--
Model 3	-0.10	-0.20	0.60	0.05	0.00	-0.07	0.30	0.07	0.02	0.03
Model 3t	-0.10	-0.20	0.60	0.05	0.00	0.10	0.30	0.05	0.02	0.00
Model 4	-0.11	-0.38	0.19	0.05	0.18	Not modeled				--
Model 5	-0.08	-0.50	0.56	0.04	0.30	Not modeled				--
Model 6	-0.11	-0.10	0.61	0.07	0.10	Not modeled				--
Model 7	-0.11	-0.50	0.57	0.04	0.30	0.21	0.10	0.00	0.02	0.23
Model 8	-0.11	-0.16	0.59	0.06	0.04	-0.02	0.34	0.31	0.04	0.28
Model 9	-0.23	-0.10	0.59	0.06	0.17	-0.08	0.28	0.18	0.03	0.22

*depth of models 1 and 4 is 0.20m

Table 18: 2D Ellipsoid inversion results (positions). Average location error 0.17m.

	60mm			Error	20mm			Error
	X	Y	Z		X	Y	Z	
True	-0.10	-0.20	0.60*		0.10	0.30	0.05	
Model 1	-0.10	-0.20	0.20	0.00	Not modeled			--
Model 2	-0.10	-0.20	0.61	0.01	Not modeled			--
Model 3	-0.10	-0.23	0.61	0.03	0.01	0.27	0.18	0.16
Model 3t	-0.10	-0.20	0.61	0.01	0.10	0.30	0.05	0.00
Model 4	-0.10	-0.38	0.21	0.14	Not modeled			--
Model 5	-0.09	-0.49	0.55	0.29	Not modeled			--
Model 6	-0.11	-0.10	0.62	0.10	Not modeled			--
Model 7	-0.10	-0.50	0.57	0.30	0.21	0.10	0.00	0.23
Model 8	-0.12	-0.17	0.58	0.04	-0.03	0.32	0.43	0.40
Model 9	-0.24	-0.10	0.58	0.17	-0.09	0.29	0.21	0.25

*depth of models 1 and 4 is 0.20m

Table 19: 2D Ellipsoid inversion results (dimensions)

	60mm			Error	20mm			Error
	A	B	C	%Vol	A	B	C	%Vol
True	0.051	0.051	0.051		0.017	0.017	0.017	
Model 1	0.10	0.04	0.04	1	Not modeled			--
Model 2	0.15	0.04	0.03	2	Not modeled			--
Model 3	0.10	0.05	0.03	3	0.04	0.02	0.01	104
Model 3t	0.10	0.05	0.03	0	0.03	0.02	0.02	1
True	0.100	0.030	0.030		0.035	0.010	0.010	
Model 4	0.14	0.03	0.02	7	Not modeled			--
Model 5	0.13	0.04	0.02	6	Not modeled			--
Model 6	0.17	0.07	0.03	256	Not modeled			--
Model 7	0.12	0.05	0.02	1	0.05	0.01	0.01	42
Model 8	0.21	0.05	0.02	170	0.36	0.01	0.01	1925
Model 9	0.11	0.06	0.03	162	0.13	0.01	0.01	613

The most notable result of the 2D inversion was that the spherical targets (Models 1-3) were better resolved than the ellipsoids. This was seen most clearly in the RMS errors. It should also be noted that the z-error was no longer the dominant position error. Horizontal errors in target location, especially for the ellipsoid targets, were larger than those previously determined by the gradient strings. The location error presented here is the total offset including both horizontal and vertical components.

The high errors in Models 4-9 were attributed to the differences in ellipsoid modeling techniques between MAGMOD and ModelVision. Codes for spherical models compare exceptionally well (Models 1-3), but as has already been stated, these codes produce significantly different results for ellipsoidal bodies. These effects can only be attributed to the difference in approach to modeling between MAGMOD and ModelVision. This is further explored in the noise-free Model 9t results presented below.

Ellipsoid inversion results for target orientation were calculated but were not explored. The ModelVision software inverts for full ellipsoids, and not cylindrical ellipsoids – it does not allow the variation in the lesser axes to be tied together. As a result, inversion targets may appear as disks or ovals rather than round cylinders, which made orientation comparisons difficult. This, added to the large errors in the target dimensions, made the orientation analysis irrelevant.

Table 20: 3D RMS error when fitting a sphere(s) or ellipsoid(s) to the data.

	RMS error (sph)	RMS error (ellip)
Model 1	1.29	1.12
Model 2	1.29	1.29
Model 3	0.74	0.71
Model 3t	0.01	0.02
Model 4	3.85	3.94
Model 5	6.23	6.26
Model 6	1.65	1.75
Model 7	3.52	3.51
Model 8	1.44	6.55
Model 9	1.25	1.27
Model 9t	1.09	1.41

Table 21: 3D Spherical inversion results (fitting a spherical model). Average location error 0.09m.

	60mm				Error	20mm				Error
	X	Y	Z	rad		X	Y	Z	rad	
True	-0.10	-0.20	0.60*	0.05		0.10	0.30	0.05	0.02	
Model 1	-0.10	-0.21	0.21	0.05	0.01	Not modeled				--
Model 2	-0.10	-0.20	0.60	0.05	0.00	Not modeled				--
Model 3	-0.10	-0.20	0.60	0.05	0.01	0.11	0.30	0.04	0.02	0.01
Model 3t	-0.10	-0.20	0.60	0.05	0.00	0.10	0.30	0.05	0.02	0.00
Model 4	-0.07	-0.32	0.17	0.04	0.13	Not modeled				--
Model 5	-0.07	-0.47	0.50	0.04	0.29	Not modeled				--
Model 6	-0.10	-0.13	0.62	0.07	0.08	Not modeled				--
Model 7	-0.08	-0.47	0.56	0.05	0.27	0.12	0.22	0.03	0.01	0.08
Model 8	-0.11	-0.14	0.63	0.07	0.07	0.10	0.33	0.05	0.02	0.03
Model 9	-0.18	-0.10	0.60	0.06	0.13	0.04	0.29	0.06	0.02	0.06
Model 9t	-0.19	-0.10	0.60	0.06	0.13	0.04	0.29	0.05	0.02	0.06

*depth of models 1 and 4 is 0.20m

Table 22: 3D Ellipsoid inversion results (positions). Average location error 0.18m.

	60mm			Error	20mm			Error
	X	Y	Z		X	Y	Z	
True	-0.10	-0.20	0.60*		0.10	0.30	0.05	
Model 1	-0.10	-0.20	0.19	0.01	Not modeled			--
Model 2	-0.10	-0.20	0.62	0.02	Not modeled			--
Model 3	-0.10	-0.19	0.60	0.01	0.10	0.30	0.05	0.01
Model 3t	-0.10	-0.20	0.60	0.00	0.10	0.30	0.05	0.00
Model 4	-0.08	-0.35	0.22	0.15	Not modeled			--
Model 5	-0.06	-0.46	0.49	0.29	Not modeled			--
Model 6	-0.10	-0.12	0.63	0.09	Not modeled			--
Model 7	-0.08	-0.46	0.54	0.26	0.12	0.22	0.03	0.09
Model 8	-0.20	-0.33	0.02	0.60	-0.05	0.10	0.64	0.64
Model 9	-0.20	-0.10	0.62	0.14	0.03	0.28	0.08	0.08
Model 9t	-0.20	-0.10	0.65	0.15	0.04	0.29	0.00	0.08

*depth of models 1 and 4 is 0.20m

Table 23: 3D Ellipsoid inversion results (dimensions).

	60mm			Error	20mm			Error
	A	B	C	%Vol	A	B	C	%Vol
True	0.051	0.051	0.051		0.017	0.017	0.017	
Model 1	0.14	0.08	0.01	2	Not modeled			--
Model 2	0.13	0.04	0.03	4	Not modeled			--
Model 3	0.11	0.04	0.03	1	0.04	0.01	0.01	7
Model 3t	0.07	0.05	0.04	1	0.02	0.02	0.02	0
True	0.100	0.030	0.030		0.035	0.010	0.010	
Model 4	0.10	0.04	0.03	37	Not modeled			--
Model 5	0.09	0.06	0.02	351	Not modeled			--
Model 6	0.21	0.05	0.03	273	Not modeled			--
Model 7	0.08	0.04	0.03	12	0.02	0.01	0.01	21
Model 8	0.01	0.01	0.01	99	0.14	0.05	0.05	8935
Model 9	0.12	0.05	0.05	206	0.05	0.02	0.01	191
Model 9t	0.13	0.06	0.04	253	0.05	0.01	0.01	61

The best results were obtained using the 3D data and spherical inversion models. The average location error and size (radius) error were approximately half those of the 2D data with spherical models. The ellipsoid inversion required a greater number of free parameters, which contributed slightly to the higher errors (Table 21 vs 22). The more significant problem is believed to be the mis-match of ellipsoid modeling techniques. Model 9t is a fully-populated noise-free version of Model 9. Comparing Models 9t and 3t in Tables 20-23 shows that even with perfect data, there is a problem with matching ellipsoidal models that is not present for spherical models.

It was also found that the raw (uninterpolated) data points produced significantly better results than the gridded results. Comparable tables for these cases are presented in Appendix B-4. The interpolation had the most detrimental effect on the 3D data. The original 300 data points were interpolated to approximately 2,000 points, many of which were beyond the range of the original 30 second data collection window. On the other hand, the 2D data were interpolated from 205 to 400 points, all of which were within the outer bounds of the data simulation. There was also a difference in the efficacy of the gridding algorithm. The 2D Geosoft minimum curvature routine is well known to produce good results for potential fields. The performance of the Rockware algorithm is relatively untested. A comparison between the two was conducted and the Rockware gridding produced location errors between 3-5times higher than the Geosoft grids (see Appendix B-4).

Conclusions

In all cases, the 3D acquisition and processing methodology has been shown to be better than the standard 2D method for detection and location of closely spaced targets. Applying 1cm of positional noise and 0.1nT of magnetometer noise to the theoretical models, the best techniques averaged location errors of 0.09m and depth errors of 0.06m. It is estimated that feedback and cooperative inversion techniques can further reduce this to a radial error of 0.05m.

The Gradient String approach detected all of the targets and located them in (x, y) more accurately than the 2D analytic signal peaks. Depth estimates using the analytic signal ratio and Euler deconvolution were five times more accurate using the 3D data. The dipole inversion code suffered from inadequate signal strength and segmentation problems. This caused the location accuracies to fall below those obtained from the simpler methods. The 3D results, however, showed significantly fewer problems than the 2D data. The solid-body inversion ran more smoothly than the dipole inversion, but highlighted a potential mis-match in theoretical models between MAGMOD and ModelVision. The best results were produced using the 3D data and spherical models, where target locations were twice as accurate as the comparable 2D data sets.

It was also shown that the Rockware 3D gridding algorithm was not as well-suited to potential fields as the Geosoft approach. Comparison tests showed an increase in location error of three times. The 3D results in the Detection, AS depth and Euler depth analysis sections relied on the Rockware algorithm and were as good or better than the 2D data. This indicates that the performance enhancement of the 3D method is still being under reported.

This study did not examine the potential benefits of the 3D methodology to techniques for discriminating between UXO and non-UXO. This was due to the limitations of simulating non-UXO signatures. Estimation of target size however, a key element in clutter discrimination, was quite accurately determined for the spherical target sets.

Transition

This project has found considerable advantage to a 3D data collection and processing methodology. Transition efforts should focus on (a) added benefits than can be obtained by refinement and cooperative use of the techniques explored here (b) extending the study to include the benefits of 3D methods to discrimination of UXO from non-UXO, (c) introduction of commercial software and hardware vendors to improve and streamline the techniques, and (d) research into extension of these techniques to electromagnetic data. The ultimate objective should be to combine these techniques into a hand-held sensor platform so that mapping, detection and discrimination can be conducted in a single pass, thereby significantly reducing field costs.

Recommendations

There are several additional benefits to 3D processing that this study did not encompass. It did not attempt to implement any sort of feedback from one technique to another. For example, Euler depth estimates can be used to refine the horizontal location and then position values can be locked to reduce the number of free parameters in the inversion process. This would free up variables to improve the resolution of target shape and size. Similarly, iterative steps through the inversion to fix parameters in sequence (invert for location, invert for size, invert for shape, invert for orientation) is another process that may prove useful. The use of irregularly shaped lattice nodes (e.g 10cm x 10cm x 5cm) may offer additional benefits by reducing the buffer zone around the 3D lattice so that depth calculations can be made a lower heights with better signal-noise ratios.

This study should be extended to include the benefits of 3D methodology to current discrimination techniques (UXO vs non-UXO), such as those reported by University of British Columbia.

Beyond studies into the benefits of 3D data are tests of the practical application of the method. In conjunction with the collection of field data for the verification phase of the project, several points relating to software need to be addressed. 3D gridding routines need to be improved to the same level of reliability as the existing 2D routines. The interpolation algorithms in the existing 3D software were shown to produce locations errors roughly twice that of the 2D software. The extrapolation of data beyond the 3D "cloud" in order to fill the 1x1x0.5m volume highlighted these problems. It also indicates that additional care must be taken to collect data throughout the data space in order to maximize the utility of the 3D method.

The discrepancies between ellipsoid modeling routines needs to be resolved by examination of field or test-stand data. Cylindrical ellipsoid inversion routines must also be developed to overcome some of the software shortcomings discovered in this study. Ultimately, a real-time system will allow technicians to digitally map, discriminate and excavate a site in a single mobilization without repeated referral to a processing geophysicist. This would considerably reduce the time and effort required for UXO investigations. Development of any new software routines should therefore be under a single processing package capable of hand-held operation for the field staff, and desktop operation for QA geophysicists. This will also facilitate a broader distribution and streamline processing during the initial commercialization period. All of these tasks will require the involvement of relevant commercial software and hardware vendors.

The final task is to extend the scope of this study to include electromagnetic (EM) sensors. This will be sensor specific, probably dealing with the Geonics EM-61HH and the Geophex Gem-300. Research into inversion routines and the effects of coil orientation are already underway through SERDP/ESTCP and should be leveraged with the 3D methodology proven here. This will allow stand-alone EM techniques to be applied in noisy magnetic environments, and will form the basis for future joint 3D inversion of mag/EM data.

Appendix A1
Abstract – SERDP/ESTCP Partners in Technology Conference
December 2003

3D visualization of 3D magnetic data

T. Jeffrey Gamey
Oak Ridge National Laboratory, Oak Ridge, TN 37831-6038
(865) 574-6316 gameytj@ornl.gov

W.E.Doll, A.M.Emond, L.P.Beard

Magnetic modeling and inversion routines that take advantage of recorded altitude or Z values have followed the development of improved 3-dimensional positioning technologies. Usually, this technique involves recording ground clearance (or ellipsoid height in the case of DGPS systems) during the course of collecting routine profile data. Technologies include laser or radar altimeters for airborne techniques, DGPS heights, or laser and/or ultra-sonic positioning for ground systems.

Visualization of the data, however, maintains a 2D approach using either profiles or grids. Tools such as 3D surface maps are often used to project gridded data into a simulated 3D surface, but this is still a representation of 2D data.

A simple approach to collecting actual 3D data is recording multiple sensors at different heights during a single profile, such as vertical magnetic and electromagnetic gradients (Geometrics G-858 and Geonics EM-61). The utility of this has been proven in many studies. Many inversion routines rely on gradients, either measured or calculated, for depth determination and ordnance discrimination.

Alternatively 3D data may be acquired with a single sensor, accurately positioned, and moved around in a volume of space above the target area in re-acquisition mode. This SERDP funded seed project investigates this approach collection of data in a 3D volume to determine the resulting improvement in inversion capabilities.

Appendix A2
Poster – SERDP/ESTCP Partners in Technology Conference
December 2003

3D Geophysical Data C
for Unexploded Ordnanc

SERDP - SEED 1357 Oak

P.I. T. Jeffrey Gamey

Traditional Approach

The traditional approach to geophysical mapping for UXO has been to collect data along transects at a nominal height (1D) and present the results on a grid (2D). Single profiles show the data with great resolution and fidelity since they are not subject to gridding interpolation, but are difficult to interpret. The most obvious short-fall being the lack of information to either side of a profile anomaly. By presenting the data with reference to neighboring points on either side, the 2D perspective makes it much simpler to pick out discrete targets from broader anomalies. This simplification is an important part of the interpretation process.

Data processing techniques based on 2D data sets also have significant advantages over their 1D counterparts. There are many advantages to analyzing data that have been spatially correlated in two dimensions. Spatial filters, for example, can remove uncorrelated noise better. FFT processes, such as analytic signal, can also enhance features more reliably and with fewer assumptions when applied to grids than to profiles.

The disadvantage of 2D presentations is that it assumes that all of the data were collected on a common plane, although this is not usually true. Whenever a data point is collected at different height than the adjacent data points, it creates an artifact in the grid. Depending on the severity and distribution of these artifacts, any interpretation based on the gridded data will be more or less flawed.

As a result, many additional 2D data processing steps must be incorporated into the work flow in order to correct for the "common plane" assumption and produce a viable interpretation. In addition to the gridding process, which generally desamples data down-line and interpolates data between lines, filtering or deletion of data points must be applied to produce a satisfactory grid. In some cases, these additional steps may reduce data quality more than they enhance it.

State-of-the-Art Approach

The impact of height on gridding is not a new phenomenon. The effects of height in both magnetic and electromagnetic data are well documented. Numerous studies have been done to either limit, quantify or correct these effects. Techniques include wheeled carts to control height, altimeters and other positioning systems to measure height, and various upward or downward continuation algorithms to correct readings to a nominal height.

Advances in positioning systems and computing capabilities now allow collection and storage of geophysical, position and height data in a single database. Software packages for data inversion are taking advantage of increased power and are inverting data with height information. The MTADS inversion code and the commercially available ModelVision from Encom are two examples.

Although the technology has incorporated several aspects of 3D data, all of these are attempts to solve the problem of continually forcing 3D data into a 2D format. To date, the best inversion solutions ignore the 2D format altogether and work entirely with profile data. Although this work flow avoids many of the problems, it does not take advantage of any of the positive elements of 2D processing such as noise reduction or FFT algorithms. It makes use of only one dimension of spatial correlation (down-line). Only filters and processes that can be applied to profiles are used.

Notes on Dimensions

For descriptive clarity, a distinction must be made between the number of dimensions of position data collected during a survey and the number of dimensions of the presentation format. The traditional survey measures two dimensions of position data (X,Y) and presents the geophysical results as 1D profiles (a projection against a single axis of time or horizontal position, with the data as the second axis), 2D grids/contours (a projection against two horizontal position axes using color to represent the data axis), or a 3D surfaces /curves /nets (a projection against two horizontal position axes, using the illusion of a third vertical axis to represent the data). Data may also be presented as profiles along survey lines plotted on 2D maps, which are similar to the 2D grids.

Even with the recording of 3D positional data (X,Y and height), none of the aforementioned presentation techniques display or accommodate the additional height information. This is a limitation of all two-dimensional media (paper and screens). It is extremely difficult to represent 3D positions on a 2D screen or map. This does not include a dimension for the geophysical data itself. Even 3D nets are technically 2D presentations using illusions of perspective and shading to appear 3D. Occasionally, a 3D presentation is rotated to enhance the illusion, thus adding time as an added dimension to a 2D image. The 3D holographic presentations of science fiction would still require rotation of the image or movement of the observer in order to fully interpret it, just as any solid object would.

Multi-dimensional data sets therefore require that we either reduce the information to it's most relevant form for presentation, or else to think and to present data in terms of matrices and functions with n-dependent variables. This applies equally to 3D positioned data from a single sensor, multiple responses from a single sensor (ie EM time gates), or integrated multi-sensor data sets. Although this makes them ideal candidates for computer analysis, which is based almost entirely on linear matrices, the human factor is still required for control and judgement.

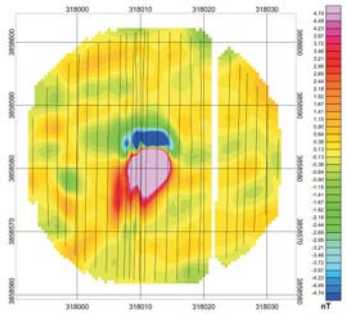

Gridded magnetic data distorted by variations in altitude

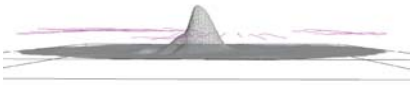

Sensor positions shown as pink lines in a 3D presentation over a surface plot of the gridded magnetic data from the sample above.

Research into control and measurement of sensor position, height and orientation.
Photos courtesy of Shaw Environmental & Infrastructure

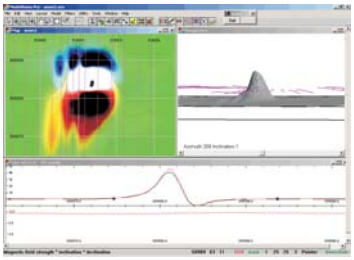

1D (profile), 2D (grid) and "3D" (surface) presentations of the magnetic anomaly from above.
Screen shot from ModelVision by Encom

3D Re-ac

Background

This project follows from the following points:

- traditional survey techniques lose much of the benefit of 2D data processing technic require additional processing to remove or diminish the effects of having forced 3 plane
- state-of-the-art processing techniques that incorporate 3D positional information benefit of 2D data processing by ignoring the potential of spatially correlating the straight to numerical inversion after 1D processing
- data collected with 3D positional information offers the potential of spatially co vertically as well as horizontally

This last point presents particularly interesting possibilities. It deals with the problem changes in height by handling 3D data in three-dimensions, as well as providing opport the state-of-the-art inversion techniques by incorporating the benefits of spatial c inversion.

Approach

For developmental purposes, the approach to creating and analyzing these new tech the data reacquisition process. After an anomaly of interest is selected, reacquisition with a similar instrument using a 3D positioning system. The effect is to collect a "clo over a suspect anomaly.

The "cloud" of data are then interpolated into a 3D lattice (grid) for processing. T opportunity for examination of 3D analogs of 2D processing techniques. Several diff techniques are available. Two of the most accessible software packages for this purpo RockWorks. Matlab, however, only offers linear and nearest-point lattice routines. eight methods, six of which are suitable for this application.

3D Filters and Products

3D data processing techniques can now be applied to the data prior to analysis. These analogs to standard 2D techniques, such as windowing and filtering, as well as mo techniques to derived products such as vertical gradient and analytic signal. The ac calculations of gradient products, of course, is the fact that far more accurate vertical g hand than ever before. Higher order gradients are also possible as directly measured p than mathematical extrapolations of total field data. New filters and new products are lattice data. Moving average filters with variable weighting based on absolute or rela used to take advantage of the variable signal-to-noise ratios produced by ground clutte

3D Gradient Strings

Although inversion routines do not rely on visualization of the data, reduction of the intrinsic qualities is essential to presentation for human interpretation and control of filt inversion parameters. Several standard presentation techniques are reviewed, a concept of Gradient Strings is introduced.

Standard presentation techniques of lattice data are layers, slices, iso-surfaces an Gradient strings, lines through the lattice tracing maximum rate of change in the field introduced here. It is applicable to both magnetic and electromagnetic data, a interpretation of the physics differs, the utility for processing and target identification is t

The visualization and manipulation of gradient strings will allow the operator to parameters and to deselect targets from noise or to pin-point multiple targets within clo underlying assumption is that maximum gradient lines for legitimate sources will be c increase in magnitude with proximity to the ground. Noise, which might otherwise be p targets, will lack this continuity through 3D space. Similarly, multiple targets that may a target at survey heights, can be resolved as distinct gradient strings. Processing gradient string information can include spatial windows, cut-off thresholds, and filter str of peaks can be controlled by length and continuity of gradient strings.

ollection and Analysis
ce (UXO) Discrimination

Ridge National Laboratory
GameyTJ@ornl.gov

ornl GEOPHYSICS

quisition

ques because they
3D data onto a 2D

lose much of the
data and moving

rrelating the data

s associated with
unities to enhance
orrelation prior to

niques centers on
will be conducted
oud" of data points

his offers the first
erent interpolation
se are Matlab and
Rockworks offers

include simple 3D
odified processing
dvantage to lattice
radient data are at
parameters, rather
also possible with
tive height can be
r.

data to their most
er, processing and
nd the innovative

d transparencies.
l is a new concept
and although the
he same.

refine processing
se proximity. The
ontinuous and will
picked as possible
appear as a single
options based on
engths. Selection

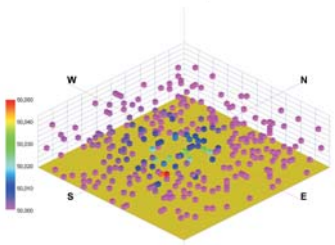

Cloud of magnetic readings over a selected anomaly

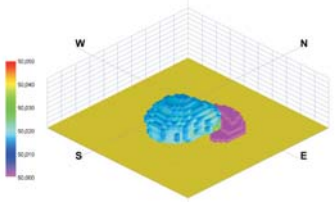

Magnetometer data rendered as two isosurfaces (one positive, one negative)

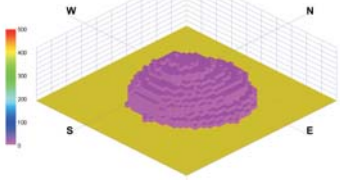

Analytic signal data derived from lattice of total field data. Isosurface at 10nT/m.

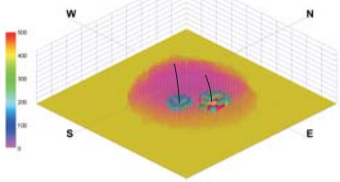

Analytic signal data rendered as solid isosurface at 250+ nT/m and transparent at 10+ nT/m

Analysis

Establish Baseline

Analysis of the benefits of 3D processing will be based on a suite of magnetic dipole models. Although this technique is equally applicable to electromagnetic models, magnetic modeling offers fewer variables and more robust inversion at this stage. Models include single dipoles at multiple depths, and pairs of dipoles of varying strengths, depths and offsets. A duplicate set of models for filter testing, with random noise added to the positions and geophysical readings has also been created. Having developed the theoretical models, 1D profiles and 2D grids are extracted and inverted using different techniques to establish a baseline performance for each of the inversion methods. These methods will include amplitude thresholds, Euler deconvolution, the MTADS and ModelVision inversion codes.

3D Gridding

Various 3D gridding algorithms are being tested to determine which produced the most acceptable results. Results at lattice nodes will be comapred to the theoretical response to determine the quality of a given routine. Input data will begin with a fully sampled space. Data density will then be reduced in stages. Noise can then be added to provide a target for filtering routines.

3D Processing

3D analogs to 2D processing procedures are then developed. These have included Hanning filters and Analytic Signal calculations. More advanced algorithms for weighted filters and gradient string calculations have also been developed. Modifications to the various presentation formats in different software suites are being explored in order to streamline analysis and itemize features for future development.

Inversion

The various inversion methods are then tested against the synthetic 3D data (with and without noise) and compared to the baseline results to quantify any improvement. This will require some modification to the standard procedures for some of the techniques. The amplitude threshold is the simplest method. In three dimensions, it is an extension of the gradient string principle. Rather than picking a peak from a grid, the peak is traced through 3D space and can include a cut-off for length as well as amplitude. The Euler routine will include the measured gradient rather than a calculated one in its algorithm. The MTADS and ModelVision codes operate on profile lines. These will be extracted from the 3D lattice and included in the inversion database.

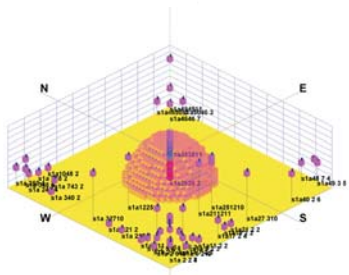

Gradient String Demo

This is a simple demonstration of the gradient string concept. Analytic Signal data are presented as a transparency, with peaks shown as solids at the appropriate node. The line of peaks at the center of the lattice are continuous and increase in intensity with decreasing height. The single point peaks are the result of noise in the lattice data. Gridded data (horizontal slices) would intersect one or more local lattice peaks and might be misinterpreted. Using the 3D spatial relationship between points allows for less ambiguous interpretation. These peaks can be used to set filter thresholds in processing, amplitude thresholds in peak selection, or continuity thresholds in gradient string selection.

Data Presentation

At right is a screen shot from ModelVision demonstrating 3D inversion of synthetic magnetic data. 2D gridded data in the top left shows magnetic response from lowest layer of lattice. Superimposed are two spheres presented as the starting model of the inversion process. Parameters of the spheres are shown in the bottom right.

The software is semi-manual, in that the user must provide a reasonable starting model before proceeding to inversion. Inversion allows for free parameters such as position, depth, radius, susceptibility and remanence of spheres. Additional shapes, such as spheroids and various regular and irregular polygons are supported with variations in free parameters as required.

Below the grid are two NS profiles, also from the lowest level of the lattice. Each one passes over one of the spheres. The black profile is the original data, the red profile is the starting model for the inversion process.

The 3D representation in the upper right shows the two spheres and the original total field data corresponding to the grid and profiles on the left. Line paths representing three layers of the complete lattice are also shown.

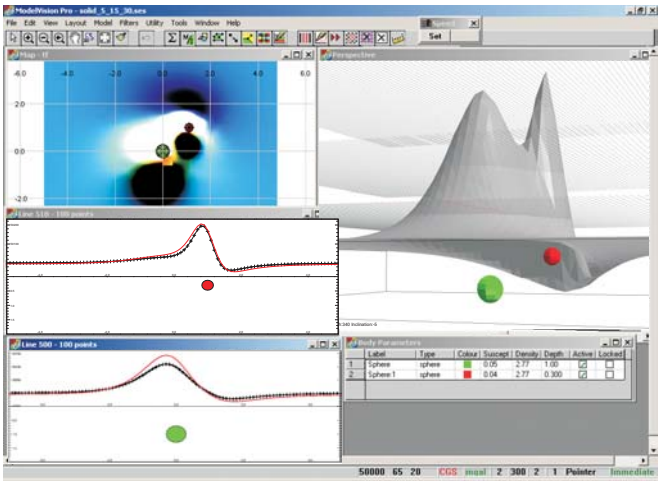

Appendix A3
Extended Abstract – SAGEEP 2004
February 2004

3D PROCESSING AND VISUALIZATION OF 3D MAGNETIC DATA

T.J.Gamey, W.E.Doll, A.M.Emond, L.P.Beard
Oak Ridge National Laboratory, Oak Ridge, TN 37831-6038

Abstract

Magnetic modeling and inversion routines that take advantage of recorded altitude or Z values have followed up on the development of improved 3-dimensional positioning technologies. Usually, this technique involves recording ground clearance or ellipsoid height during the course of collecting routine profile data. Technologies include laser or radar altimeters, DGPS heights, or laser and/or ultra-sonic positioning systems. Visualization of the data, however, maintains a 2D approach using either profiles or grids. This is an obvious limitation of 2D media such as paper and computer screens. Tools such as 3D surface maps are often used to project gridded data into simulated 3D, but this is not the same thing as presenting 3D data. Processing of these data often takes a step backwards and is limited to 1D tools. The noise reduction and interpretive capabilities derived from spatially correlating data across lines is lost.

This paper presents a justification for 3D collection, processing and interpretation of data for small, discrete objects such as drums, pipes and unexploded ordnance that are common to many environmental surveys. In addition to traditional visualization techniques, the concept of "gradient strings" and their utility in data analysis is introduced. While this paper focuses on magnetic data, the basic principles are equally applicable to electromagnetic data.

Introduction

Many geophysical data sets, collection procedures and presentation techniques are described as 3-dimensional. For the purposes of clarity, a distinction must be made between the number of dimensions of the position data collected during the survey and the number of dimensions of the presentation format. The traditional survey measures two dimensions of position data (X,Y) and presents the geophysical results as:

- 1D profiles (a projection against a single axis of time or horizontal position, with the data as the second axis),
- 2D grids/contours (a projection against two horizontal position axes using color to represent the data axis),
- or 3D surfaces /curves /nets (a projection against two horizontal position axes, using the illusion of a third vertical axis to represent the data).

Data may also be presented as profiles along survey lines plotted on 2D maps, which are similar to the 2D grids, although this format has apparently fallen out of fashion since the advent of simple gridding and contouring packages.

Even with the recording of 3D positional data (X,Y and height), none of the aforementioned presentation techniques display or accommodate the additional height information. Generally, the height is assumed to be constant and the data are forced into a 2D grid. This is a limitation of all two-dimensional media (paper and screens). Even 3D surfaces are technically 2D presentations using illusions of perspective and shading to appear 3D. It is

extremely difficult to represent 3D points on a 2D screen or map, and this does not yet include a dimension for the geophysical data itself. Occasionally, the perspective of a 3D presentation is rotated, thus adding time to enhance the illusion of dimension. Exchanging our 2D media for the 3D holographic presentations of science fiction would still require some form of transparency plus rotation of the image or movement of the observer in order to fully interpret it, just as any solid object would. A 3-dimensional representation therefore presents several fundamental obstacles to the observer.

Multi-dimensional data sets therefore require that we either reduce the information to its most relevant form for presentation, or else to think and to present data in terms of matrices and functions with n-dependent variables. This applies equally to 3D positioned data from a single sensor, multiple responses from a single sensor (ie EM time gates), or integrated multi-sensor data sets. Although this makes them ideal candidates for computer analysis, which is based almost entirely on linear matrices, the human factor is still required for control and judgment.

Traditional Data Collection

A single reading at one point in space rarely has any geophysical significance. Until the reading is presented with respect to neighboring points it has little relevance. It is this spatial correlation that gives a data profile meaning. Similarly, consecutive profiles allow the data to be spatially correlated in two dimensions – down line and across line. The traditional approach to geophysical mapping therefore is to collect data along transects (1D) at a nominal height and present the results as a grid (2D). Each added dimension brings a new level of relevance to the interpretation, but there are drawbacks.

Single profiles show the data with great resolution and fidelity since they are not subject to gridding interpolation, but are difficult to interpret. The most obvious short-fall is the lack of information to either side of a profile anomaly. By presenting the data with reference to neighboring points on either side, the 2D perspective makes it much simpler to pick out discrete targets from broader anomalies. This simplification is an important part of the interpretation process.

Data processing techniques based on 2D data sets also have significant advantages over their 1D counterparts. There are many advantages to analyzing data that have been spatially correlated in two dimensions. Spatial filters, for example, can remove uncorrelated noise better. FFT processes, such as analytic signal, can also enhance features more reliably and with fewer assumptions when applied to grids than to profiles.

The disadvantage of 2D presentations is that it assumes that all of the data were collected on a common plane, although this is not usually true. Whenever a data point is collected at different height than the adjacent data points, it creates an artifact in the grid. Depending on the severity and distribution of these artifacts, any interpretation based on the gridded data will be more or less flawed.

As a result, many additional 2D data processing steps must be incorporated into the work flow in order to correct for the “common plane” assumption and produce a viable interpretation. In addition to the gridding process, which generally desamples data down-line and interpolates data between lines, filtering or deletion of data points must be applied to produce a satisfactory grid. In some cases, these additional steps may reduce data quality more than they enhance it.

State-of-the-Art Data Collection

The impact of height on gridding is not a new phenomenon. The effects of height in both magnetic and electromagnetic data are well documented. Numerous studies have been done to limit, quantify or correct these effects. Techniques include wheeled carts to control height, altimeters and other positioning systems to measure height, and various upward or downward continuation algorithms to correct readings to a nominal height.

Advances in positioning systems and computing capabilities now allow collection and storage of geophysical, position and height data in a single database. Software packages for data inversion are taking advantage of increased power and are inverting data with height information.

Although the technology has incorporated several aspects of 3D data, all of these are attempts to solve the problem of continually forcing 3D data into a 2D format. To date, the best inversion solutions ignore the 2D format altogether and work entirely with profile data. Although this work flow avoids many of the problems, it does not take advantage of any of the positive elements of 2D processing such as noise reduction or FFT algorithms. It makes use of only one dimension of spatial correlation (down-line). Only filters and processes that can be applied to profiles are used.

3D Data Collection

The only way to take advantage of spatial correlation of data collected with 3D positioning, is to process it in three dimensions. Not only does this effectively deal with the problems associated with changes in height, but it offers the potential of spatially correlating the data vertically as well as horizontally. This also provides an opportunity to enhance the state-of-the-art inversion techniques by incorporating the benefits of spatial correlation prior to inversion.

For logistical and testing purposes, this paper assumes that the data are collected as part of a cued investigation (to follow-up a previously detected anomaly) using magnetometer sensors, although the techniques are equally applicable to traditional survey collection and to electromagnetic data after additional experimentation with 3D gridding and inversion techniques. After an initial geophysical survey, specific anomalies are identified for additional follow-up. Prior to excavation, the operator collects a “cloud” of data points at irregularly spaced intervals around the pre-determined location. The processing and inversion are then applied to this data set (Figure 1).

The “cloud” of data is then interpolated into a 3D lattice (grid) for processing. This offers the first opportunity for examination of 3D analogs of 2D processing techniques. Several different interpolation techniques are available. Two of the most accessible software packages for this purpose are Matlab and RockWorks. Matlab, however, only offers linear and nearest-point lattice routines. Rockworks offers eight methods, six of which are suitable for this application. The most reliable of these was their “inverse distance/anisotropic” technique. This method interpolates nodes based on an average of the closest points within each octant weighted by their proximity to the interpolated node (Figure 2).

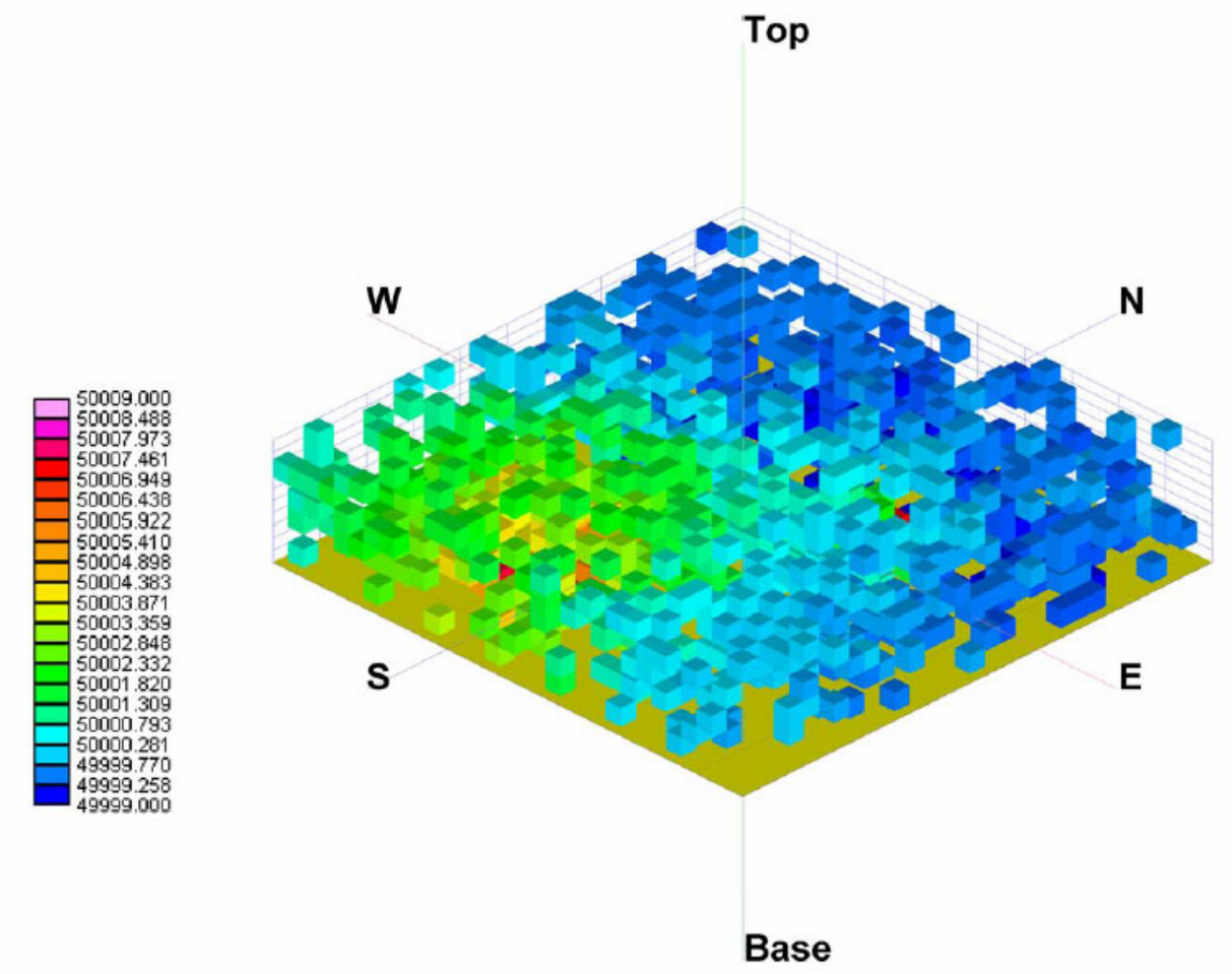

Figure 1: Total field magnetic data (in nT) collected as a "cloud" of points in three dimensions above two synthetic targets. Data are presented as a 10cm cube at each reading location. Data space is 300cm x 300cm x 60cm. Sample density is $1/6^{th}$ of the total volume (comparable to a fully populated 2D grid over the same area).

The targets for the sample data set presented here are two spherical dipoles with different sizes and depths in close proximity to one another. The large, deep target appears in the SW quadrant of the figures, while the smaller, shallower target appears in the NE quadrant. Additional target details are provided in Table 1. The collected data set ranges from -100cm to +200cm in X and Y, and from 10cm to 60cm above ground level. It will be seen that the sensor height is a critical element of the interpretation. The response of the larger target is visible at all heights, but the rapid increase in gradient of the shallower target makes it much more definitive at lower heights. Since cued investigations typically use analog instruments held very close to the ground, it is a debatable and subjective call as to which target would actually be excavated by a field crew – the larger target, the stronger response, or both. Unless both are excavated and documented, the measured data will be difficult to use as a calibration tool to judge system performance, future results and/or QA assessment.

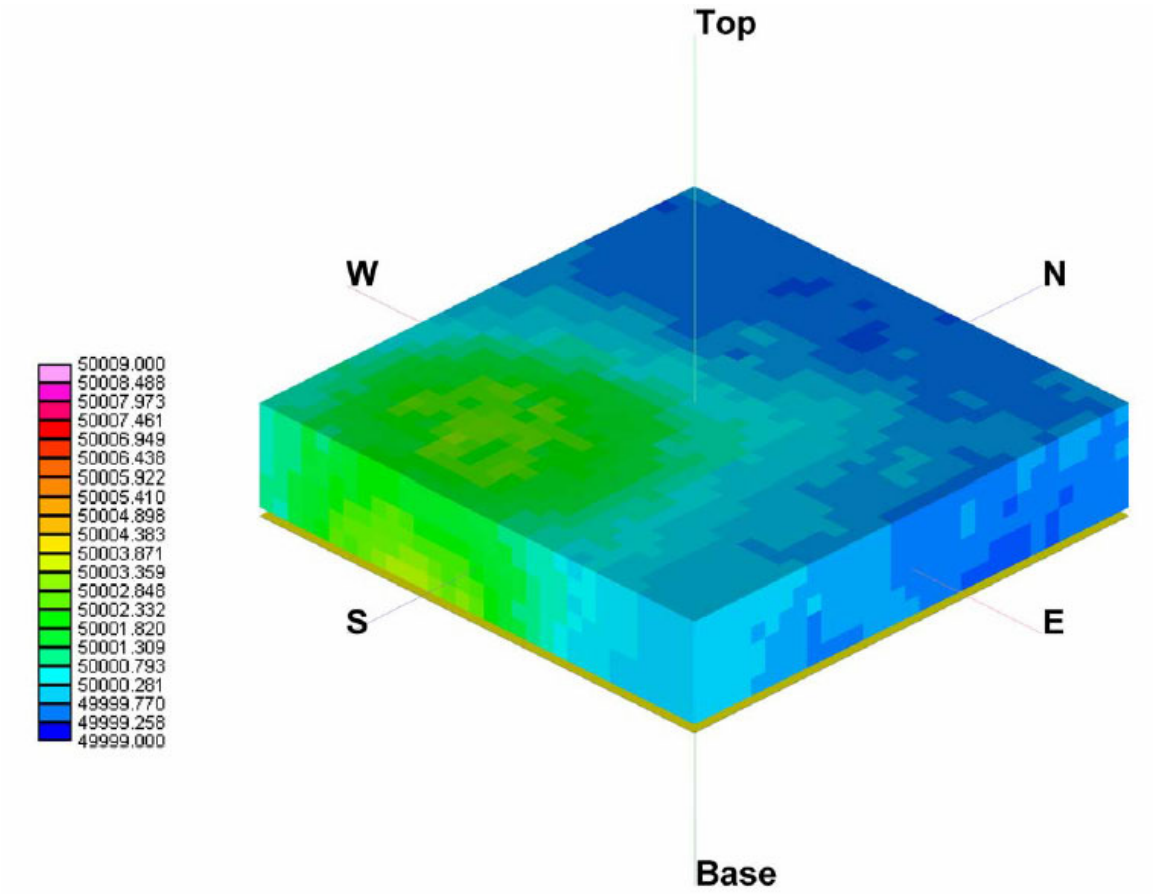

Figure 2: Total field magnetic data (nT) interpolated from "cloud" of points in figure 1 using an inverse distance algorithm. Data space is 300cm x 300cm x 60cm.

This 3D data set has been sampled at random locations throughout this data space at 1/6th the total volume so as to be more directly comparable to a fully populated 2D grid over the same area. At this density and distribution, the 3D gridding routine demonstrates a 0.32nT rms error between the interpolated results and the true modeled values. Gaussian noise of 2.5cm was added to the XY positions, 5.0cm to the Z positions, and 0.1nT was added to the magnetic data prior to 3D interpolation and processing.

3D data processing techniques can now be applied to the data prior to analysis. These include simple 3D analogs to standard 2D techniques, such as windowing and filtering, as well as modified processing techniques to derived products such as vertical gradient and analytic signal. For example, the coefficients for a 3-point symmetric 3D Hanning filter are provided in Table 2. The advantage to lattice calculations of gradient products, of course, is the fact that far more accurate vertical gradient data are at hand than ever before. Higher order gradients are also possible as directly measured parameters, rather than mathematical extrapolations of total field data. New filters and new products are also possible with lattice data. Moving average filters with variable weighting based on absolute or relative height can be used to take advantage of the variable signal-to-noise ratios produced by ground clutter. The result is a data set that has been enhanced with spatial correlation in all three directions without requiring excessive filters to correct for 2D assumptions.

Table 1: Synthetic target parameters used for sample data set. Targets were modeled as spherical dipoles with a magnetization of 120 A/m in a field of 50,000nT at 60° inclination and 20° West declination.

ID	X (cm)	Y (cm)	Z (cm)	radius (cm)
1	0.0	0.0	100.0	5.0
2	100.0	100.0	20.0	1.5

Table 2: Coefficients of 3-point 3D Hanning filter

lower grid			middle grid			upper grid		
0.006	0.030	0.006	0.030	0.074	0.030	0.006	0.030	0.006
0.030	0.074	0.030	0.074	0.148	0.074	0.030	0.074	0.030
0.006	0.030	0.006	0.030	0.074	0.030	0.006	0.030	0.006

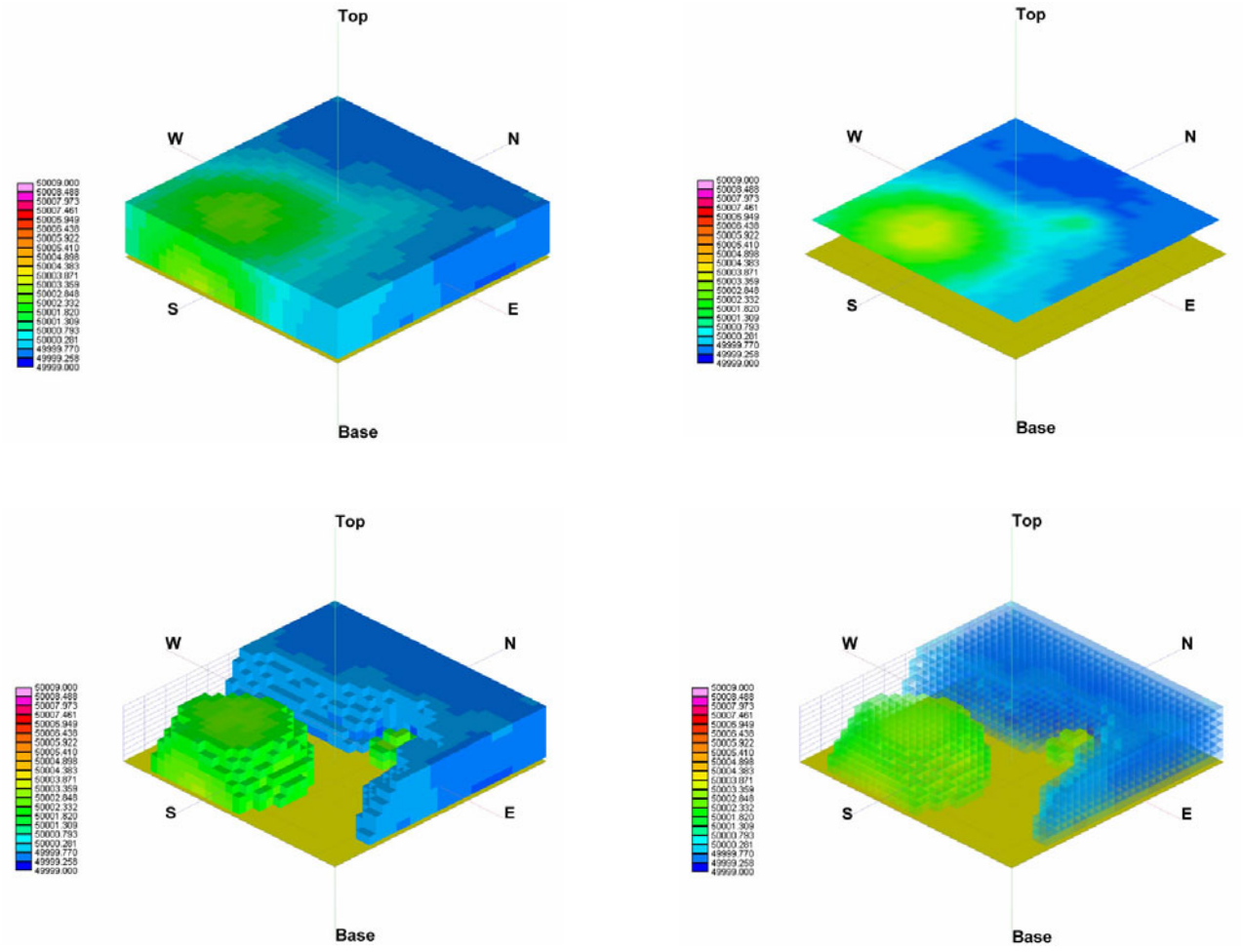

Figure 3: Total field magnetic data (nT) after application of a 3-point, 3-dimensional Hanning filter. Data space is 300cm x 300cm x 60cm. (top-left) solid volume shows faces only. (top-right) horizontal slice at 40cm above the ground. (bottom-left) two pairs of iso-surfaces showing volumes below 50,000nT, and above 50,002nT. (bottom-right) the same iso-surfaces as before, with a 75% transparency.

Visualization techniques must now be applied to view the interior of the 3D data set. Several different techniques are demonstrated in Figure 3. These include solids, slices, iso-surfaces and transparencies. Slices are simply planes cut through the lattice at varying angles. Multiple vertical slices are often called fences. Horizontal slices are equivalent to 2D grids, except that they can have been interpolated onto a plane, rather than assumed to have been collected that way. Iso-surfaces are the 3D equivalent of 2D contour lines. They appear as three-dimensional blobs encompassing all values greater than the specified threshold. Unlike contour maps only a single surface value can be displayed at a time, although multiple iso-surfaces, such as the positive/negative lobes demonstrated in Figure 3, are possible. Successive increments, fluctuations or depressions within the iso-surfaces cannot easily be represented. Transparencies attempt to do this by taking the solid colors and reduce their intensity, allowing visual space for underlying colors and shapes to be presented. All of these techniques require interactive manipulation in order to be useful to the interpreter. This requires additional time and effort that is ill-suited to a production setting where hundreds of targets must be analyzed.

3D Gradient Strings

Although inversion routines do not rely on visualization of the data, reduction of the data to their most intrinsic qualities is essential to presentation for human interpretation and control of filter, processing and inversion parameters. Gradient strings are a new concept introduced here to simplify the visualization of 3D data sets typical in magnetic and electromagnetic detection of UXO and other discrete environmental targets. Although the interpretation of the physics differs between magnetics and electromagnetics, the utility for processing and target identification is the same. These are essentially lines through the lattice tracing maximum rate of change in the field. For magnetic data, one can imagine layers of analytic signal grids with a line connecting the peaks from one layer to the next.

The aim of this technique is to reduce the data set to its most important qualities and allow simple visualization with as few control parameters as possible. The underlying assumption is that maximum gradient lines for legitimate sources will be continuous and will increase in magnitude with proximity to the ground. Noise, which might otherwise be picked as a possible target, will lack this continuity through 3D space. Similarly, multiple targets that may appear as a single target on the original survey data can be resolved as distinct gradient strings. Processing options based on gradient string information can include spatial windows, cut-off thresholds, and filter strengths. Selection of peaks can be controlled by length and continuity of gradient strings. If the line branches with depth, the operator is faced with the possibility of multiple targets or a single large target in the very near surface.

For a string to be valid, therefore, it must (a) exceed an intensity threshold (b) be continuous over several layers and (c) increase in intensity with depth. The result is a line through the 3D data space that points directly to the target. To further aid in interpretation, the line is color-coded to gradient intensity.

These gradient strings and the numerical inversion provide mutual feedback into the decision making process. The visualization and manipulation of gradient strings will allow the operator to refine processing parameters and to deselect targets from noise or to pin-point multiple targets within close proximity to one another. In return, the inversion will provide quantitative results in the form of fit coefficients.

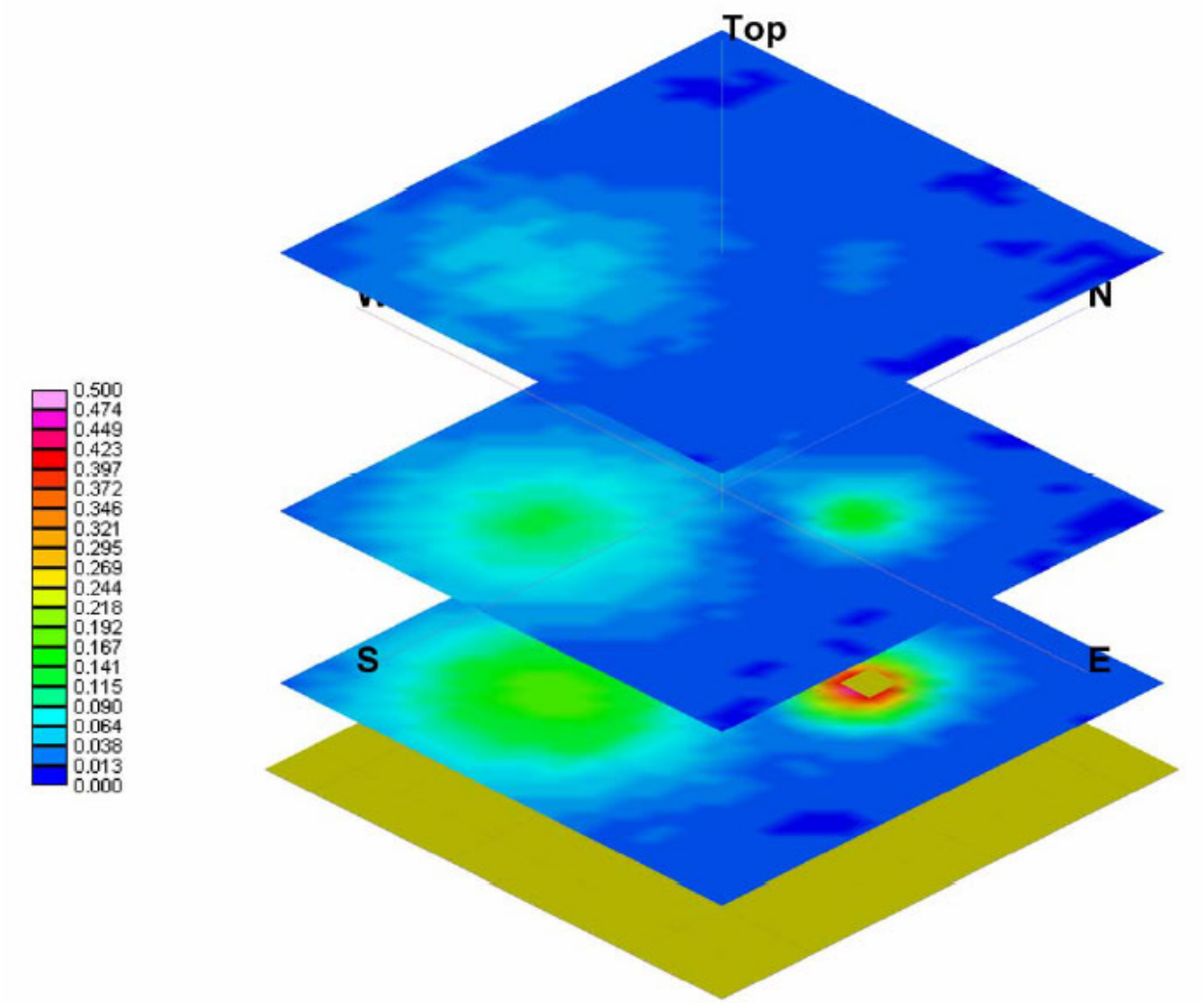

Figure 4: Analytic signal (nT/cm) calculated from the 3D total field data. Slices represent data at 10cm, 30cm and 60cm above the ground level. Data space is 300cm x 300cm with an expanded vertical scale. Note the effect of second order gradient effects. The smaller (shallower) target in the NE quadrant shows a much stronger gradient response at lower heights, but has almost disappeared at greater heights, although the larger (deeper) target is visible at all heights.

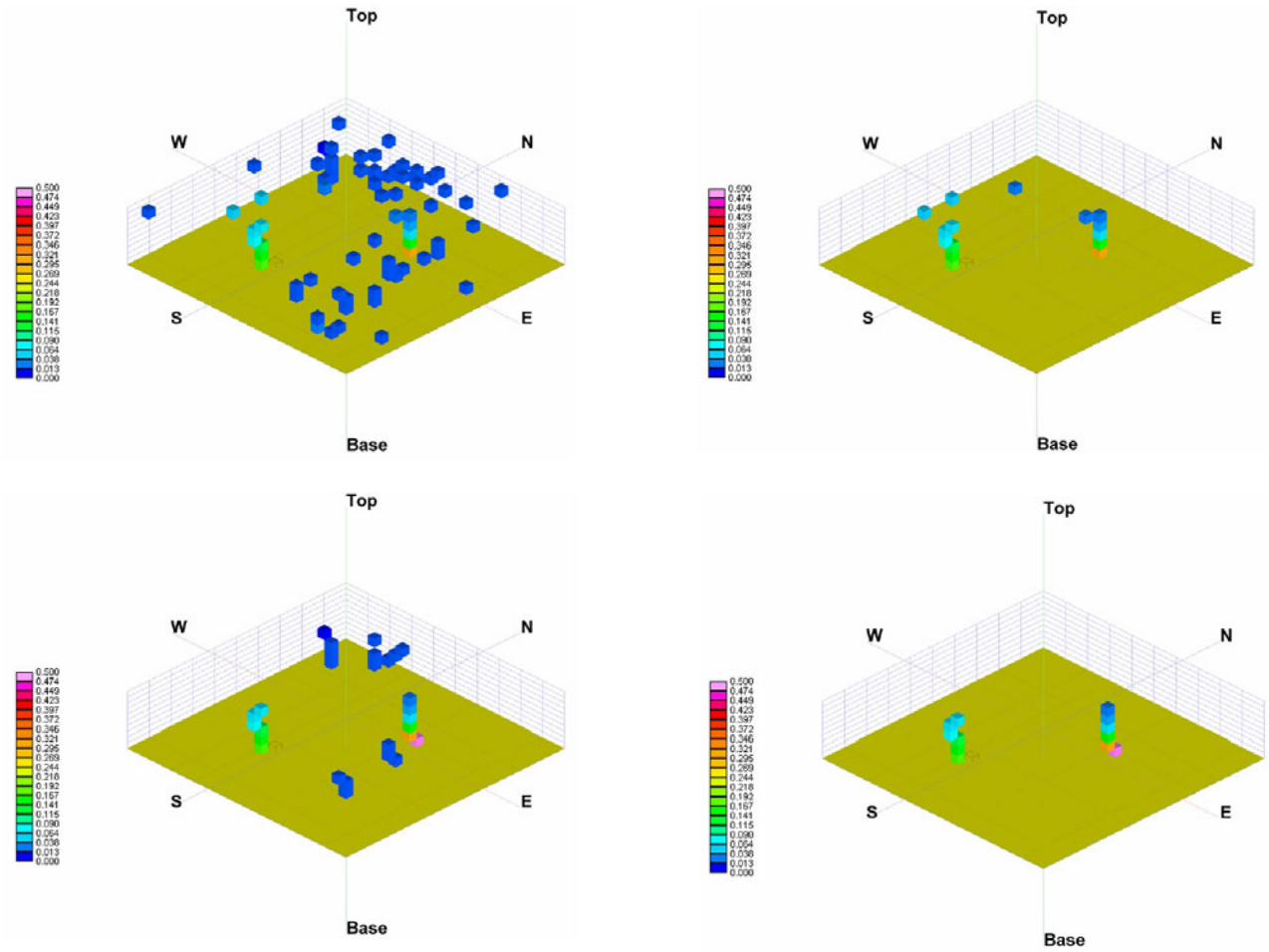

Figure 5: Gradient strings of analytic signal (nT/cm). (top-left) all strings regardless of length, amplitude or continuity. (top-right) strings after application of 0.3nT/cm threshold. (bottom-left) strings with three or more points, regardless of amplitude. (bottom-right) strings with three or more points and amplitudes greater than 0.3nT/cm.

3D Inversion

To compare inversion results from 2D vs 3D data collection, three different data collection scenarios were modeled on the sample target set used above. The first was a set of parallel survey lines at 0.5m spacing and 0.4m height, the second was a 2D grid at 0.1m spacing and 0.4m height, and the third was a 3D lattice at randomly sampled locations. The number of data points for the 2D grid and the 3D lattice were the same. Each scenario was inverted using the Encom ModelVision software. The same poorly fit starting model was used for all inversions. Results of the inversion are presented in Table 3. Figure 6 shows a screen capture of the inversion software for the noise-free case.

Adding a small amount of noise (Gaussian noise 2.5cm to XY, 5.0cm to Z, 0.1nT to magnetics), produced correspondingly poorer results. If the 0.5m survey lines crossed directly over the two targets, the inversion fit was 2.8% rms. If the survey lines are offset by 10cm from the target center, the error increases to 3.6% rms. Given that most geophysical surveys use 1m line spacing (rather than the 0.5m used here) and experience 2-5x the positional error, this is probably better than most traditional survey results can produce. The fully populated 2D grid inverted with a fit of 2.9% error, while the 3D lattice inverted with a fit of 2.2% error.

In each case, the 3D lattice produced slightly better numerical inversion results than the fully populated 2D grid using the same number of data points. This reflects the predictive nature of potential fields. An electromagnetic system would presumably show an even greater difference in performance. It must be recognized, however, that this is not a typical 2D magnetic grid. It is a fully populated grid with a raw data spacing of 10cm and tight vertical controls. Since this is best accomplished in practice using a 3D positioning system and the data collection procedure outlined above, the true measure of the 3D inversion results for field applications is the comparison to the 10cm offset lines.

Table 3: Inversion parameters and results. The same starting model was used for all inversions.

	X (cm)	Y (cm)	Z (cm)	Rad (cm)	Susc (cgs)	X (cm)	Y (cm)	Z (cm)	Rad (cm)	Susc (cgs)	fit err (%)
Model											
True	0	0	100	5.0	0.24	100	100	20	1.5	0.24	0.02
Start	10	-10	20	2.0	0.30	90	110	20	2.0	0.30	18.4
Noise-free											
Lines*	0.97	0.85	102.3	6.3	0.12	89.9	100.6	0.0	4.5	0.00	1.5
Grid	0.00	0.01	100.1	7.2	0.08	100.0	100.1	20.0	2.2	0.07	0.05
Lattice	0.00	0.02	100.0	5.6	0.17	100.0	100.0	20.0	1.9	0.13	0.02
Noise-added											
Lines*	0.01	0.48	103.0	7.4	0.08	97.5	96.5	12.6	4.3	0.01	2.8
Lines**	0.71	0.69	101.2	5.3	0.20	100.0	98.6	13.7	1.9	0.10	3.6
Grid	-0.36	-0.01	101.0	7.7	0.07	100.1	98.2	15.5	2.1	0.07	2.9
Lattice	0.81	-0.47	99.6	5.6	0.16	95.3	101.1	18.6	1.3	0.39	2.2

* lines pass directly over both of the targets, required tighter limits on XY to resolve small target
** lines pass 10cm offset from center of both targets
susceptibility conversion: $k_{SI} = 4\pi\, k_{cgs}$

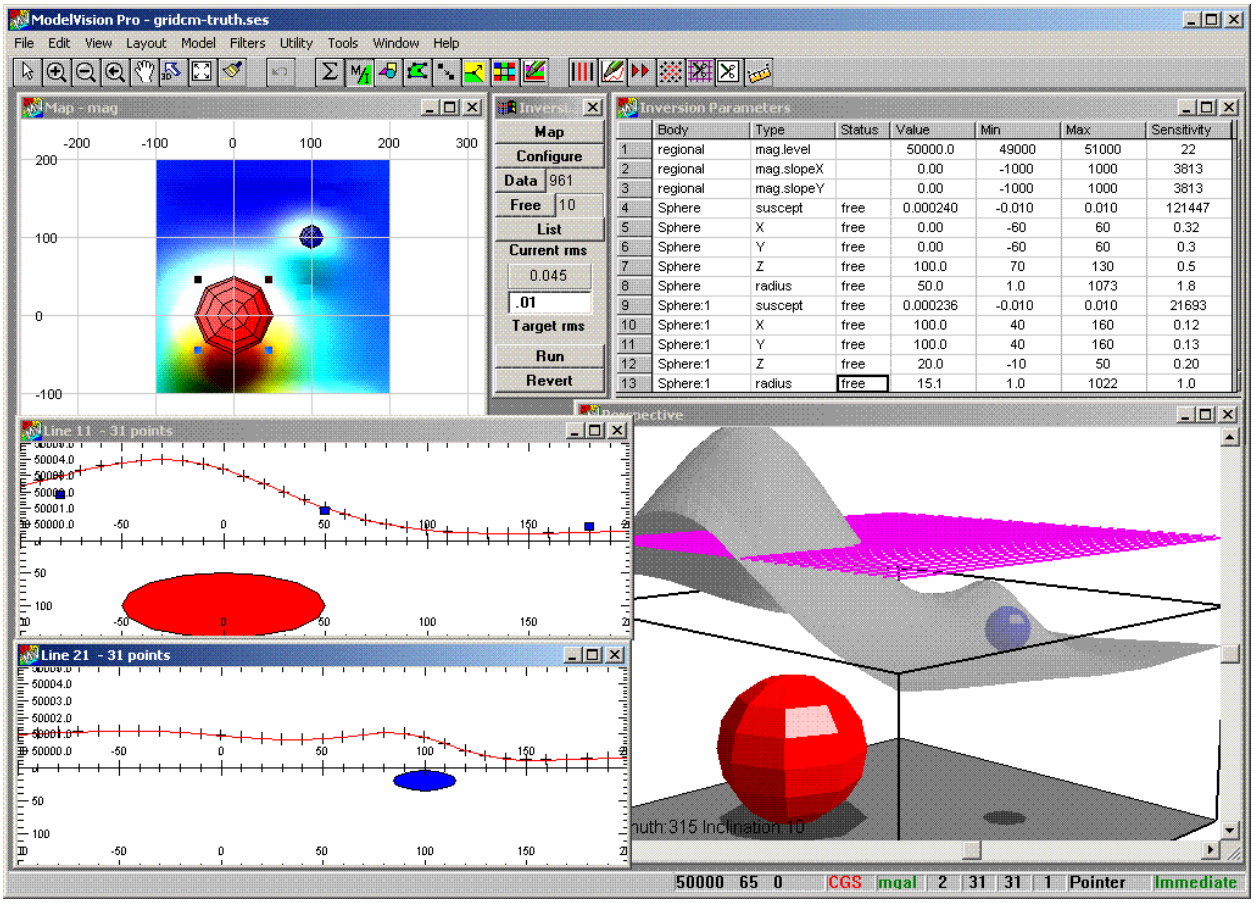

Figure 6: Screen capture from the Encom ModelVision software. It includes 2D plan, 2D profile, and 3D data-surface visualization capabilities and inversion parameter control.

Conclusion

Three-dimensional processing and presentation of geophysical data collected with 3D positioning offers several advantages. The primary benefit is the ability to improve noise levels by spatially correlating data in three dimensions without forcing the data onto a common plane. A new visualization technique using gradient-strings was introduced to enable a full 3D lattice to be reduced to its most intrinsic qualities for interpretation. For a string to be a representation of a true ground source, it must (a) exceed an intensity threshold (b) be continuous over several layers and (c) increase in intensity with depth. By eliminating strings that do not meet these criteria, the result is a simple line through the 3D data space that points directly to the target(s). To further aid in interpretation, the line is color-coded to gradient intensity.

The effects of second order gradients were also briefly demonstrated. The response of the larger target was visible at all heights, but the gradient of the shallower target increased much more quickly with proximity. Since cued investigations typically use analog instruments held very close to the ground, it is a debatable and subjective call as to which target would actually be excavated by a field crew – the larger target, or the stronger response. This digital 3D approach would make it much simpler for field crews to assess multiple targets in close proximity to the single dig location they may be provided.

Inversion results of 3D data were shown to be equivalent to an equal density of highly controlled 2D data, but significantly better than typical line survey results. The combination of gradient strings for simple visualization and the numerical inversion provide mutual feedback into the decision making process. The visualization and manipulation of gradient strings will allow the operator to refine processing parameters and to deselect targets from noise or to pin-point multiple targets within close proximity to one another. In return, the inversion will provide quantitative results in the form of depths, sizes and fit coefficients.

Acknowledgements

Funding for this work was provided as a SEED project by the SERDP UXO office under Anne Andrews. Oak Ridge National Laboratory is managed by UT-Battelle, LLC for the U.S. Department of Energy under contract DE-AC05-00OR22725. The submitted manuscript has been authored by a contractor of the U.S. Government. Accordingly, the U.S. Government retains a nonexclusive, royalty-free license to publish or reproduce the published form of this contribution, or allow others to do so for U. S. Government purposes.

Appendix A4
Oral Presentation – SAGEEP 2004
February 2004

3D Processing and Visualization of 3D Magnetic Data

T. Jeffrey Gamey, William E. Doll, Abraham Emond, Les P. Beard
Oak Ridge National Laboratory, Oak Ridge, TN

Background

- OE Techs don't trust digital geophysics
- They DO trust analog geophysics !!
- Decision making is taken out of their hands
- Ultimate objective is to simplify the visualization and discrimination tools to the point where Techs can use and trust them to make decisions that will speed clearance
- Still retains digital record of each decision as required by regulators

Overview

- Definitions
- Traditional Methods
- State-of-the-Art Methods
- 3D Method
- Generalized example with modeled data
- Gradient strings
- 3D vs 2D inversion comparison
- Conclusions

Definitions: Collection - Presentation - Inversion

- Collection refers to number of dimension coordinates collected with the geophysical data
  - rarely 1D (distance down line)
  - usually 2D (includes XY)
  - recently 3D (XYZ)
- Z measurement techniques include DGPS, laser, radar, ultra-sonic
- Z accuracy varies with technology; DGPS Z measure is roughly half as good as XY
- Z reference planes vary with technology; HAE is good for inversion, not so good for ground follow-up

Definitions:
Collection - Presentation - Inversion

- Presentation: number of *dimension* axes on map, profiles (1D), grids (2D), solids (3D)
  - same definition applies to processing techniques
  - note some "3D maps" use *geophysical* axis for Z
  - note limitations of 2D media (paper, screens)
- Presenting third axis (dimension or geophysical) on 2D media uses perspective and shading to create illusion of three dimensions
- Presenting "4D" data requires additional techniques to visualize the interior of the data space (slice, fence, transparency, iso-surface)

Definitions:
Collection - Presentation - Inversion

- Inversion refers to number of *variable* dimension coordinates in geophysical data used in target calculation
- Standard techniques to locate discrete targets such as Analytic Signal peaks and Euler are based on grids with 2D positions (fixed Z, very fast, simple)
- Newer techniques use a collection of points (line or set of lines) with measured Z positions (3D)

Traditional Methods

- Data are collected in 2D at nominal height AGL
- Then processed in 1D (freq filters), gridded, additional processing in 2D (filters, AS)
- Then interpreted in 2D (peaks, Euler)
- Pro: Fast-simple-intuitive, relates anomalies on adjacent lines for discrimination of target shapes
- Con: Ignores differences in collection height; forces all data onto common plane; converts height changes into grid artifacts; spends more effort removing height artifacts than improving quality

Traditional Methods

- Data collected at different heights along adjacent lines with differences forced into gridding artifacts

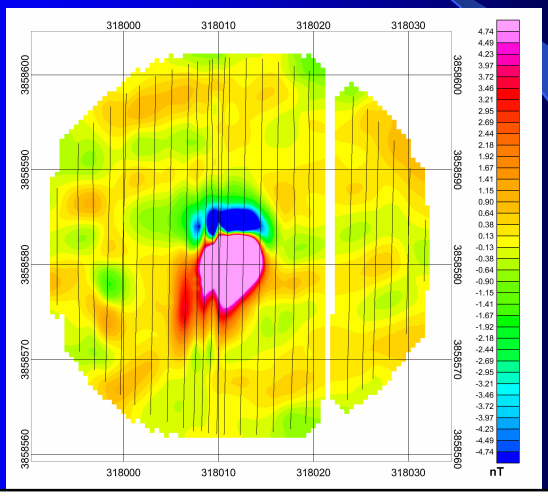

State-of-the-Art Methods

- Data are collected in 3D at nominal height AGL
- Then processed in 1D (freq filters), gridded, additional processing in 2D (filters, AS, peaks)
- Then interpreted in 3D from pre-grid data
- Pro: Uses height data, bypass grid artifacts
- Con: Misses opportunity to reduce noise for data inversion through cross-line correlation; target selection still distorted by forcing height differences onto common plane

State-of-the-Art Methods

- Data collected in 3D at nominal height AGL
- Gridded data still show artifacts, but inversion avoids these problems by stepping back to use profile data only

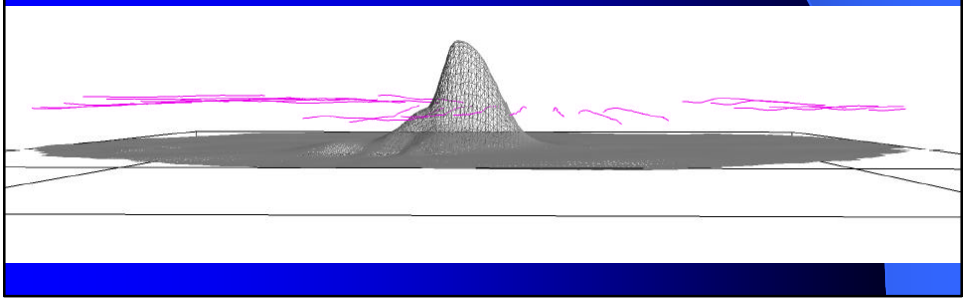

3D Method

- Data are collected in 3D at random heights AGL
- Then processed in 1D (filters?), gridded (3D), additional processing in 3D (filters, AS, strings)
- Then interpreted in 3D from 3D gridded data
- Pro: Uses height data and three dimensional correlation to reduce noise prior to target selection and inversion
- Con: Practical only for cued investigations; integrated system not yet available

Example of 3D Method

- Modeled response from two small spherical targets with different radii and burial depths, simulating 60mm mortar and 20mm shell
- Data were collected at random positions within 3D space (100cm x 100cm x 50cm)
- Sampled at 1/6th full density (same number of data points as fully populated grid at 10cm interval)
- Sample heights from 10-60cm AGL
- Random noise added to positions and magnetic data for testing purposes

Example of 3D Method

- Data are collected in 3D at random heights AGL

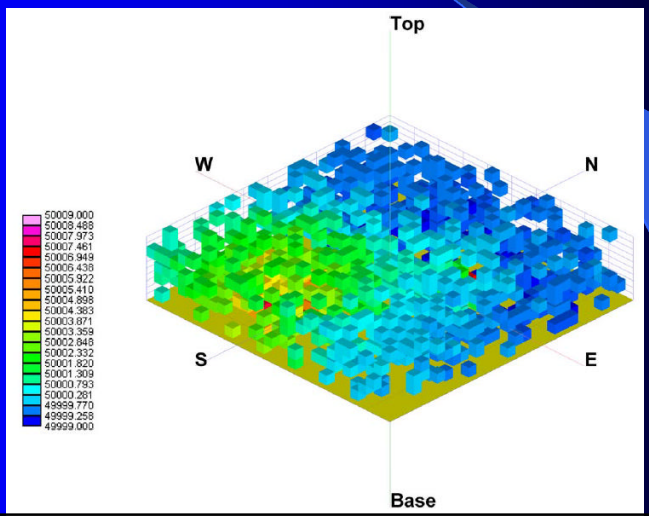

Example of 3D Method

- Data are "gridded" in 3D onto a lattice of regularly spaced points, creating a solid volume of data
- Six different 3D gridding techniques were tested using Rockware SolidModel routines
- "anisotropic inverse-distance weighting" produced the best results based on least error between interpolated and modeled response regardless of degree of interpolation tested
- 3D Hanning (cosine roll-off) and triangular (linear roll-off) filters were designed to supplement square (vertical roll-off) filter provided

Example of 3D Method

- Data are "gridded" in 3D onto a lattice of regularly spaced points, creating a solid volume of data

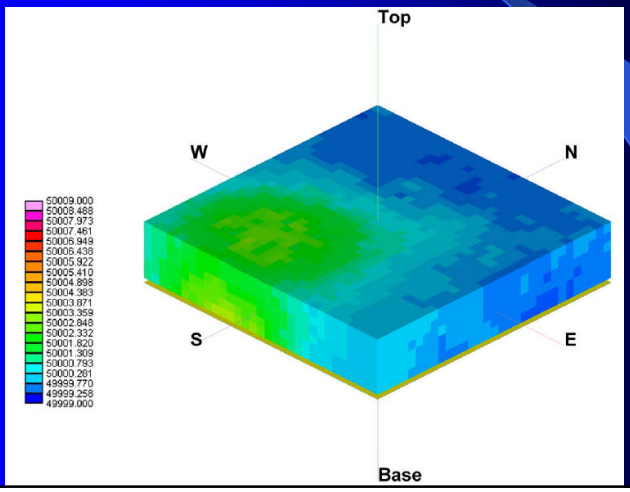

Example of 3D Method

- Visualization not required for inversion, but it *is* required for interpretation
- Interpreter must at least specify initial target shape (sphere, ellipsoid, continuous pipeline) and whether to invert for single or multiple targets
- Additional visualization techniques are required for 3D
  - Solids only show surface readings
  - Total field after 3D Hanning

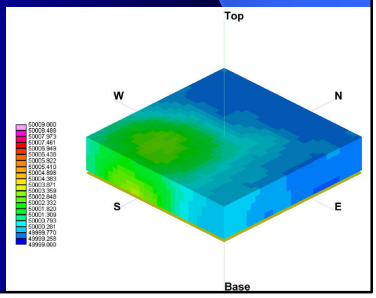

Example of 3D Method

- Additional visualization techniques are required for 3D
  - grids
  - slices
  - fences

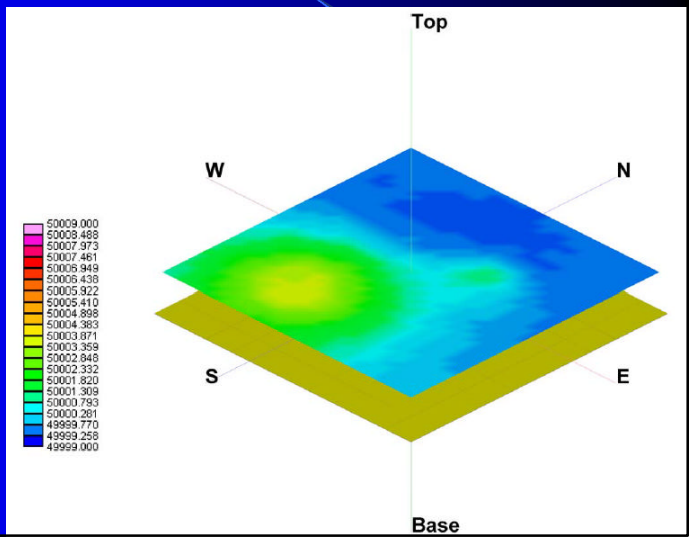

Example of 3D Method

- Additional visualization techniques are required for 3D
  - iso-surfaces (<50,000nT and >50,002nT)

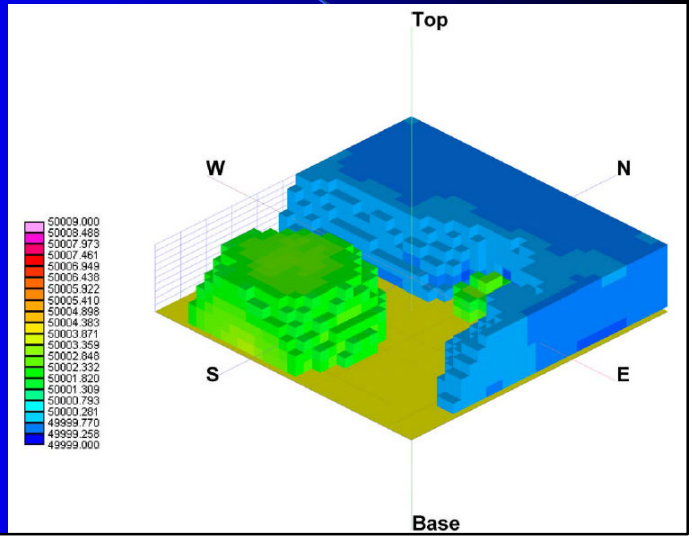

Example of 3D Method

- Additional visualization techniques are required for 3D
  - transparency (iso-surface with 75% transparency)

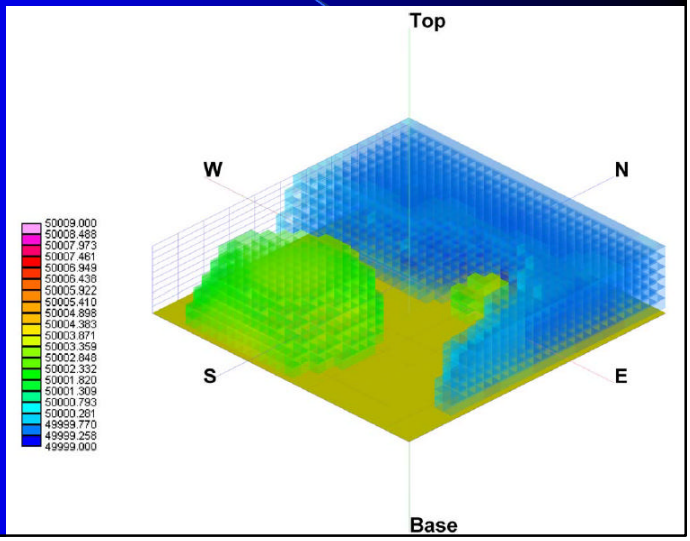

Gradient Strings

- Locating small targets (UXO) in 2D often uses analytic signal peaks
- AS can be calculated directly from 3D lattice
- Peaks from individual slices will align to form strings along lines of maximum gradient
- For a string to be legitimately associated with an object it must:
  - exceed a minimum amplitude threshold
  - be continuous over some length (noise peaks in individual slices will be non-continuous with height)
  - decrease in signal strength with height (strongest gradient is closest to target at ground level)

Gradient Strings

- After calculating the AS from the TF, visualize connecting the peaks through multiple grids to form strings of maximum gradient

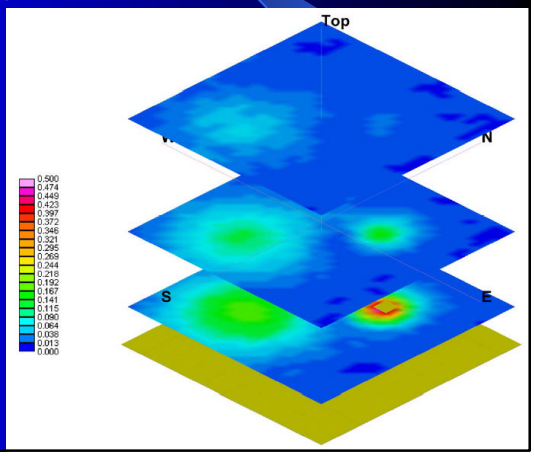

Gradient Strings

- Isolate individual peaks and display
- Numerous peaks will be caused by noise

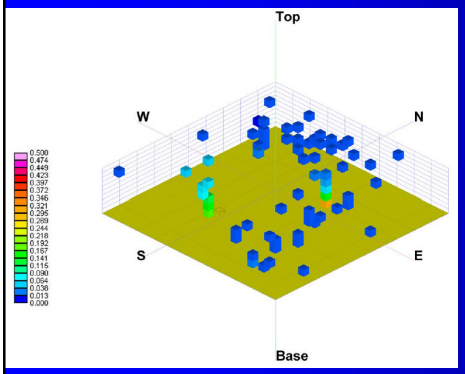

all strings

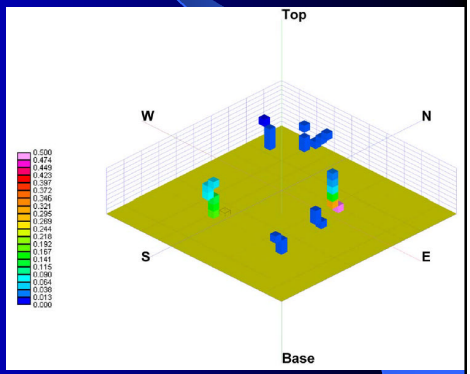

strings > 2pts

Gradient Strings

- Number of strings can be reduced by length, strength and continuity

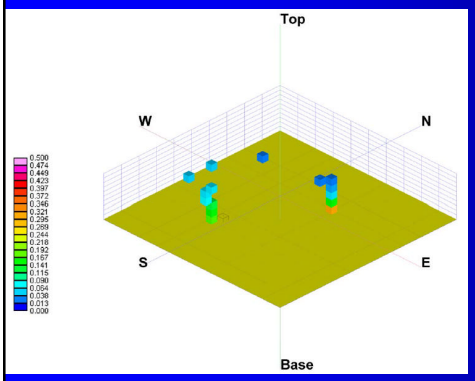

strings > 0.3nT/m

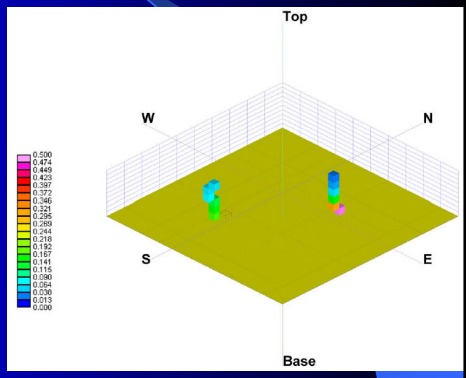

strings > 2pts and > 0.3nT/m

Inversion Comparison

- Modeled data from two targets based on traditional survey lines and 3D data collection
- Survey lines at 0.5m spacing 0.4m height; one set directly over targets, one offset by 10cm
- Line data required 5:1 interpolation to fill 2D grid, but still twice the density of typical 1m survey
- 3D data collected at random locations
- 3D data required 6:1 interpolation to fill 3D solid (same number of data points as 2D grid)
- Noise-free and noise-added sets compared

Inversion Comparison

- Line data detection of smaller target problematic (insufficient density)
- Inversion of line data had trouble resolving location of smaller target, especially if line offset from target
- 3D strings detected both targets
- Inversion of 3D data showed better fit results (line data 2cm off large target, 3D exact fit on both)
- Adding positioning noise evened up the comparison by degrading quality of 3D faster than line data due to higher gradients at lower heights, but 3D still better (line data 3/10cm off, 3D 1/5cm off)
- 3D resolved target size better (10% vs 50-150%)

Conclusions

- Traditional collection methods suffer from gridding artifacts caused by height variations
- Modern inversion methods eliminate this by collecting 3D positions and inverting collections of lines, but this loses the noise reduction capabilities of cross-line correlation
- 3D data collection solves both of these problems plus it improves inversion results, but is practical only for cued investigations
- Gradient strings were introduced to aid visualization of 3D solids prior to setting inversion parameters
- The technique is as applicable to EM as to magnetic methods

Acknowledgements

Jeff Marqusee, Anne Andrews
at SERDP Program Office

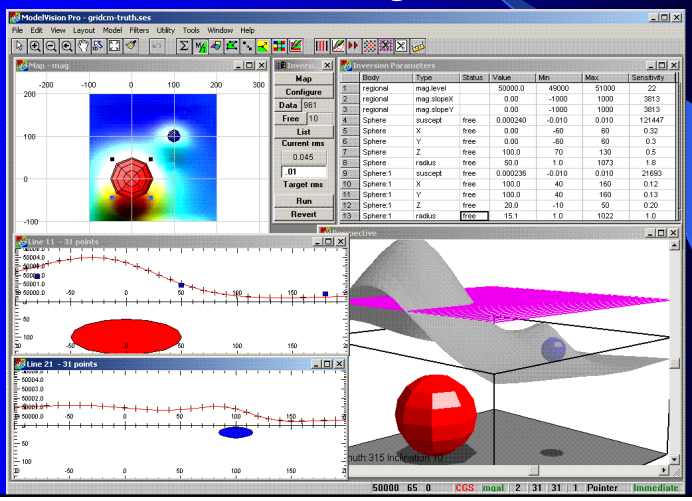

3D Method

- Data are collected in 3D at random heights AGL then gridded in 3D for processing and interpretation

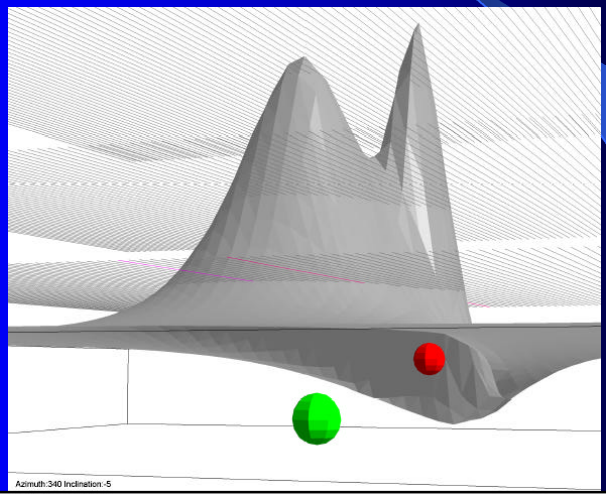

Appendix B1
Color Contours with Targets

Color contours of 2D Total Field Magnetic data with synthetic targets in their true locations and orientation. Horizontal units in cm, total field units in nT.

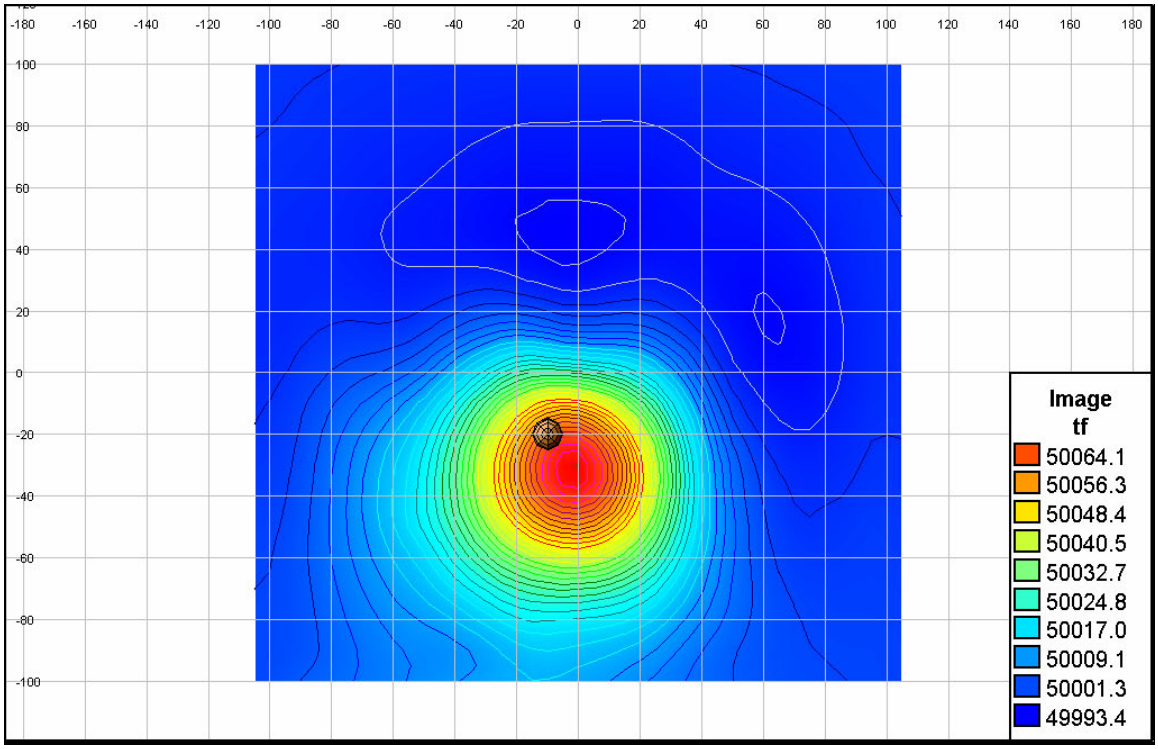

Model 1 (sphere at depth 0.2m)

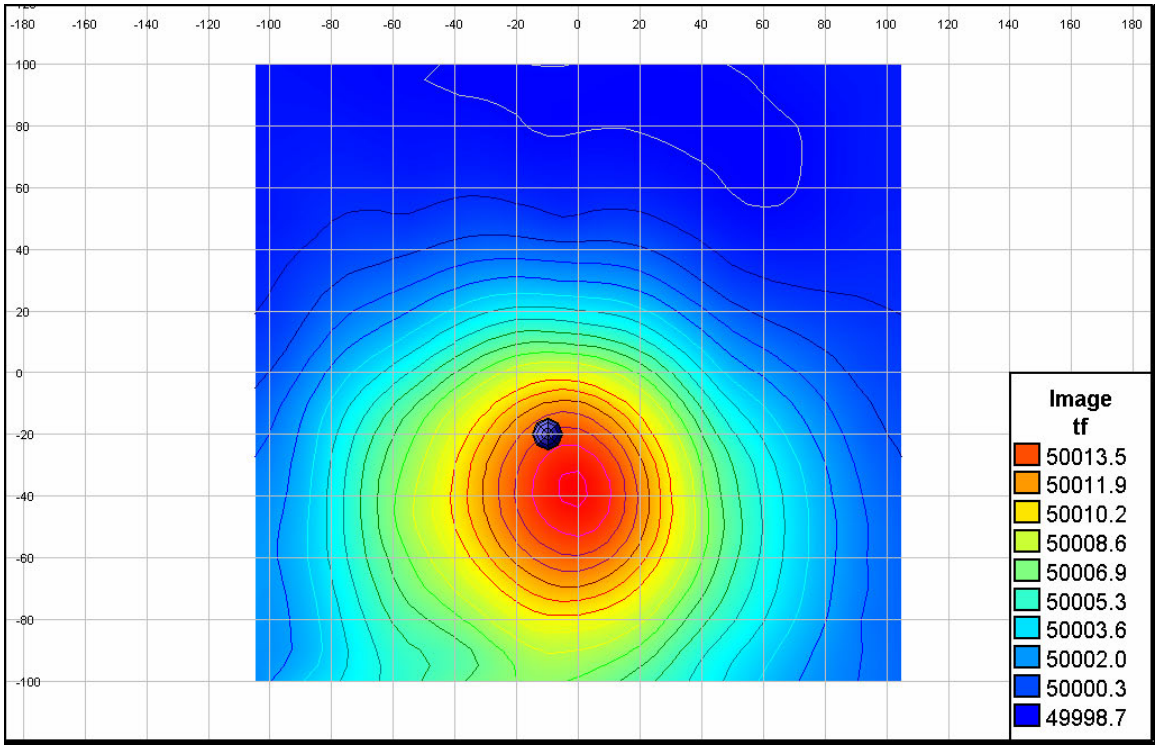

Model 2 (sphere at depth 0.6m)

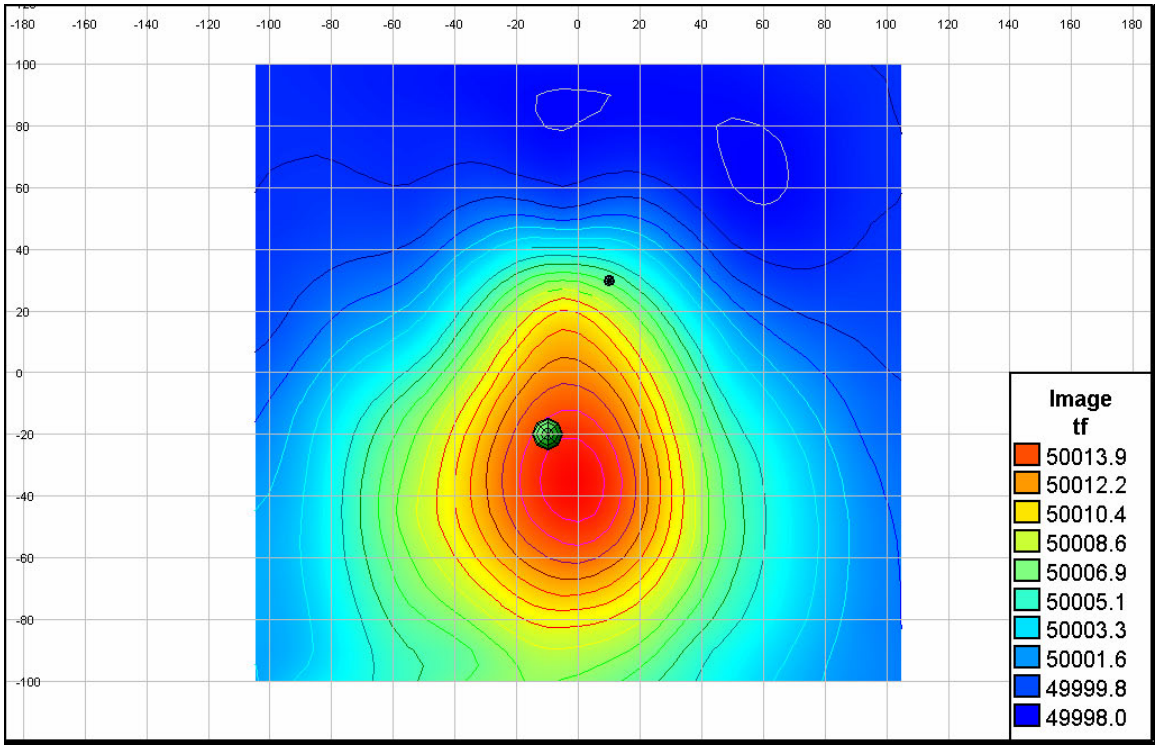

Model 3 (spheres at depths 0.6m and 0.05m)

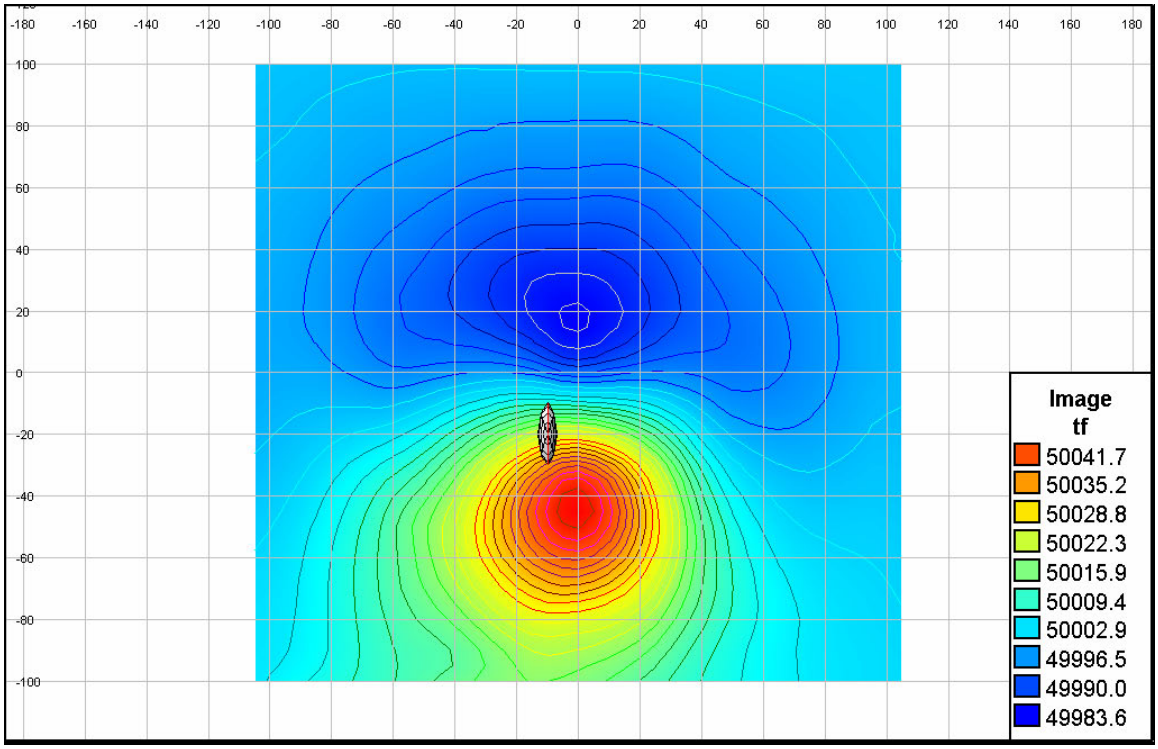

Model 4 (Horizontal ellipsoid at depth 0.2m)

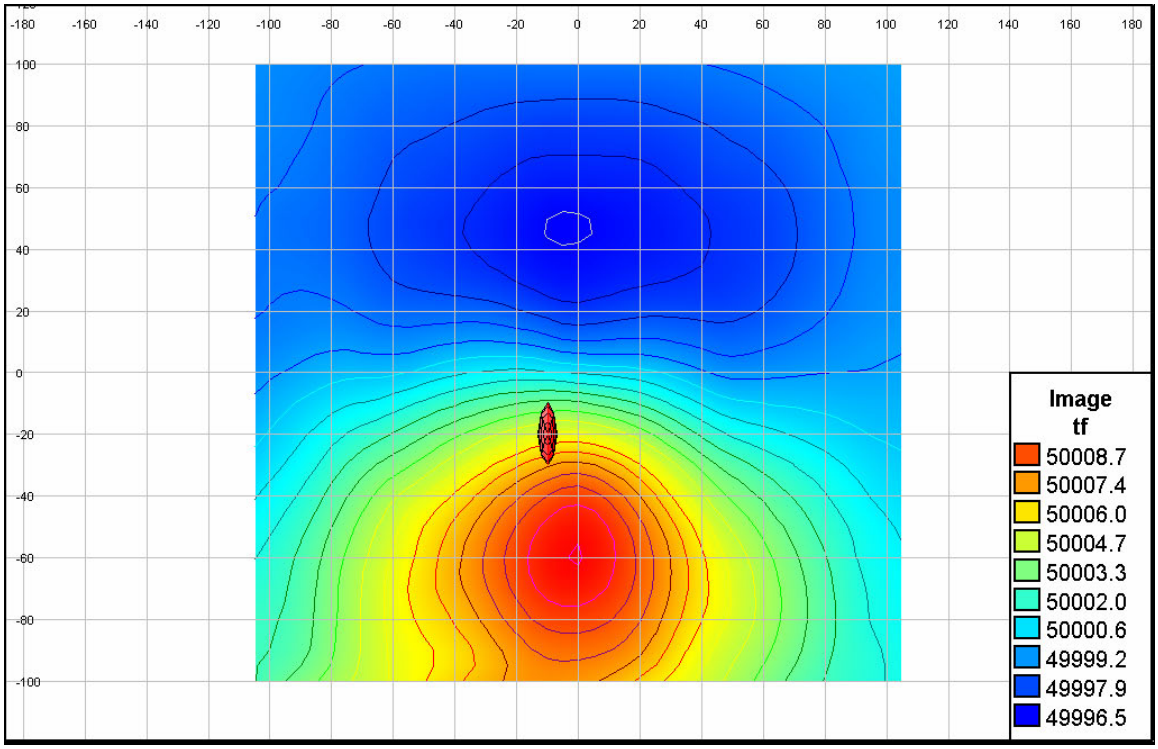

Model 5 (Horizontal ellipsoid at 0.6m)

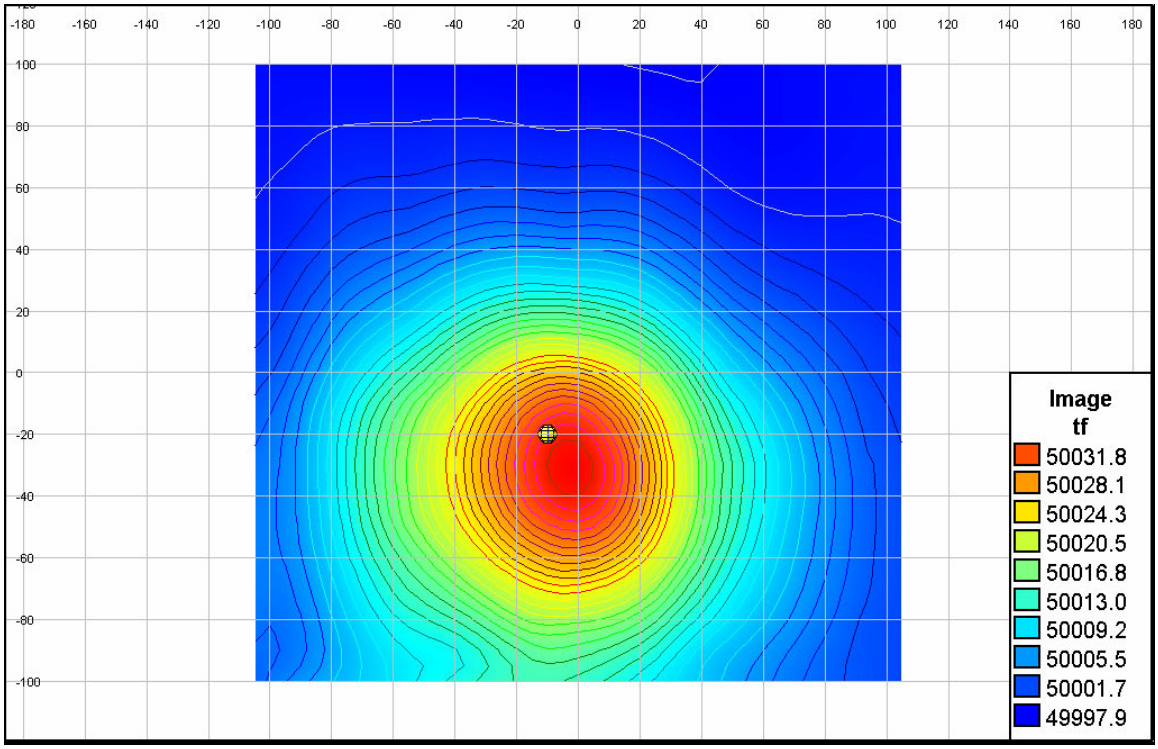

Model 6 (Vertical ellipsoid at depth 0.6m)

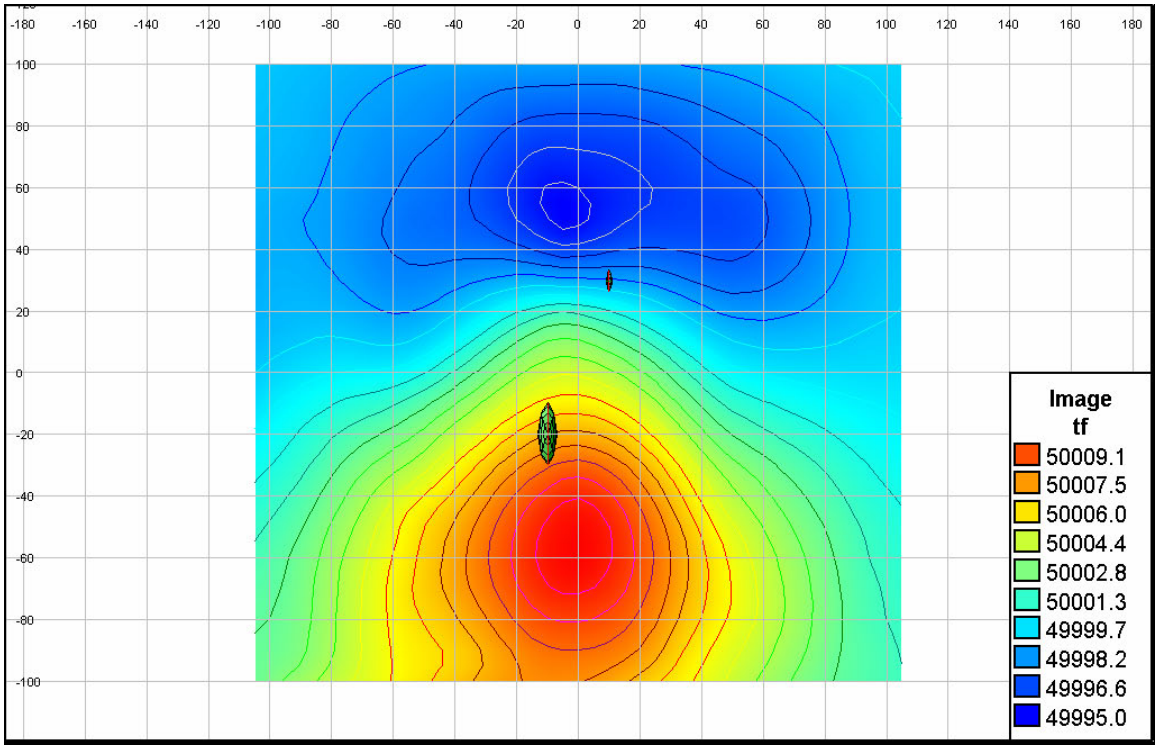

Model 7 (Horizontal ellipsoids at depths 0.6m and 0.05m)

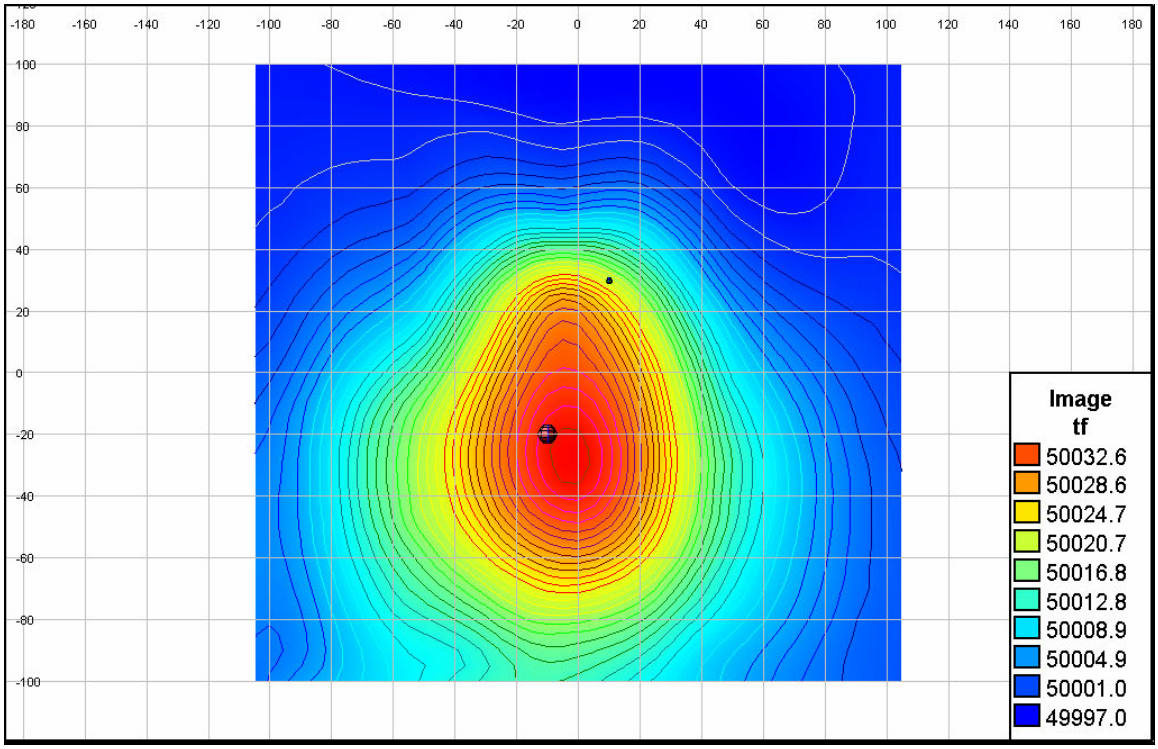

Model 8 (Vertical ellipsoids at depths 0.6m and 0.05m)

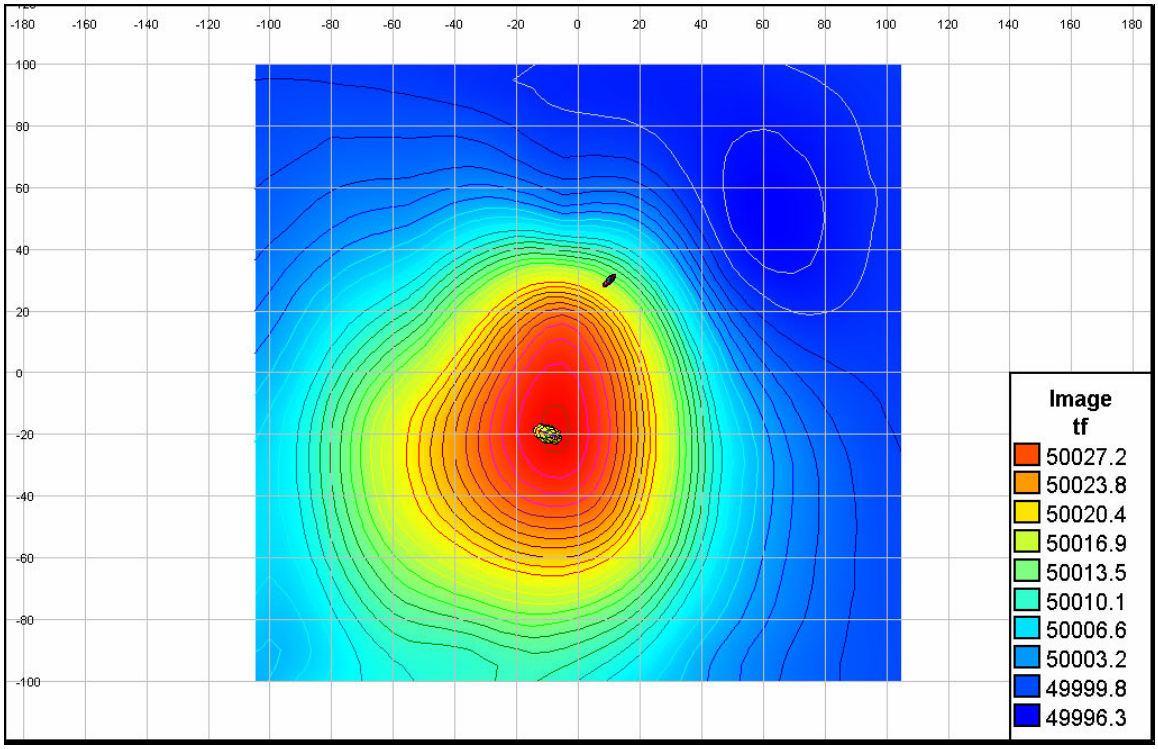

Model 9 (Randomly oriented ellipsoids at depth 0.6m and 0.2m)

Appendix B2
Gradient Strings

Gradient Strings of 3D Analytic Signal data. Data space is 2m x 2m x 0.5m. Viewed above from the SE. Analytic Signal units in nT/m.

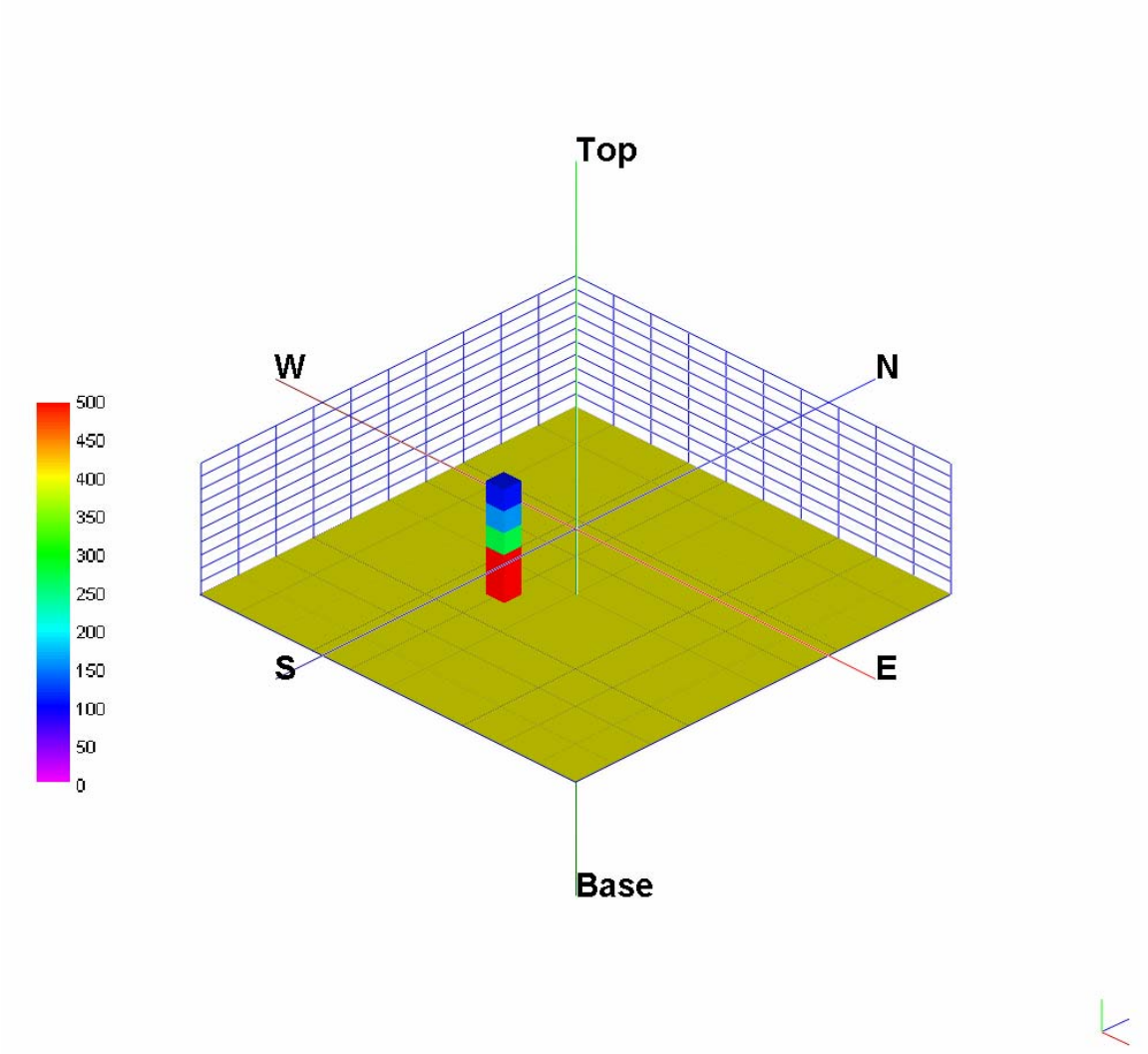

Model 1 (sphere at depth 0.2m)

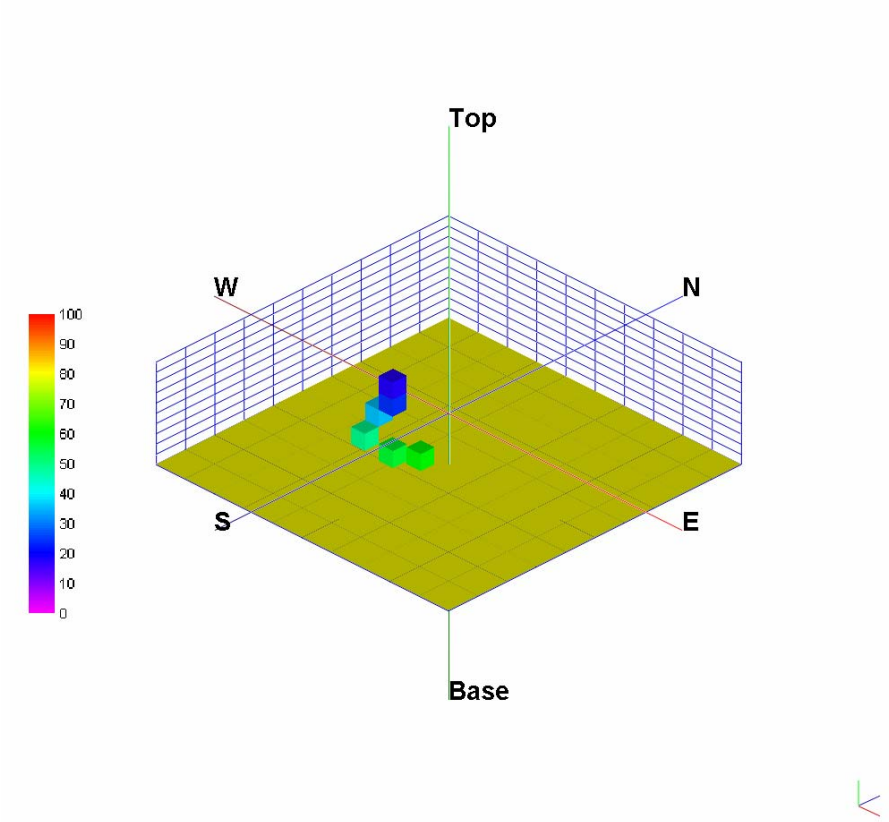

Model 2 (sphere at depth 0.6m)

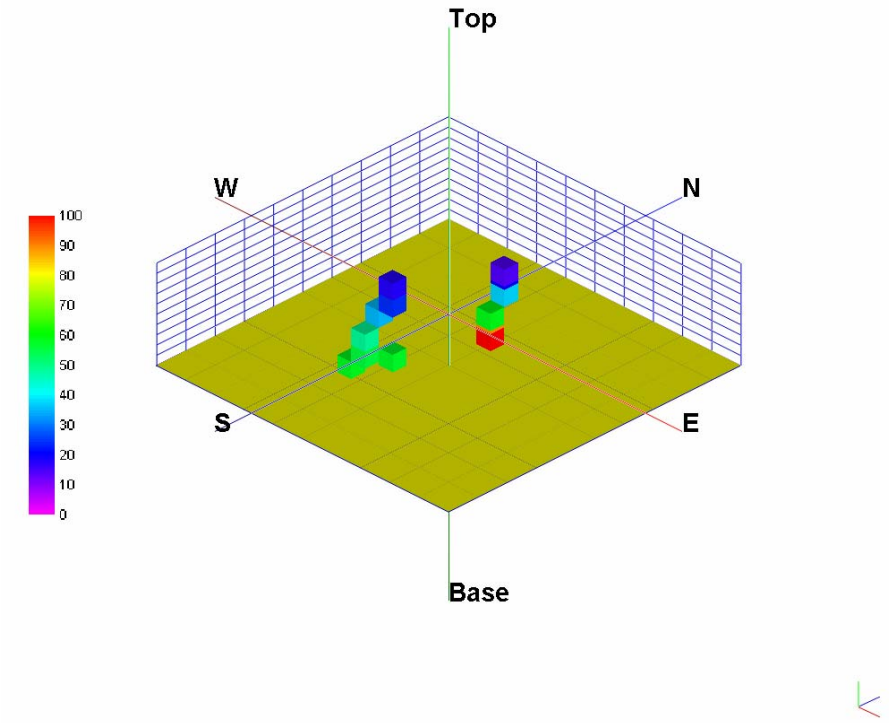

Model 3 (spheres at depths 0.6m and 0.05m)

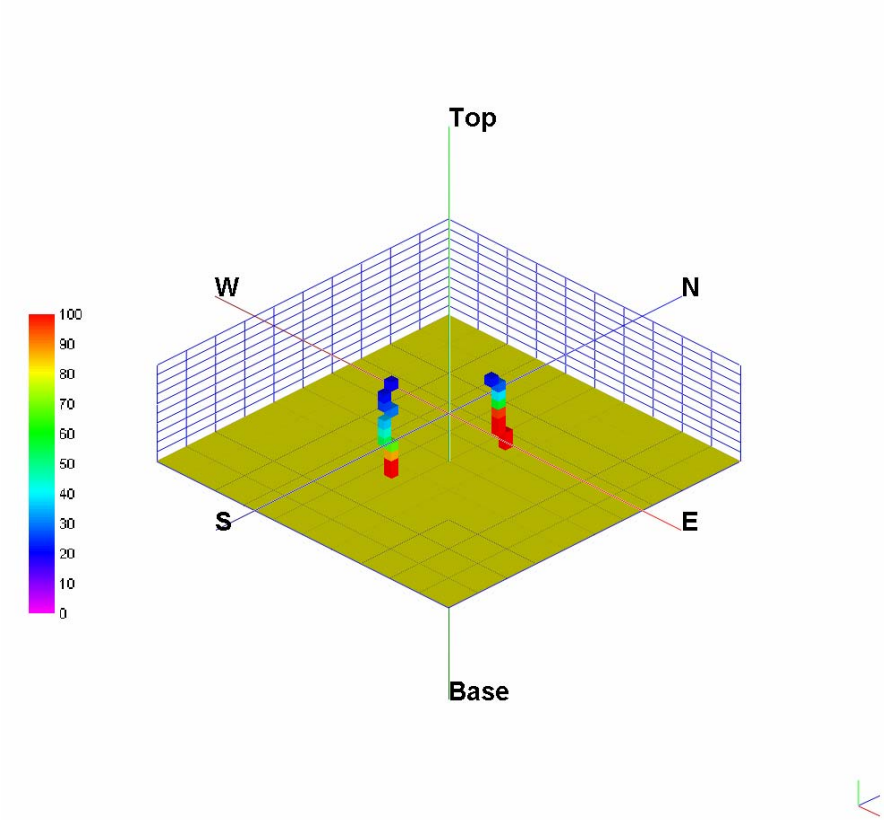

Model 3t (spheres at depths 0.6m and 0.05m)

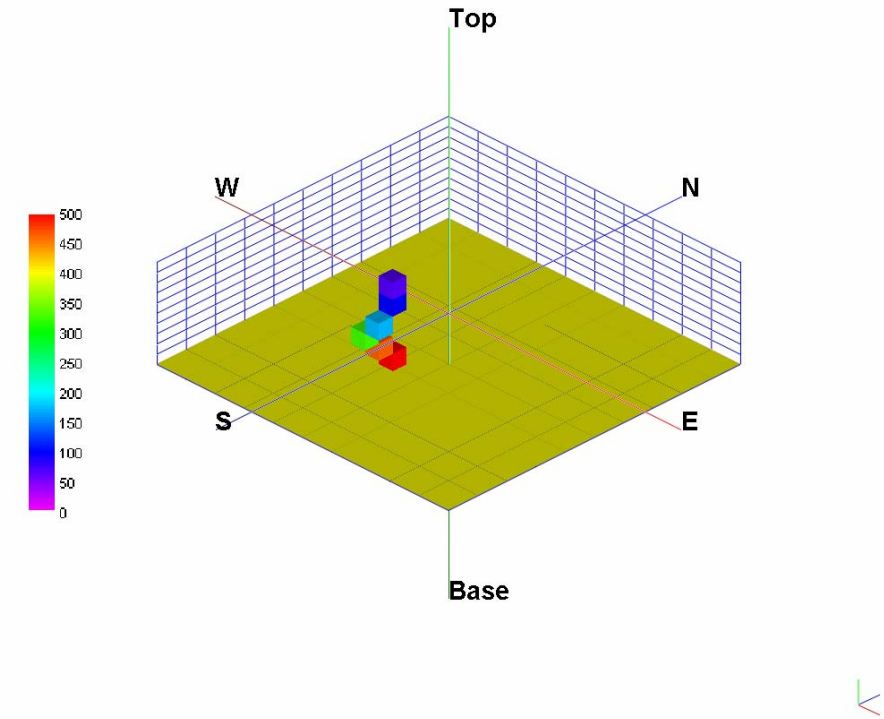

Model 4 (Horizontal ellipsoid at depth 0.2m)

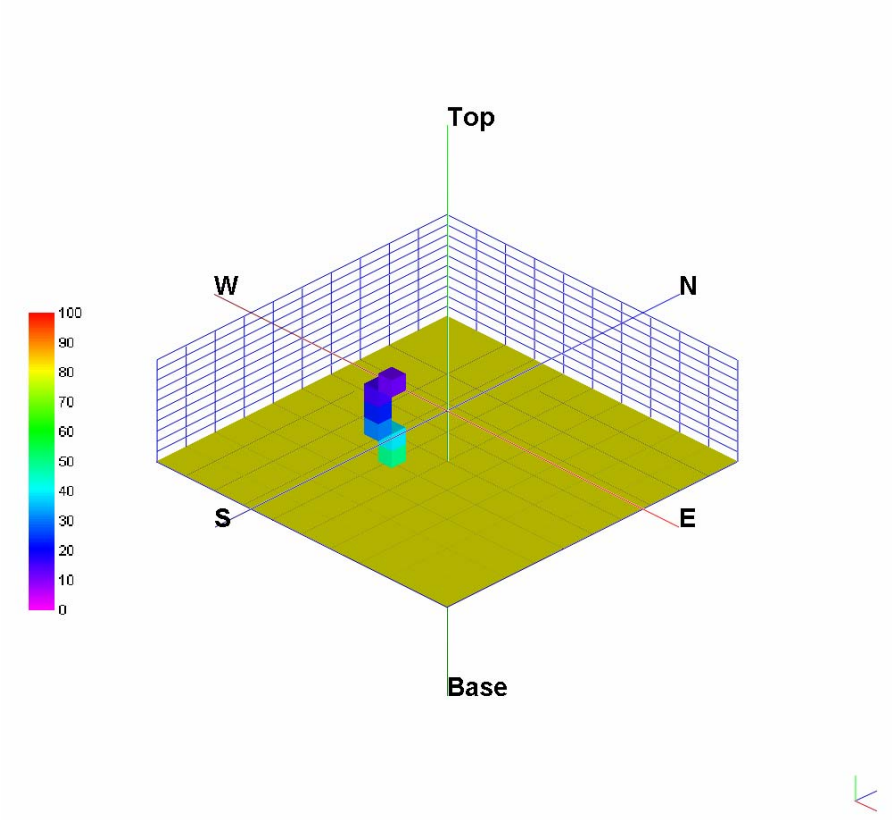

Model 5 (Horizontal ellipsoid at 0.6m)

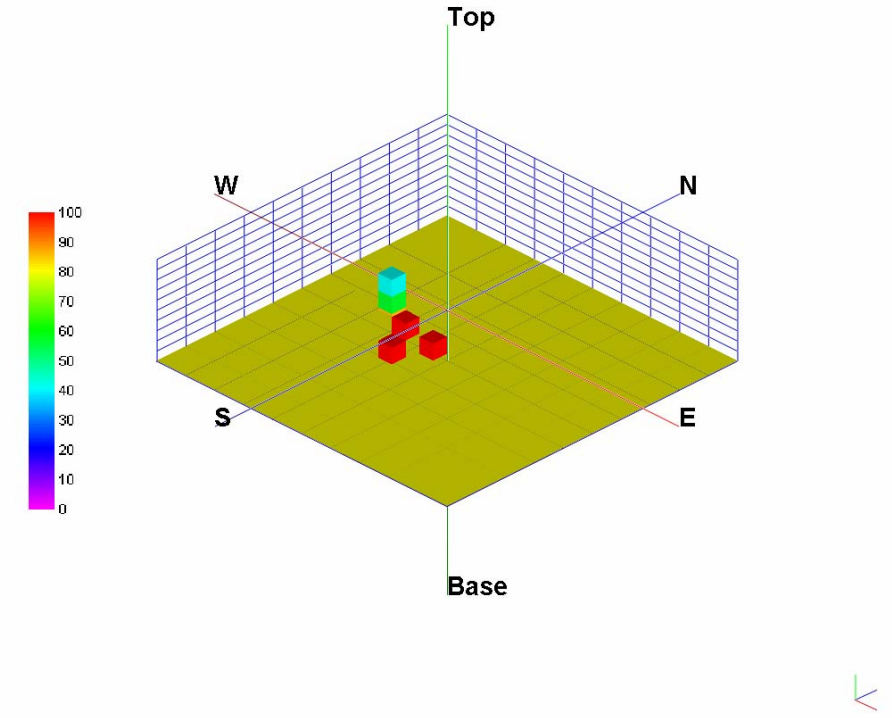

Model 6 (Vertical ellipsoid at depth 0.6m)

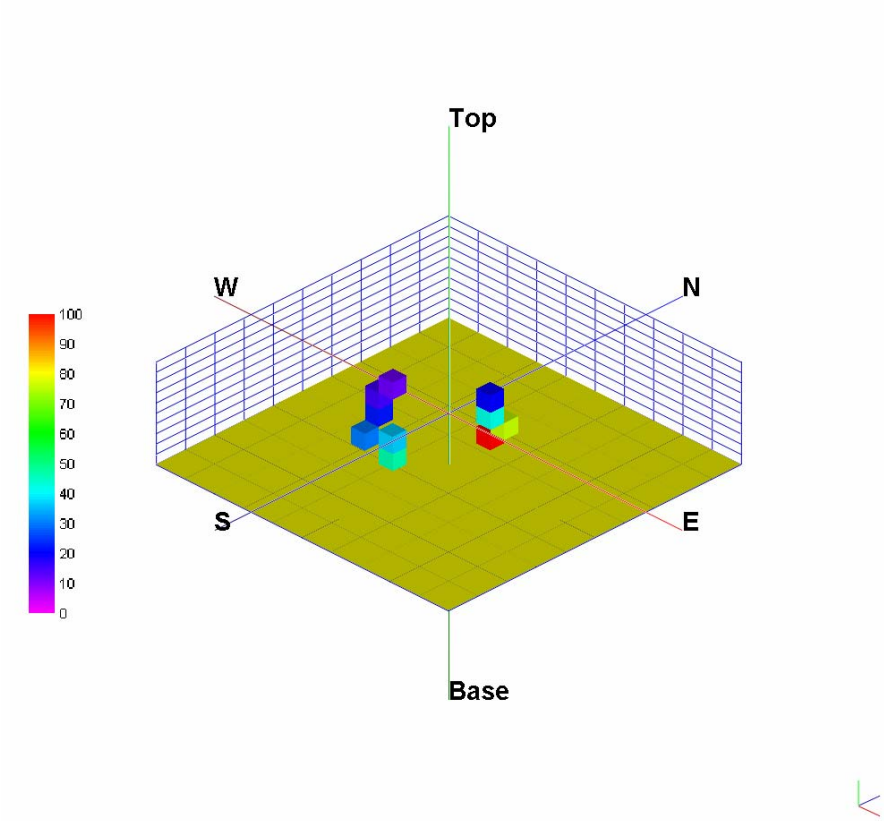

Model 7 (Horizontal ellipsoids at depths 0.6m and 0.05m)

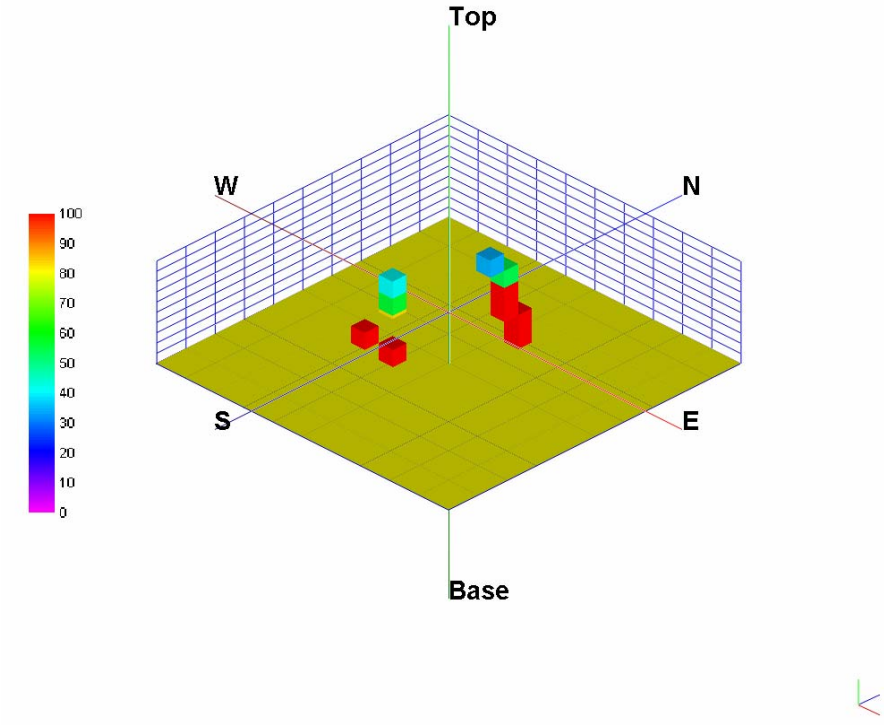

Model 8 (Vertical ellipsoids at depths 0.6m and 0.05m)

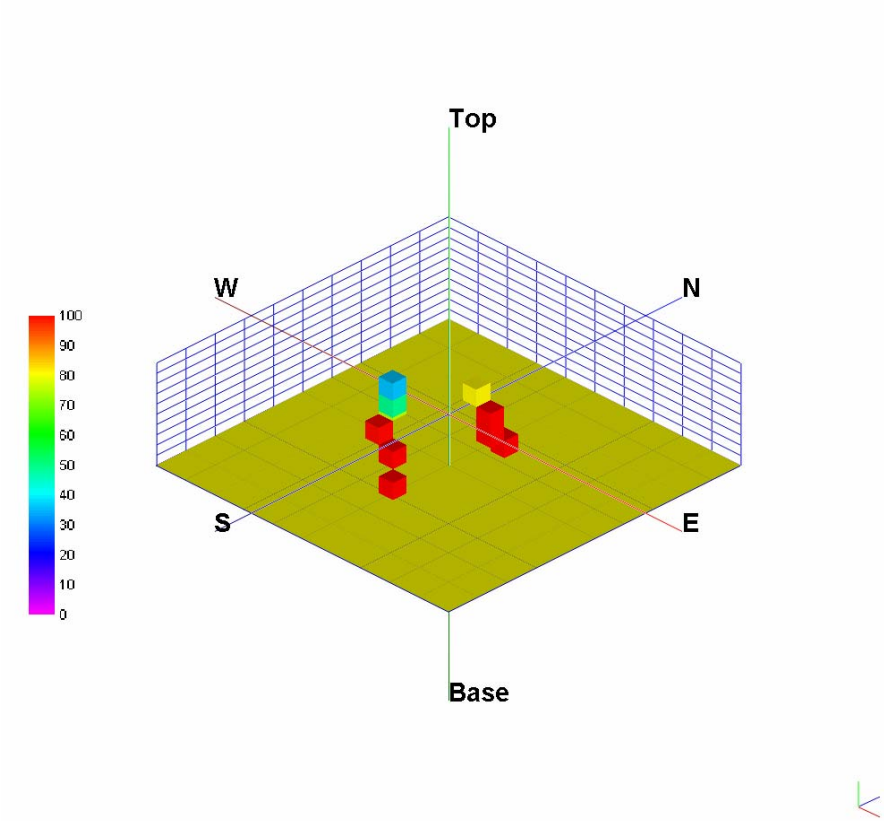

Model 9 (Randomly oriented ellipsoids at depth 0.6m and 0.2m)

Appendix B3
UXAnalyze Dipole Inversion Results

This code is currently under development by AETC and Geosoft under a concurrent ESTCP project. The authors would like to extend their gratitude to AETC for running these models for us when our original attempts to run the older IDL-based MTADS-DAS code failed to invert several of the 2D input data sets. The positional accuracy of the two runs are comparable, but the UXAnalyze version inverted the 2D data with greater success.

As with the IDL-based code, this code operates on one anomaly at a time. Where signatures overlap, data must be manually divided between anomalies based on position. For the data in this Appendix, no segmentation of anomalies was attempted. Targets generally appear as single asymmetric anomalies in the 2D data, and the 3D data cannot be satisfactorily gridded. As a result, all Models are treated as single targets for purposes of inversion and results should be compared to the "combined" targets presented in the body of the text. Position errors are reported as the linear distance from the detection point to the closest true target location including both horizontal and vertical components.

This inversion process is essentially the same as the "combined" target inversion presented in the body of the text. When these "combined" targets are taken in to consideration, the results both in terms of fit and accuracy are virtually the same for both the IDL and UXAnalyze codes.

Table B3-1: 2D data fit coefficient.

	Fit (2D data)	Fit (3D data)
Model 1	0.972	0.000
Model 2	0.928	0.925
Model 3	0.939	0.497
Model 3t	0.960	0.002
Model 4	0.957	0.835
Model 5	Not strong enough	0.495
Model 6	0.983	Too much change
Model 7	Not strong enough	0.331
Model 8	0.952	0.628
Model 9	0.975	0.570

Table B3-2: 2D and 3D dipole inversion results. Average location error of 0.16m with two failures for 2D input data. Average location error of 0.29m with one failure for 3D input data.

	2D data				Error	3D data				Error
	X	Y	Z	size		X	Y	Z	size	
True	-0.10	-0.20	0.60*	0.10		-0.10	-0.20	0.60*	0.10	
Model 1	-0.17	-0.21	0.15	0.05	0.09	-0.05	-0.28	-0.12	0.00	0.33
Model 2	-0.03	-0.17	0.52	0.04	0.11	-0.16	-0.26	0.43	0.04	0.19
Model 3	-0.06	-0.02	0.50	0.05	0.21	0.00	-0.26	0.78	0.05	0.21
Model 3t	-0.08	-0.02	0.53	0.05	0.19	0.10	0.36	-0.15	0.00	0.21‡
Model 4	-0.07	-0.18	0.21	0.05	0.04	-0.17	-0.24	0.14	0.04	0.10
Model 5	--				--	-0.33	-0.24	0.19	0.02	0.47
Model 6	-0.06	-0.11	0.49	0.06	0.15	--				--
Model 7	--				--	0.02	0.35	0.00	0.01	0.11‡
Model 8	-0.02	0.03	0.49	0.06	0.27	0.00	0.17	0.83	0.07	0.45
Model 9	-0.01	0.03	0.48	0.06	0.28	0.02	0.23	0.51	0.05	0.45

*depth of models 1 and 4 is 0.20m

‡position error with respect to 20mm target at (0.10, 0.30, 0.05).

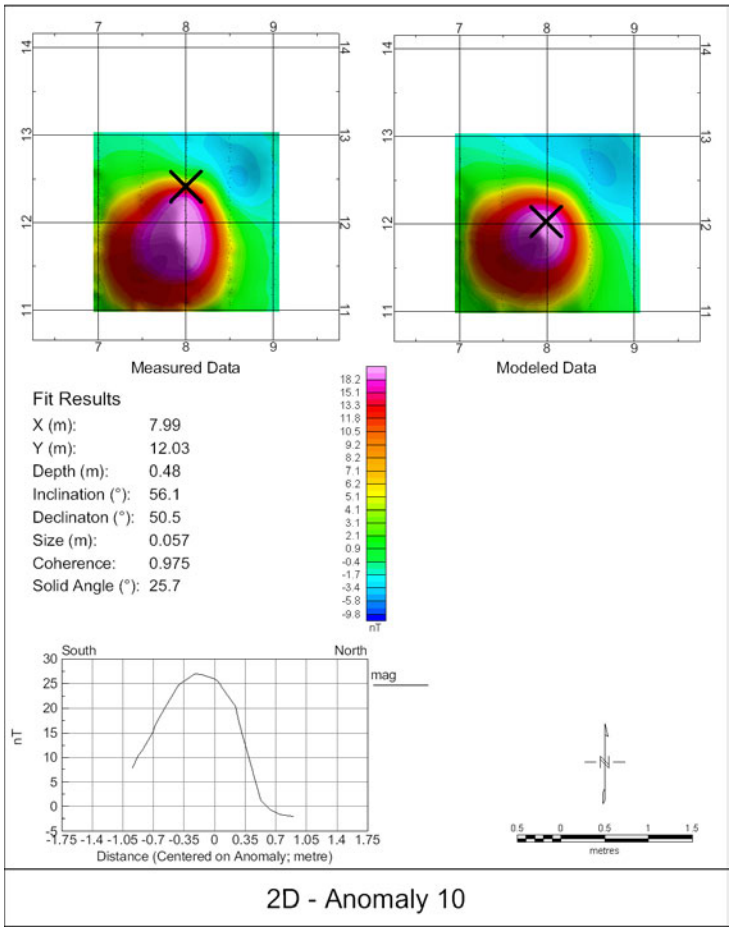

Figure B3-1: Screen capture of UXAnalyze results from Model 9.

Appendix B4
Solid-body Inversion of Interpolated Data

In addition to the solid-body inversion of the 2D lines and 3D "cloud" of data points, inversion was also run on the interpolated 2D grids and 3D lattices. The results are significantly skewed by the introduction of interpolation errors. This impacted the 3D data more than the 2D data due to the poorer algorithms and the greater requirement for interpolation. The 2D data required interpolation from 205 to 441 points (1:2), whereas the 3D data required interpolation from 300 to2,205 points (1:7).

The weakness in the Rockware gridding algorithm (used for all 3D data) is demonstrated using Model 9rw. In this case, the Rockware routines were used to grid the 2D data, and can be compared directly to the results using the Geosoft routines as shown in the 2D Model 9 results. The entire 2D data set was not treated with the Rockware processing in order to illustrate the performance of the 3D method against the current standard of processing algorithms.

The Model 9t reported in the 3D results is the fully-populated noise-free version of Model 9. Since this model is fully-populated it does not rely on interpolation of any kind. The errors in this case are strictly the result of the mis-match in treatment of ellipsoids between the MAGMOD forward modeling code and the ModelVision inversion code.

Note that, unlike the tables in the body of the report, the positioning errors reported here are the z-error and not the radial-error.

Table B4-1: 2D RMS error when fitting a sphere or ellipsoid to the data.

	RMS error (sph)	RMS error (ellip)
Model 1	2.30	2.21
Model 2	1.80	1.63
Model 3	1.82	1.64
Model 3t	0.01	0.08
Model 4	5.70	5.68
Model 5	8.76	8.67
Model 6	2.58	2.56
Model 7	8.32	8.94
Model 8	2.40	2.36
Model 9	4.71	4.60
Model 9rw	6.12	5.26

Table B4-2: 2D Spherical inversion results (fitting a spherical model)

	60mm				z-error	20mm				z-error
	X	Y	Z	rad		X	Y	Z	rad	
True	-0.10	-0.20	0.60*	0.10		0.10	0.30	0.05	0.03	
Model 1	-0.05	-0.19	0.24	0.05	0.04	Not modeled				--
Model 2	-0.07	-0.20	0.63	0.05	0.03	Not modeled				--
Model 3	-0.07	-0.21	0.64	0.05	0.04	-0.02	0.29	0.15	0.02	0.10
Model 3t	-0.10	-0.20	0.60	0.05	0.00	0.10	0.30	0.05	0.02	0.00
Model 4	-0.04	-0.38	0.23	0.04	0.03	Not modeled				--
Model 5	-0.05	-0.50	0.56	0.04	0.04	Not modeled				--
Model 6	-0.08	-0.10	0.65	0.06	0.05	Not modeled				--
Model 7	-0.05	-0.50	0.60	0.04	0.00	-0.01	0.10	0.03	0.01	0.02
Model 8	-0.07	-0.14	0.62	0.06	0.02	-0.03	0.35	0.32	0.03	0.27
Model 9	-0.20	-0.12	0.62	0.05	0.02	-0.09	0.29	0.34	0.03	0.29
Model 9rw	-0.23	-0.20	0.50	0.05	0.10	-0.10	0.23	0.43	0.04	0.38

*depth of models 1 and 4 is 0.20m

Table B4-3: 2D Ellipsoid inversion results (positions)

	60mm			z-error	20mm			z-error
	X	Y	Z		X	Y	Z	
True	-0.10	-0.20	0.60*		0.10	0.30	0.05	
Model 1	-0.06	-0.20	0.25	0.05	Not modeled			--
Model 2	-0.10	-0.30	0.65	0.05	Not modeled			--
Model 3	-0.08	-0.21	0.63	0.03	-0.02	0.28	0.16	0.11
Model 3t	-0.10	-0.20	0.61	0.01	0.10	0.30	0.05	0.00
Model 4	-0.04	-0.38	0.23	0.03	Not modeled			--
Model 5	-0.04	-0.50	0.56	0.04	Not modeled			--
Model 6	-0.08	-0.10	0.65	0.05	Not modeled			--
Model 7	-0.04	-0.43	0.57	0.03	-0.10	0.10	2.00	1.95
Model 8	-0.08	-0.16	0.61	0.01	-0.03	0.34	0.36	0.21
Model 9	-0.22	-0.10	0.63	0.03	-0.06	0.27	0.31	0.14
Model 9rw	-0.27	-0.12	0.68	0.08	-0.04	0.19	0.26	0.34

*depth of models 1 and 4 is 0.20m

Table B4-4: 2D Ellipsoid inversion results (dimensions)

	60mm			error	20mm			Error
	A	B	C	%Vol	A	B	C	%Vol
True	0.051	0.051	0.051		0.017	0.017	0.017	
Model 1	0.12	0.03	0.03	20	Not modeled			--
Model 2	0.28	0.02	0.02	25	Not modeled			--
Model 3	0.26	0.02	0.02	29	0.04	0.01	0.01	30
Model 3t	0.10	0.03	0.03	29	0.02	0.02	0.02	28
True	0.100	0.030	0.030		0.035	0.010	0.010	
Model 4	0.09	0.03	0.03	21	Not modeled			--
Model 5	0.17	0.03	0.01	33	Not modeled			--
Model 6	0.57	0.15	0.01	162	Not modeled			--
Model 7	1.00	0.03	0.01	27	0.02	0.02	0.01	71
Model 8	0.19	0.06	0.05	104	0.12	0.03	0.02	1145
Model 9	0.18	0.06	0.05	83	0.04	0.03	0.01	701
Model 9rw	0.13	0.06	0.03	158	0.04	0.04	0.02	841

Table B4-5: 3D RMS error when fitting a sphere(s) or ellipsoid(s) to the data.

	Error (sph)	Error (ellip)
Model 1	1.79	1.68
Model 2	3.57	3.49
Model 3	1.91	2.36
Model 3t	0.01	0.01
Model 4	2.43	2.36
Model 5	4.99	4.92
Model 6	3.17	3.55
Model 7	3.44	1.99
Model 8	1.98	2.35
Model 9	1.73	1.72
Model 9t	0.66	0.63

Table B4-6: 3D Spherical inversion results (fitting a spherical model)

	60mm				z-error	20mm				z-error
	X	Y	Z	rad		X	Y	Z	rad	
True	-0.10	-0.20	0.60*	0.10		0.10	0.30	0.05	0.03	
Model 1	-0.11	-0.24	0.30	0.06	0.10	Not modeled				--
Model 2	-0.14	-0.30	0.86	0.06	0.26	Not modeled				--
Model 3	-0.14	-0.30	0.90	0.07	0.30	0.08	0.27	0.13	0.02	0.08
Model 3t	-0.10	-0.20	0.60	0.05	0.00	0.10	0.30	0.05	0.02	0.00
Model 4	-0.12	-0.39	0.35	0.06	0.15	Not modeled				--
Model 5	-0.15	-0.50	1.10	0.07	0.50	Not modeled				--
Model 6	-0.13	-0.20	0.76	0.08	0.16	Not modeled				--
Model 7	-0.15	-0.50	0.78	0.05	0.18	0.22	0.21	0.14	0.01	0.09
Model 8	-0.14	-0.22	0.77	0.08	0.17	0.09	0.30	0.15	0.03	0.10
Model 9	-0.30	-0.16	0.87	0.08	0.27	0.04	0.24	0.11	0.02	0.06
Model 9t	-0.20	-0.10	0.58	0.06	0.02	0.07	0.28	0.05	0.02	0.00

*depth of models 1 and 4 is 0.20m

Table B4-7: 3D Ellipsoid inversion results (positions)

	60mm			z-error	20mm			z-error
	X	Y	Z		X	Y	Z	
True	-0.10	-0.20	0.60*		0.10	0.30	0.05	
Model 1	-0.11	-0.25	0.25	0.05	Not modeled			--
Model 2	-0.15	-0.31	0.87	0.27	Not modeled			--
Model 3	-0.12	-0.24	0.92	0.32	0.08	0.29	0.02	0.03
Model 3t	-0.10	-0.20	0.60	0.00	0.10	0.30	0.05	0.00
Model 4	-0.12	-0.41	0.36	0.16	Not modeled			--
Model 5	-0.18	-0.50	1.09	0.49	Not modeled			--
Model 6	-0.14	-0.22	1.10	0.50	Not modeled			--
Model 7	-0.27	-0.50	0.91	0.31	0.07	0.22	0.07	0.02
Model 8	-0.17	-0.31	0.86	0.26	0.03	0.22	0.35	0.30
Model 9	-0.30	-0.16	0.88	0.28	0.04	0.25	0.10	0.05
Model 9t	-0.22	-0.10	0.60	0.00	0.06	0.29	0.05	0.00

*depth of models 1 and 4 is 0.20m

Table B4-8: 3D Ellipsoid inversion results (dimensions)

	60mm			error	20mm			Error
	A	B	C	%Vol	A	B	C	%Vol
True	0.051	0.051	0.051		0.017	0.017	0.017	
Model 1	0.29	0.07	0.01	50	Not modeled			--
Model 2	0.24	0.04	0.03	102	Not modeled			--
Model 3	0.12	0.06	0.05	147	0.01	0.01	0.01	80
Model 3t	0.07	0.07	0.03	1	0.02	0.02	0.02	0
True	0.100	0.030	0.030		0.035	0.010	0.010	
Model 4	0.44	0.04	0.04	122	Not modeled			--
Model 5	0.25	0.14	0.01	306	Not modeled			--
Model 6	0.57	0.15	0.01	872	Not modeled			--
Model 7	1.00	0.03	0.01	258	0.02	0.02	0.01	21
Model 8	0.19	0.06	0.05	433	0.12	0.03	0.02	1659
Model 9	0.18	0.06	0.05	503	0.04	0.03	0.01	208
Model 9t	0.20	0.08	0.02	179	0.06	0.01	0.01	153

The spherical inversion of the spherical targets slightly out-performed the other combinations (e.g. spherical inversion of ellipsoidal targets). The most disturbing result is the very poor (x, y) positioning the noise-free ellipsoid data (Model 9t), even though the depth is accurately calculated.

Inversion using the 2D Geosoft grids showed a slightly poorer overall fit, especially for Models 5 and 7. The ellipsoid inversion for the 20mm in Model 7 should be classified as a non-detection since the results pushed the target to the extreme limits set for distance and depth (Table B4-3, blue text). The radial distance to the target center was comparable between the 2D and 3D data sets, averaging 0.31 and 0.28m respectively, but the depth error in the 2D data was nearly an order of magnitude better than the 3D data. The size estimates based on target volume were also about twice as good for the 2D data. This is attributed to the superiority of the 2D Geosoft "minimum curvature" gridding algorithms over the 3D "inverse-distance" algorithm in Rockware. This is supported by the considerably poorer performance of the Model 9rw. In this case, the 2D data were gridded and processed using the Rockware code rather than the standard Geosoft code.

Appendix B5
Rockware Gridding Algorithms

These descriptions are taken directly from the Rockware help manual provided by the software company. They cover the six gridding algorithms tested under this project.

1) Closest-Point gridding algorithm
Click in this radio button to select the Closest-Point algorithm, in which the value of a voxel node is set to be equal to the value of the nearest data point, regardless of its distance from the point or the value of its other neighbors.

This method is useful when generating models in which the values are not gradational.

2) Isotropic Distance gridding algorithm
Click in the Inverse-Distance/Isotropic radio button to select the Inverse-Distance algorithm which assigns a voxel node value based on the weighted average of neighboring data points. Unlike the "Anisotropic" method, this method uses all data points in interpolating node values.

During the interpolation of solid model nodes, the value of each data point is weighted according the inverse of its distance from the node, taken to the second power (Inverse-Distance squared). By raising this to an exponent of "2", this method assures that distant points will have less influence on the node value than closer points.

This method is useful when modeling uniformly distributed data in non-stratiform environments.

3) Anisotropic Distance gridding algorithm
Click in this radio button to select the Octant-Based Inverse-Distance algorithm, which assigns a voxel node value based on the weighted average of neighboring data points. Unlike the "Isotropic" method, this method includes only the closest data point within each octant around the node when computing the inverse-distance weighted average.

This is useful for modeling drill-hole based data in stratiform deposits.

4) Weighted Distance gridding algorithm
Click in this radio button to select the Inverse-Distance algorithm that will use all of the available data points when computing a node's value.

But, instead of automatically using a weighting exponent of "2", the program allows the user to assign different weighting exponents to control points oriented vertically versus horizontally from the node. The greater the exponent you enter, the less influence those data points will have.

Expand this heading to establish the weighting values.

5) Directional Weighted gridding algorithm
Click in the Directional Weighting radio button to select the Directional-Weighting algorithm. This method will bias the modeling in a user-specified direction.

Expand this heading to specify the direction and strength.

6) Vertical Biasing gridding algorithm
This modeling method uses Inverse-Distance modeling, in which the value of each of the data points is weighted according to the inverse of its distance from the voxel node being computed, taken to a user-selected power. The difference with Horizontal Biasing is that the user can define a vertical distance from each voxel node beyond which points will no longer be used in computing the node value. This allows the user to horizontally bias the interpolation process such that stratiform deposits such as sand and gravel may be modeled more effectively

Expand this heading to establish the biasing "bubble."